NASA CR 168024
VOUGHT REPORT 2-53200/3R53497

TANDEM FAN MODEL-FRONT FAN NOZZLE TEST APPLICABLE TO A TYPE A V/STOL AIRCRAFT

DAVID F. PENNINGTON

CONTRACT NAS3-21467
JULY 1983

LTV Vought

NASA

1. Report No.	2. Government Accession No.	3. Recipient's Catalog No.
NASA CR-168024		

4. Title and Subtitle	5. Report Date
Tandem Fan Model - Front Fan Nozzle Test Applicable to a Type A V/STOL Aircraft	July 1983
	6. Performing Organization Code: 80378
7. Author(s): D. F. Pennington	8. Performing Organization Report No.: TR-2-53200/3R-53497
	10. Work Unit No.
9. Performing Organization Name and Address: Vought Corporation, P.O. Box 225907, Dallas, TX 75265	11. Contract or Grant No.: NAS3-21467
	13. Type of Report and Period Covered: Contractor Report
12. Sponsoring Agency Name and Address: National Aeronautics and Space Administration, Washington, DC 20546	14. Sponsoring Agency Code: 505-42-62

15. Supplementary Notes: FINAL REPORT

Project Manager, Mr. Albert L. Johns, V/STOL Propulsion Section, NASA Lewis Research Center, Cleveland, OH 44135

16. Abstract

An approximately 0.25 scale model of a tandem fan nozzle designed for a Type A V/STOL Aircraft configuration was tested in the NASA Lewis Research Center Vertical Thrust Stand static test facility. A.3 040 meter (12 inch) diameter, tip driven, turbofan simulator was used to provide the airflow source for the nozzle. Model variables consisted of 0, 3.81, 12.7 and 79.45 cm. spacers between the fan and duct (fan duct spacers), shaft simulator, two fan exit hub designs, two different nozzle areas in the deflected mode and two nozzle areas in the cruise mode. Static and total pressures and temperatures were measured over the range of fan corrected airflows. Thrust vector angle and thrust coefficient were calculated as a function of nozzle pressure ratio and normalized specific corrected nozzle flow.

High nozzle performance in the deflected and cruise mode was verified for all of the spacer distances and corrected fan speeds. The three major contributors to performance improvement were determined to be hub design, nozzle exit area and spacer distance. Shaft removal, or adding a contour plate and sideplates had very little or no effect on performance. The highest thrust coefficient in the deflected mode occurs with no fan-duct spacer while the best thrust coefficient for the cruise mode occurs with the largest fan-duct spacer installed ($\triangle X$ = 79.45 cm).

17. Key Words (Suggested by Author(s))	18. Distribution Statement
V/STOL Nozzle Tandem Fan Nozzle Vented Nozzle Type A V/STOL Aircraft Thrust Deflecting	Unclassified - Unlimited Category 02

19. Security Classif. (of this report)	20. Security Classif. (of this page)	21. No. of Pages	22. Price*
Unclassified	Unclassified	120	

* For sale by the National Technical Information Service, Springfield, Virginia 22161

NASA CR-168024
Vought Report 2-53200/3R-53497

TANDEM FAN MODEL-FRONT FAN NOZZLE TEST APPLICABLE TO A TYPE A V/STOL AIRCRAFT

by
David F. Pennington

July 1983

Prepared Under Contract No. NAS3-21467
by
Vought Corporation
Dallas, Texas
75265

for
Lewis Research Center
National Aeronautics and Space Administration
Cleveland, Ohio
44135

THIS PAGE BLANK

TABLE OF CONTENTS

THIS PAGE BLANK

TABLE OF CONTENTS (Continued)

THIS PAGE BLANK

TABLE OF CONTENTS (Continued)

THIS PAGE BLANK

LIST OF FIGURES

THIS PAGE BLANK

LIST OF FIGURES (Continued)

THIS PAGE BLANK

LIST OF FIGURES (Continued)

THIS PAGE BLANK

LIST OF TABLES

THIS PAGE BLANK

LIST OF TABLES (Continued)

THIS PAGE BLANK

1.0 Summary

An approximately 0.25 scale model of a front Tandem Fan nozzle designed for a Type A (Subsonic Cruise) V/STOL aircraft configuration has been tested in the Vertical Thrust Stand static test facility at NASA Lewis Research Center. A 0.3048 meter diameter (12 inch) tip driven turbofan was used to provide the airflow source for the nozzle. This series of nozzle tests were conducted with fan-duct spacer distances of 0., 3.81, 12.7 and 79.45 cm between the fan exit and the nozzle entrance planes. The nozzle performance for these tests are reported herein. Model variables include cruise and deflected nozzle positions, two (2) Hub designs, simulated turbine fan shaft installed and removed, a nozzle contour plate and nozzle sidewall extensions. The corrected fan speed was varied over the range of approximately 50 to 100 percent. The nozzle pressure ratio was in the range of 1.1 to 1.35.

High nozzle performance in the deflected mode was verified for all of the fan-duct spacer distances and corrected fan speeds. The thrust vector angle was usually between 88^{0} and 92^{0}, the thrust coefficient, was in the range of 0.90 to 0.98. The three major contributors to performance improvement were Hub design, nozzle exit area and fan-duct spacer distance. Shaft removal or adding a contour plate and sideplates had very little or no effect on performance. The better Hub design resulted in a 1.8 to 3.3 percent improvement in the thrust vector angle, and a 1.0 to 3.6 percent improvement in thrust coefficient. Additional improvements occured when the nozzle area was reduced. The highest thrust coefficient in the vertical mode occurred when no fan-duct spacer was included while the best thrust coefficient in the cruise mode occurred with the largest fan-duct spacer installed.

2.0 Introduction

Thrust deflecting V/STOL aircraft require propulsion system nozzles which can provide high thrust coefficients and efficient turning over a wide range of deflection angles. Requirements placed on the nozzles (as well as inlets) can be especially severe due to the operating environment on board various types of combat ships. Thus considerable research and configuration development is required to design nozzles (and inlets) for such an application.

The V/STOL aircraft being developed by the Vought Corporation for Navy Type A (Subsonic Cruise) applications employs two tandem fan propulsion systems arranged in two nacelles, integrated structurally with the fuselage. Each nacelle contains a complete propulsion unit consisting of a core engine, two fixed pitch fans with variable inlet guide vanes, and associated inlets and nozzles (Figure 1). The fans are located ahead of the core engine and are mounted co-axially with the engine. Small fan diameters result from the use of two fans in each nacelle. A vectoring nozzle for the front fan and an inlet for the aft fan are incorporated between the two fans. Flow through the two fans is maintained separate at all times. The core engine is located immediately behind the aft fan and is supercharged by it. The core and aft fan flows are mixed and discharged through a vectoring nozzle.

Flow paths through the Tandem Fan nacelle are shown in Figure 2. During conventional flight, fan flows are vectored directly aft. For VTOL, nozzles are repositioned as shown to vector thrust vertically. Intermediate thrust vector angles are achieved by corresponding intermediate positions of each nozzle. Thrust vector response is rapid and smooth transitions are achieved by the control forces achievable through combined thrust modulation and vectoring.

The nozzles are designed to provide high thrust coefficients and efficient turning of the flow over a range of deflection angles from 0^{o} (cruise) to 110^{o} (V/STOL). Both nozzles are a "vented" configuration which allows the inside turn radius to be set aerodynamically. Although this results in lower discharge coefficients, wall separation is eliminated and

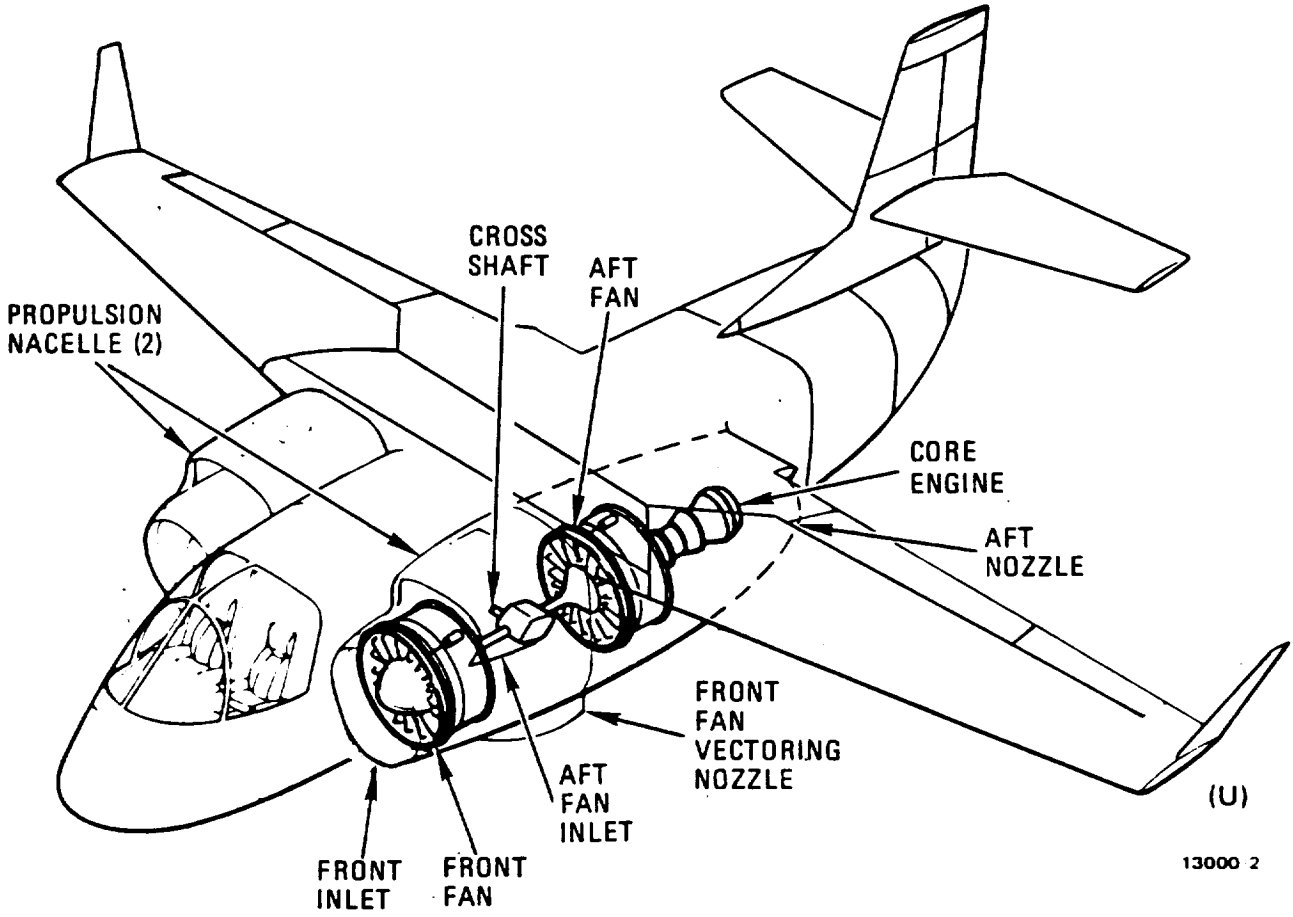

FIGURE 1 V/STOL TYPE "A" TANDEM FAN POWERED AIRCRAFT

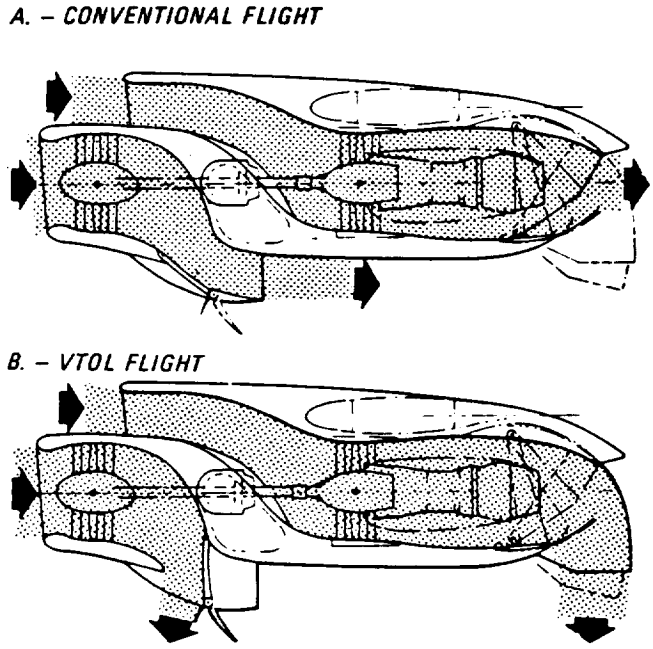

FIGURE 2 SINGLE STAGE TANDEM FAN NACELLE

higher thrust coefficients result. The forward nozzle, which is two-dimensional for good integration with the nacelle and ease in vectoring, uses a simple two-piece deflector to vector thrust. Variation of nozzle area in cruise is achieved with a small flap mounted on the nacelle surface. The aft nozzle, which vectors mixed flow from the core engine and the aft fan, is two-dimensional for ease in vectoring the flow. The nozzle deflector is hinged along the lower portion of the nacelle and is rotated downward for V/STOL. A rotating lower flap is used to achieve the nozzle areas required for cruise.

The inlets have been designed to provide good performance and low distortion in a minimum length. Large inlet lip radii are used for good VTOL performance and to reduce inlet flow distortion. The front inlet was close coupled to the fan for improved crew visibility. The aft inlet has been arranged to benefit from the favorable flow field of the front inlet and to integrate well into the nacelle. Low diffusion rates are provided for low flow distortion and high turning of the flow through the bend to the aft fan provides for a short drive shaft.

Several years ago NASA Lewis Research Center (LeRC) and the Vought Corporation began a research effort to develop a broad data base for the design of the inlet and nozzle systems that will contribute to an effective, efficient, lightweight low drag Tandem Fan propulsion system that operates satisfactorily at the conditions applicable to the Navy Type A V/STOL aircraft. The effort began with the foward and aft inlet model tests as described in References 1 and 2.

This report covers, under contact NAS3-21467 (Reference 3), the performance evaluation of the front fan nozzle in the Vertical Thrust Stand static test facility.

3.0 Symbols and Abbreviations

A	Area, cm^2
CD	Discharge coefficient; ratio of bellmouth corrected airflow to fan stream ideal airflow
CFN, CFNAD	Thrust coefficient, Tg/WSN·VIF or Tg/W7SPCA·VIN
D	Diameter, cm
ΔX	Incremental length added by a spacer, cm
ENPR	Nozzle mass weighted total pressure (at fan exit) to freestream total pressure ratio, PT/PTO
FSPS	Fan stator static pressure, Pa
g	Standard gravitational constant, 9.8066 m/sec^2
H	Height, cm
PAMB	Ambient pressure, Pa
PCDSPD	Fan corrected speed, percent
PHID	Thrust vector deflection angle, deg
PR16AD	Nozzle mass weighted total pressure at nozzle entrance for ΔX = 79.45 cm test to freestream total pressure ratio, PT/PTO
PS	Static pressure, Pa
PT/PTO	Total pressure ratio to the freestream total pressure
R	Radius, cm
R/H	Instrumentation probe radius to flow passage height ratio
T	Thrust vector at angle PHID, N
VIF	Fan stream ideal velocity, m/sec
VIN	Fan stream plus turbine stream ideal velocity, m/sec
WSN	Specific corrected nozzle flow based on area A_0 = 612.9 cm^2 (95 in^2), fan exit total pressure and temperature and non-dimensionalized by 1 $lbm/sec\text{-}in^2$
W7SPCA	Specific corrected nozzle flow based on area A_0 = 612.cm^2 (95 in^2), nozzle entrance total pressure and temperature and non-dimensionalized by 1 $lb/sec\text{-}in^2$ and turbine flow added to fan flow

X/D		Length from duct entrance face (station 10) to fan diameter (30.48 cm) ratio

Subscripts

e	-	Exit plane

4.0 Program Objectives and Description

The objectives of this test program were to develop a data base for the design of a close coupled tandem fan-nozzle geometry. The nozzle is variable in that it can be transitioned to a cruise or hover (VTOL) mode. The primary area of investigation was to determine the nozzle performance for different fan-nozzle coupling distances and two different deflected nozzle exit areas. Other areas of investigation included the effect of Hub shape, shaft (with or without) and cruise modes.

The model hardware was designed to be compatible with the installation in the NASA Lewis Research Center Vertical Thrust Stand. The nozzle tests were conducted using a government furnished short bellmouth inlet and a 30.48 cm (12 inch) diameter tip turbine fan.

The nozzle was tested over a nozzle total pressure ratio range of approximately 1.10 to 1.35 by varying the fan corrected speed from 50 to 100 percent. Model variations were also made by installation of hub and duct spacers at the fan exit station. Additionally, configurations were tested with the fan shaft simulator removed and installed, two lower duct exit lip sections removed which modified the nozzle area and bottom exit lip venting, the addition of a top duct contour plate in the nozzle to smooth the flow between the duct and nozzle flap interface, and the addition of sidewalls to improve two-dimensional nozzle flow.

The nozzle configurations were evaluated in terms of the fan exit total and static pressures and surface static pressures on the downstream duct, Hub and nozzle surfaces. Results from a series of tests using a 79.45 cm (31.28 inch) spacer between the fan and duct were also evaluated based on additional total and static pressure measurements at the spacer-duct interfaces. Model forces and moments were determined with output from a Task Corporation Mark VII, 10.2 cm. (4 in.) diameter strain gage balance. All six components and their second order interactions were used to determine normal force, axial force, and pitching moment.

5.0 Test Apparatus

This section describes the front tandem fan nozzle model and the associated instrumentation. In addition, the NASA Lewis Vertical Thrust Stand test conditions, procedures, and data reduction techniques are also described.

5.1 Model Description

The front tandem fan nozzle model is an approximate 0.25 scale geometric representation of the full scale nozzle geometry. The model consists of a short bellmouth inlet, tip turbine drive turbofan, fan exit Hub, duct spacer (different lengths), fan exit duct, nozzle section and nozzle flaps. A photograph of the complete front tandem fan nozzle model installed in the test facility is shown in Figure 3.

Bellmouth Inlet

As can be seen in Figure 3, a short bellmouth inlet was utilized in the test apparatus. This standard inlet bellmouth has been utilized by NASA Lewis on other similar tests. Based on bellmouth calibration, bellmouth static pressures, freestream total temperature and pressure and inlet diameter, 30.48 cm, the flow rate in the bellmouth for any test condition can be calculated.

Turbofan

Fan engine airflow simulation was provided to the model by a 30.48 cm (12 inch) diameter, tip-driven, warm-air powered turbofan which was designed and fabricated by Tech Development Inc. (Reference 4). Fan speed was controlled by the drive air to the turbine tip. The exit nozzle was provided with two flaps to vary the exit area and control the back pressure. A schematic of the turbofan is shown in Figure 4. Figure 5 shows actual fan performance as a function of fan pressure ratio, fan flow rate, fan corrected speed, and exit area.

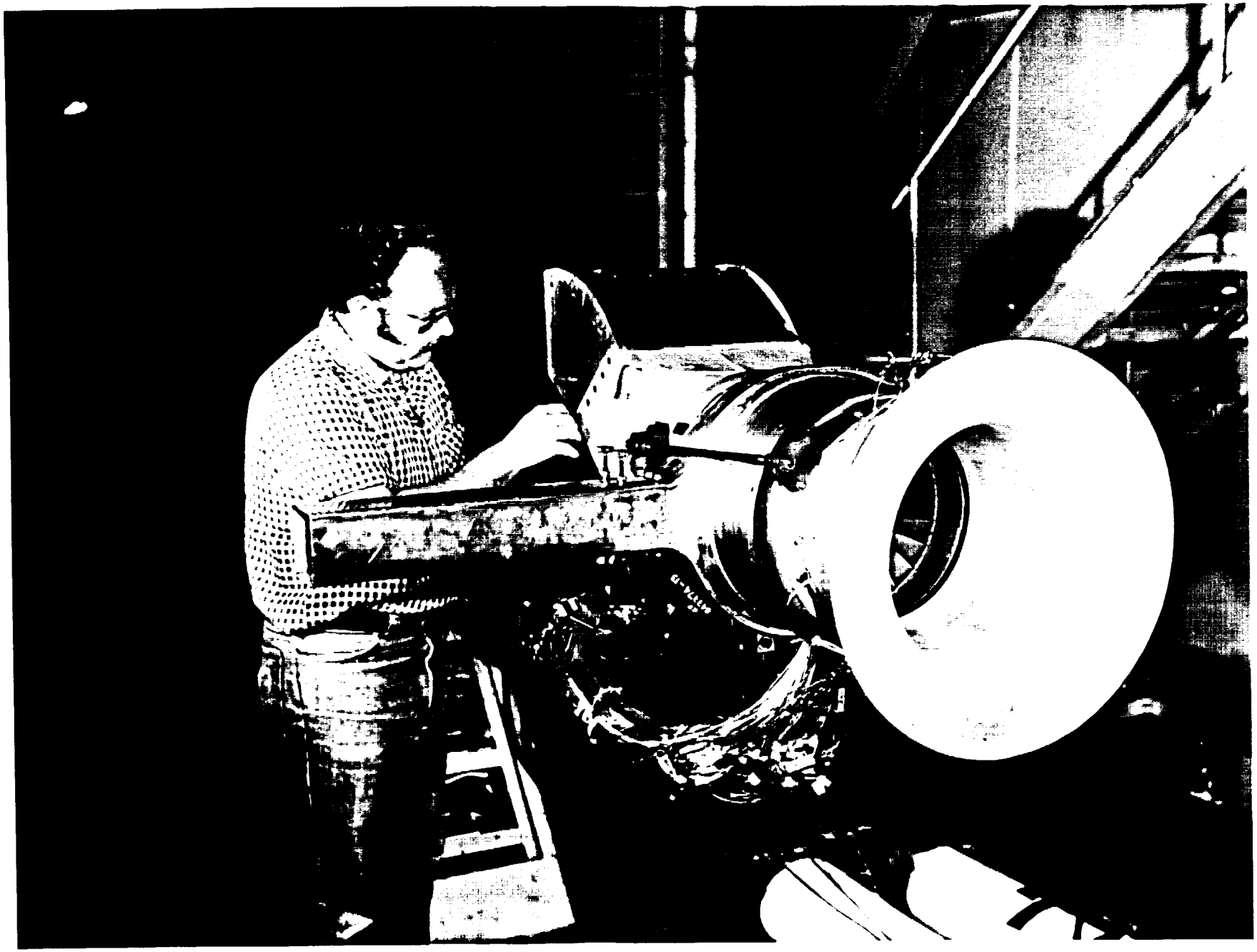

FIGURE 3 FRONT TANDEM FAN NOZZLE MODEL INSTALLED IN NASA LEWIS RESEARCH CENTER VERTICAL THRUST STAND STATIC TEST FACILITY

THIS PAGE BLANK

COURTESY TECH DEV (REF 4)

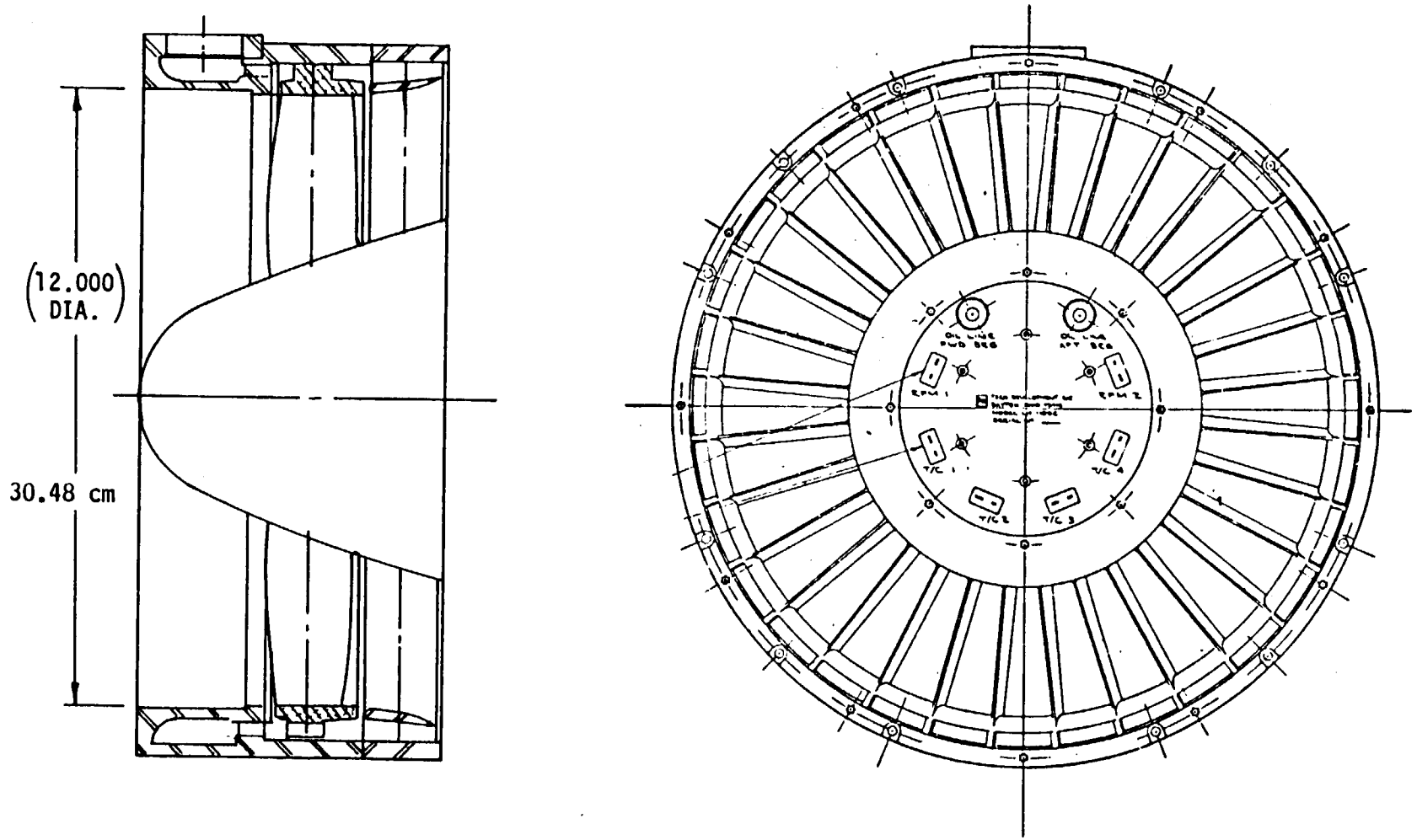

FIGURE 4 .3048 Meter Diameter Powered Simulator Assembly

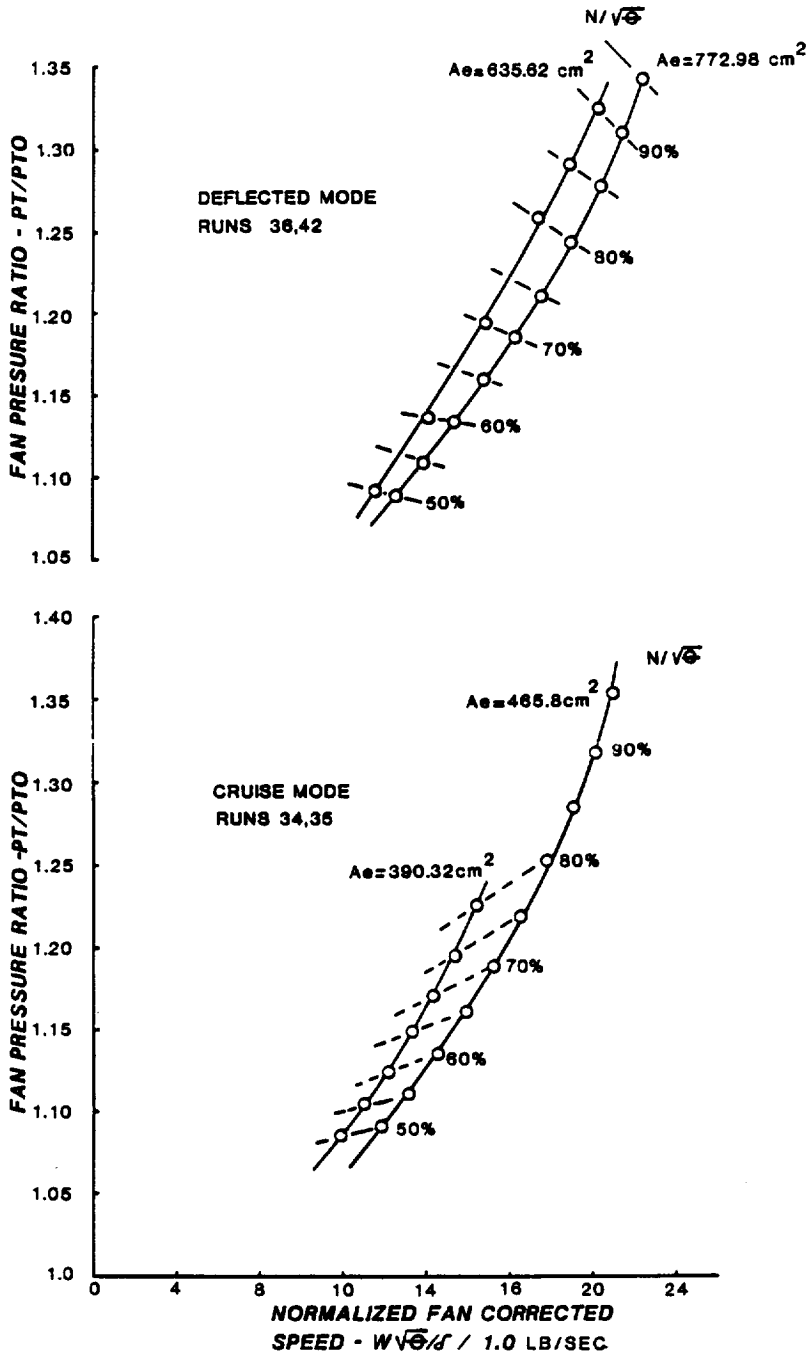

FIGURE 5 .3048 Meter Diameter Fan Operation

Fan Hub

The two different fan Hub designs shown in Figure 6 were utilized to determine the flow effects in the duct and nozzle. Hub No. 1 is a semi-axisymmetric bullet nose shape that is slightly offset below the centerline. This design tends to provide a uniform flow distribution in the duct with the offset directing the flow in the direction of the nozzle exit. This Hub design can have radial curvilinear flow caused by the swirl from the fan stators and short turning couple between the duct inlet and the nozzle exit. Hub No. 2 transitions from the 19.05 cm fan Hub exit diameter to a flat whale tail shaped surface curved in the direction of the nozzle exit. The tip offset slightly exceeds the 9.525 cm radius of the fan Hub, i.e., the tip droops about 1 cm below the bottom reference line of the Hub-fan interface. Hub No. 2 is 3.94 cm longer than Hub No. 1. Both Hubs have a 2.54 cm diameter hole that is used to locate the simulated fan shaft. When the shaft is removed a plug fairing is installed as a replacement.

Duct-Nozzle

The Vought designed and manufactured assembly shown in Figure 7a is made up of a duct, nozzle and flap assembly. The duct is made of fiberglass layup which has a 0.813 cm typical wall thickness and a 1.27 cm thick forward circular flange which bolts to the fan assembly. On the bottom of the duct is a removable block assembly (fairing) which is used to modify the nozzle exit area and degree of nozzle venting. The nozzle has two sidewalls which are 1.27 cm thick 7075-T6 aluminum and a top wall that is also 7075-T6 aluminum which is shaped like a segment of a circle. The segment being 3.81 cm at the maximum thickness. The curved surface forms the inside nozzle wall flow surface and the flat surface is the exterior of the duct. The nozzle exit area is modified from the cruise mode to the V/STOL mode (see Figure 2) by a two piece hinged aluminum flap that is approximately 42.42 cm in length in the full extended position. The duct-nozzle with the 79.45 cm spacer is shown in Figure 7(b). The spacer removed the nozzle-fan away from a close-coupled position. In addition, the tip turbine exit flow was dumped into the fan stream which resulted in a reduced total pressure distortion entering the nozzle. Details of the total pressure profile will be shown later.

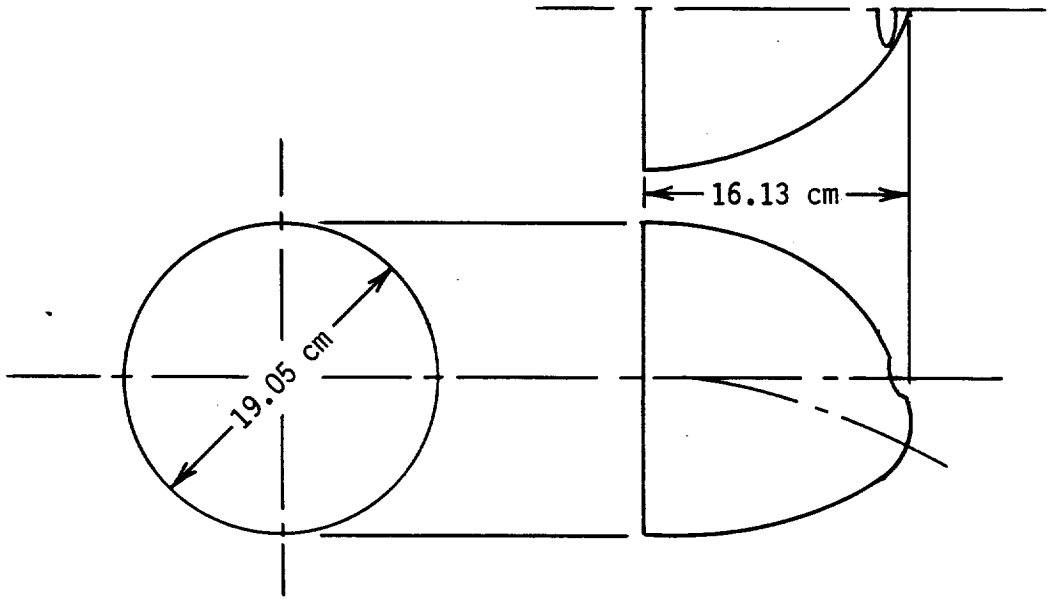

HUB DESIGN 1

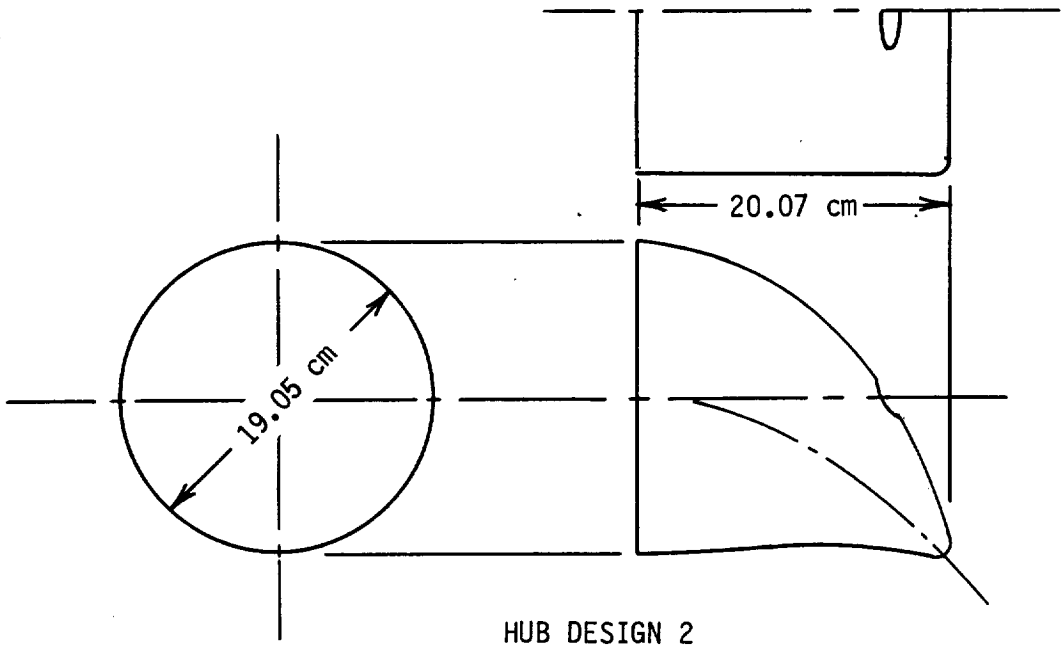

HUB DESIGN 2

Figure 6 Fan Exit Hub Design

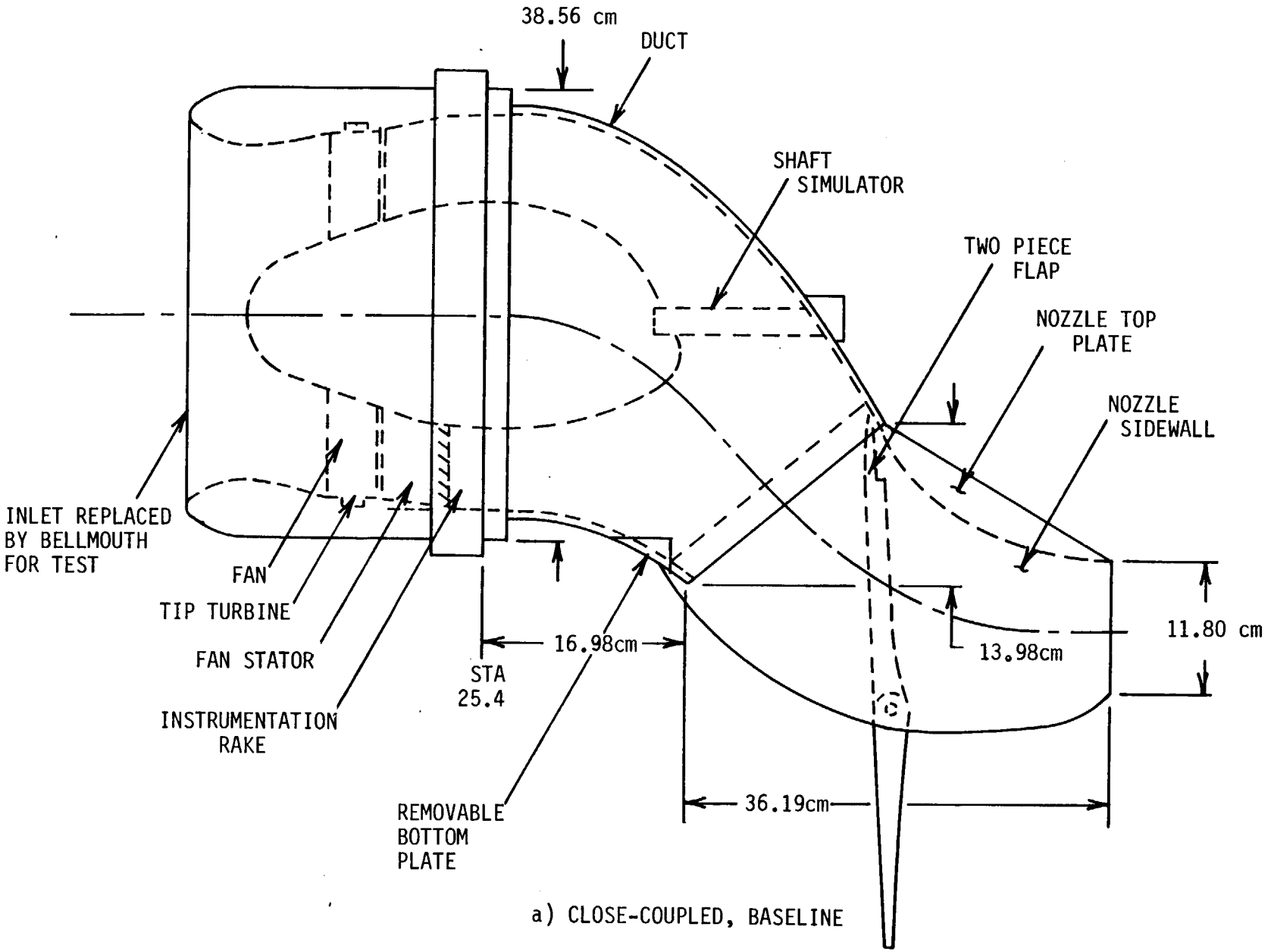

FIGURE 7 DUCT-NOZZLE ASSEMBLY

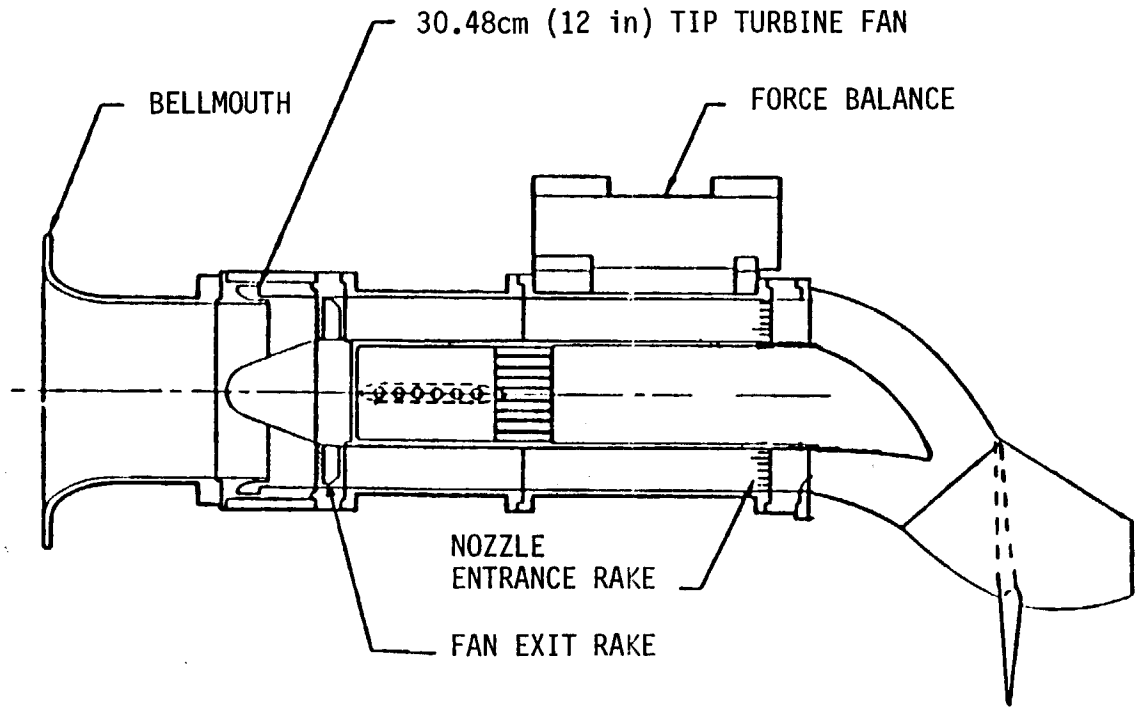

b) DUCT-NOZZLE WITH 79.45cm SPACER

FIGURE 7 (concluded)

Configuration Definition

The various nozzle configurations tested are listed in Table I. The nozzle cruise mode is identified as configuration C'X'. The symbol 'X' represents 2 or 3 which will correspond to cruise nozzle area openings of 390.32 and 465.81 cm^2, respectively. The nozzle deflected mode is identified as D'Y'. The symbol 'Y' will represent 2 or 3 which corresponds to deflected nozzle area openings of 635.62 and 772.98 cm^2, respectively. No tests were performed where the nozzle flaps were in a combination of partial deflected and partial cruise modes (transition mode).

TABLE I
MODEL CONFIGURATION TESTING DEFINITION

CONFIG. NO.	FAN SHAFT		HUB		FAN DUCT SPACER			
	IN	OUT	1	2	0	3.81	12.70	79.45
C3	X			X			X[2]	
C3	X		X		X[2]			
C3	X		X			X[2]	X[2]	X[2]
C3	X			X	X[2]	X[2]	X[2]	X[2]
C3		X	X			X[2]		
C3		X		X		X[2]		
C2	X			X				X[2]
C2	X		X		X[2]			
C2	X		X					X[2]
C2	X		X			X[2]	X[2]	X[2]
C2	X			X	X[2]	X[2]	X[2]	X[2]
C2		X		X		X[2]		
D3	X		X		X[1,2,3]	X[2]	X[2]	X[1,2]
D3	X			X	X[1]	X[2]	X[2]	X[2]
D3		X		X		X[2]		X[2,3]
D3		X	X					X[1]
D2	X		X		X[1,2,3]	X[2]	X[2]	X[2]
D2	X			X	X[1]	X[2]	X[2]	X[1,2]
D2		X	X				X[2]	
D2		X		X	X[1]		X[2]	X[1]

NOTES:

1. With contour plate
2. Without contour plate
3. With Sidewall No. 1

5.2 Instrumentation

The test model was instrumented to provide extensive pressure and temperature data so that the turbine and fan performace could be monitored during testing and nozzle performance could be analyzed. This section describes the model instrumentation which includes the bellmouth inlet, turbine and turbofan simulator, Hub, duct walls, nozzle walls and nozzle flaps.

5.2.1 Inlet Instrumentation

The bellmouth inlet was instrumented with four static pressure taps located at 0^{o}, 90^{o}, 180^{o}, 270^{o} and 22.86 cm, aft of the bellmouth lip as shown in Figure 8. These four static pressures are averaged to provide the bellmouth average static pressure, PBAV. Located at the same circumferential position as the static pressure taps and on the backside of the bellmouth lip are four thermocouples which are used to measure freestream temperature.

5.2.2 Fan Instrumentation

The fan tip turbine instrumentation consists of static pressure, total pressure and total temperature measurements which are located at eight circumferential positions in the turbine discharge plenum. These instrumentation locations are shown in Figure 9. The turbine drive air weight flow was measured using a venturi flow meter.

The fan exit is instrumented in the stator wall section with eight (8) static pressure wall taps as shown in Figure 9. An instrumentation rake is also positioned downstream of the fan and is shown in Figure 10. In this rake section there are located eight (8) additional static pressure wall taps. The instrumentation rake has (8) arms and on each arm there are five (5) total pressure and two (2) total temperature measurements.

The fan speed in revolutions per minute is also monitored so that corrected fan speed can be calculated. The design speed of the fan is 18144 rpm (100 percent corrected speed).

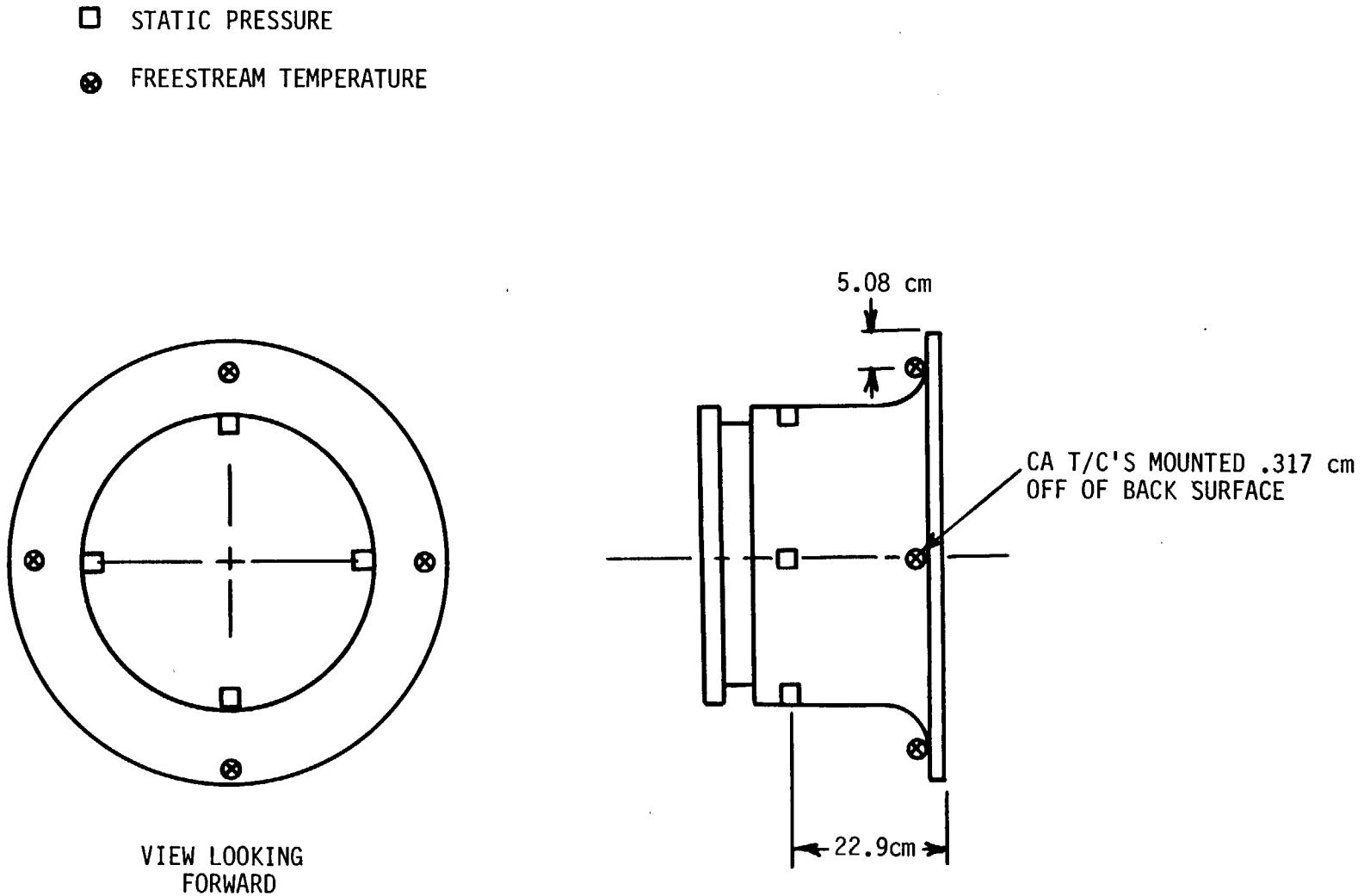

FIGURE 8 BELLMOUTH INLET INSTRUMENTATION

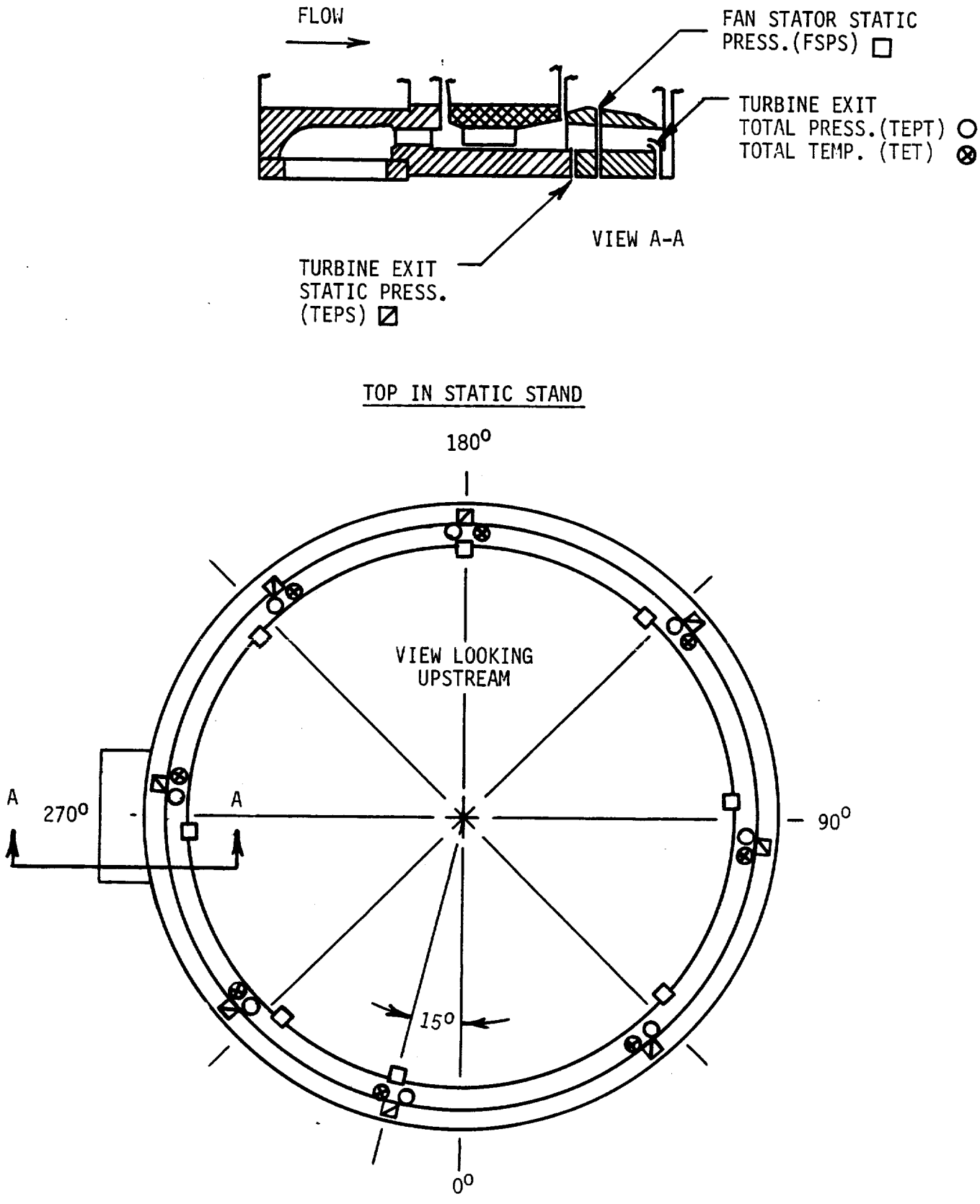

Figure 9 Turbine Instrumentation-and-Fan Stator Wall Static Pressure Taps

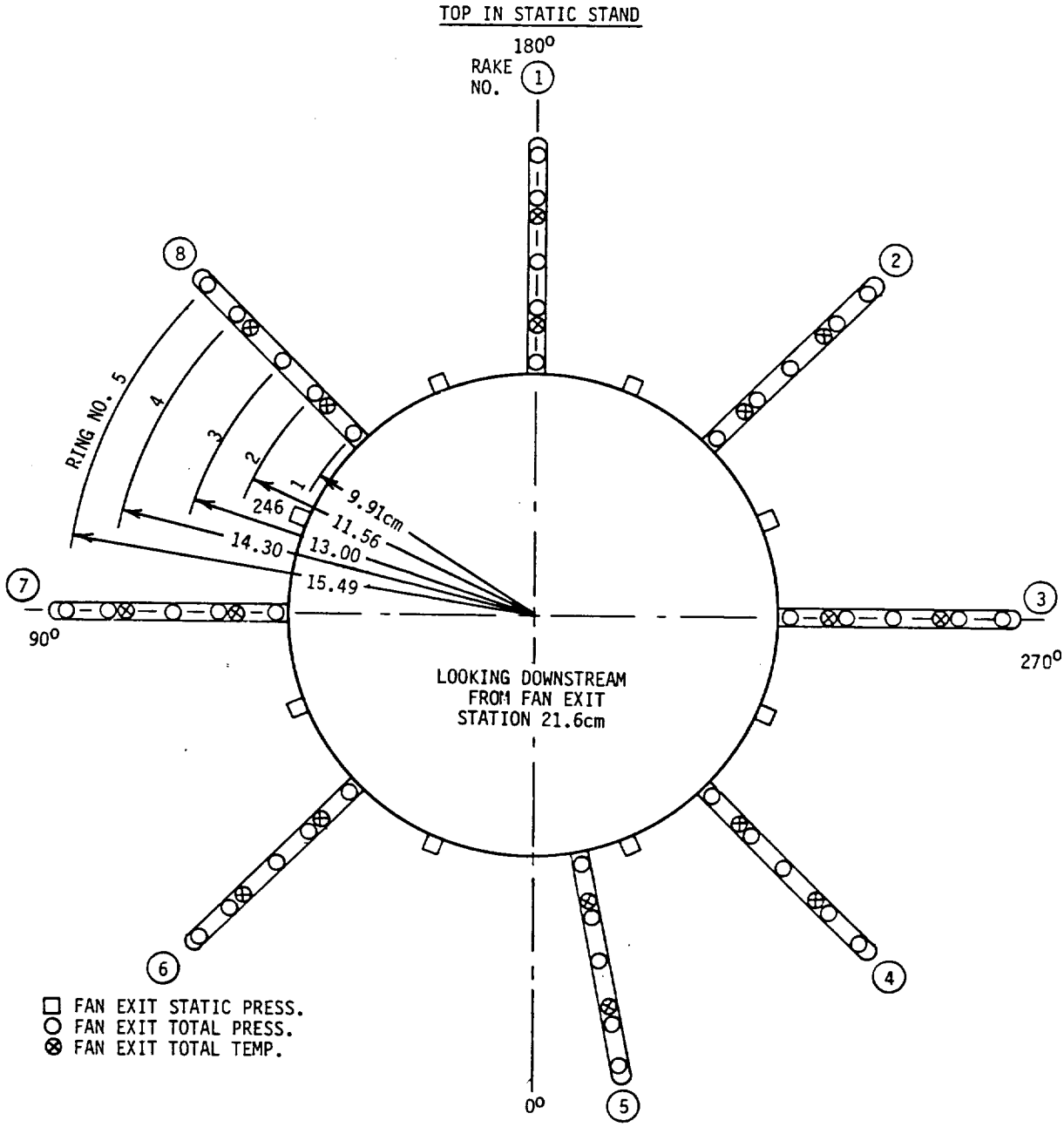

Figure 10 Fan Exit Rake Assembly - Located at Station 21.6 cm (8.5 in)

5.2.3 Duct-Nozzle Instrumentation

The duct and nozzle static pressure instrumentation is shown in Figure 11. The duct was instrumented with eighteen (18) static pressure taps. Seven (7) are located on the top centerline, five (5) in the sidewall and six (6) on the bottom centerline. The fan exit Hub fairing which extends downstream into the duct was instrumented with two (2) centerline static pressure taps on both the top and bottom surfaces. The nozzle body had ten (10) static pressure taps. Four (4) were located on the top wall centerline and six (6) were located on the sidewall centerline. The nozzle flaps contained a total of six (6) static pressure wall taps. Four (4) taps were on the duct forward deflection flap and two (2) were on the aft cruise flap.

A series of tests were also performed where a spacer length of 79.45 cm was placed between the fan and duct housing. As shown in Figure 12 the 79.45 cm spacer was instrumented with twelve (12) static pressure taps. Additionally, an instrumentation rake was installed at the spacer-duct interface (nozzle entrance station) and is shown in Figure 13. The rake wall contained twelve (12) static pressure taps. The rake assembly has six (6) arms. Five (5) of these arms contained one (1) static pressure tap and five (5) total pressure measurements. One (1) arm contained one (1) static pressure tap and six (6) total temperature measurements.

5.3 Test Facility

The test program was conducted in the NASA Lewis Research Center Vertical Thrust Stand static test facility. A schematic of the model installed on the test stand is shown in Figure 14. As shown in the figure the model was sting mounted on the end of the thrust stand with the deflected nozzle directed vertically. The thrust stand was equipped with a Task Corporation Mark VIIA, 10.2 cm diameter strain gage balance. The nozzle forces and moments were determined from the six component strain gage readings measured on the thrust stand. These data were used to calculate the thrust vector, exit flow angle and pitching moment arm.

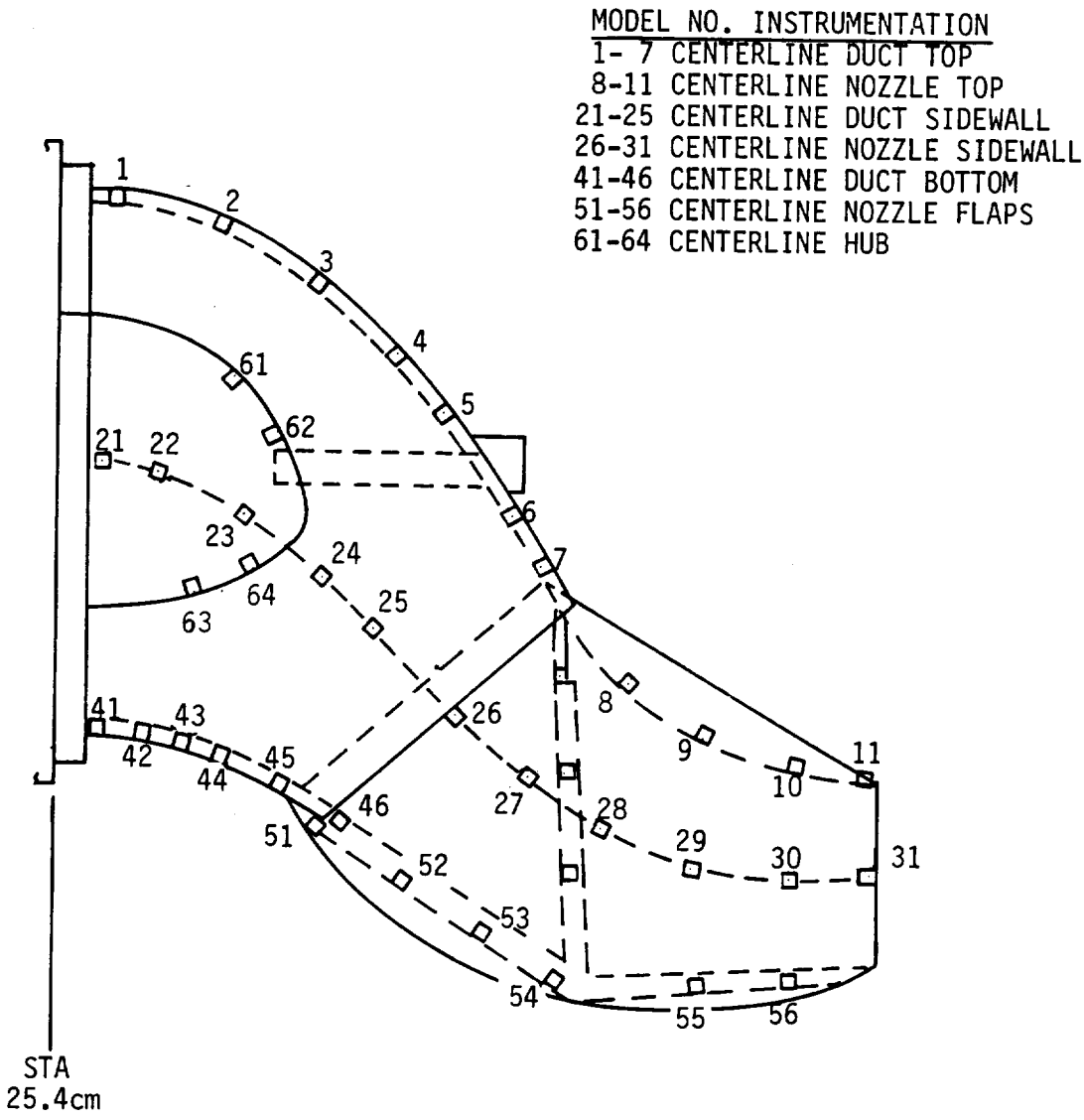

Figure 11 Duct-Nozzle Static Pressure Wall Taps

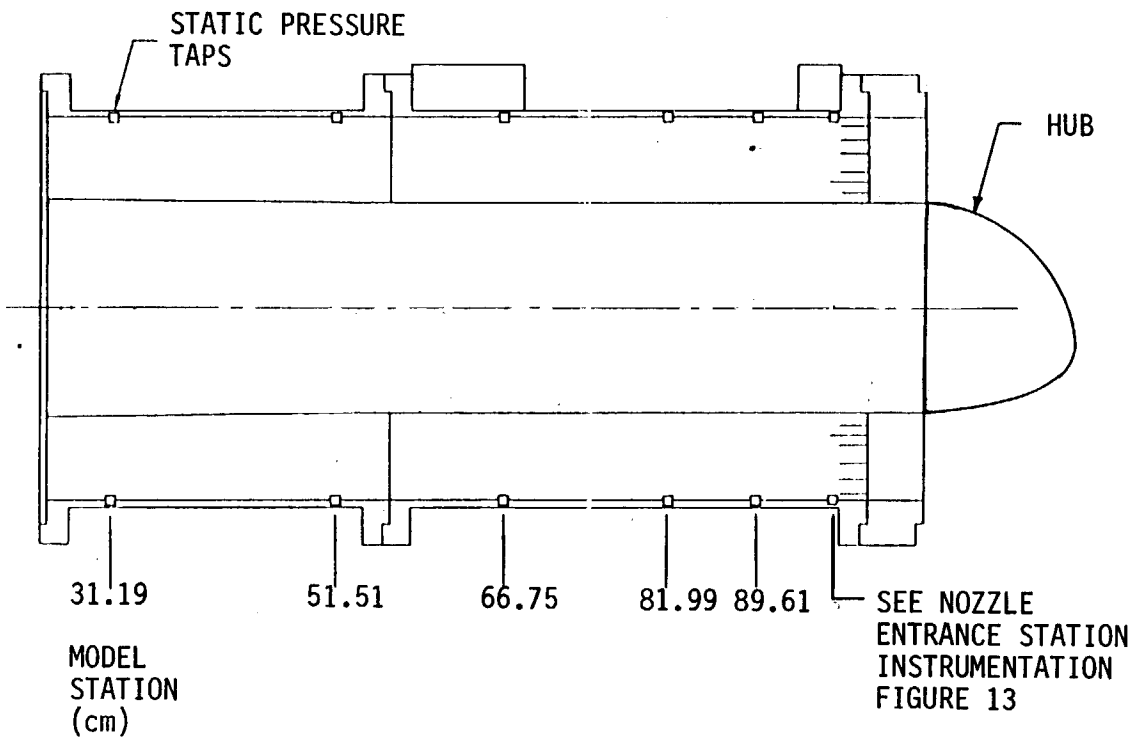

NOTE: 2 TAPS IN VERTICAL PLANE AT EACH STATION

FIGURE 12 79.45cm SPACER WALL
STATIC PRESSURE INSTRUMENTATION

TOP IN STATIC STAND

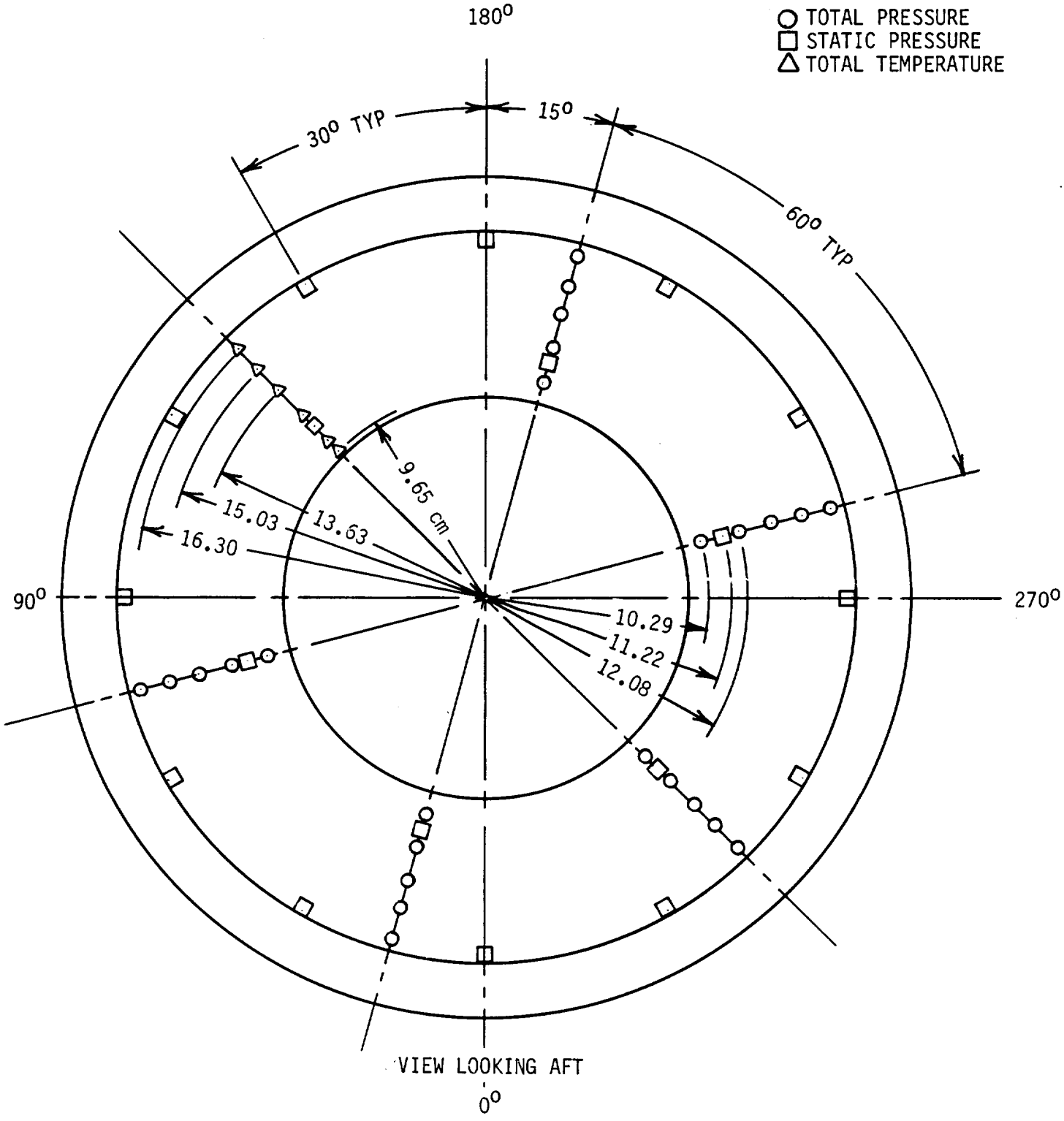

Figure 13 79.45 Cm Spacer Exit Instrumentation for Static and Total Pressures and Total Temperatures

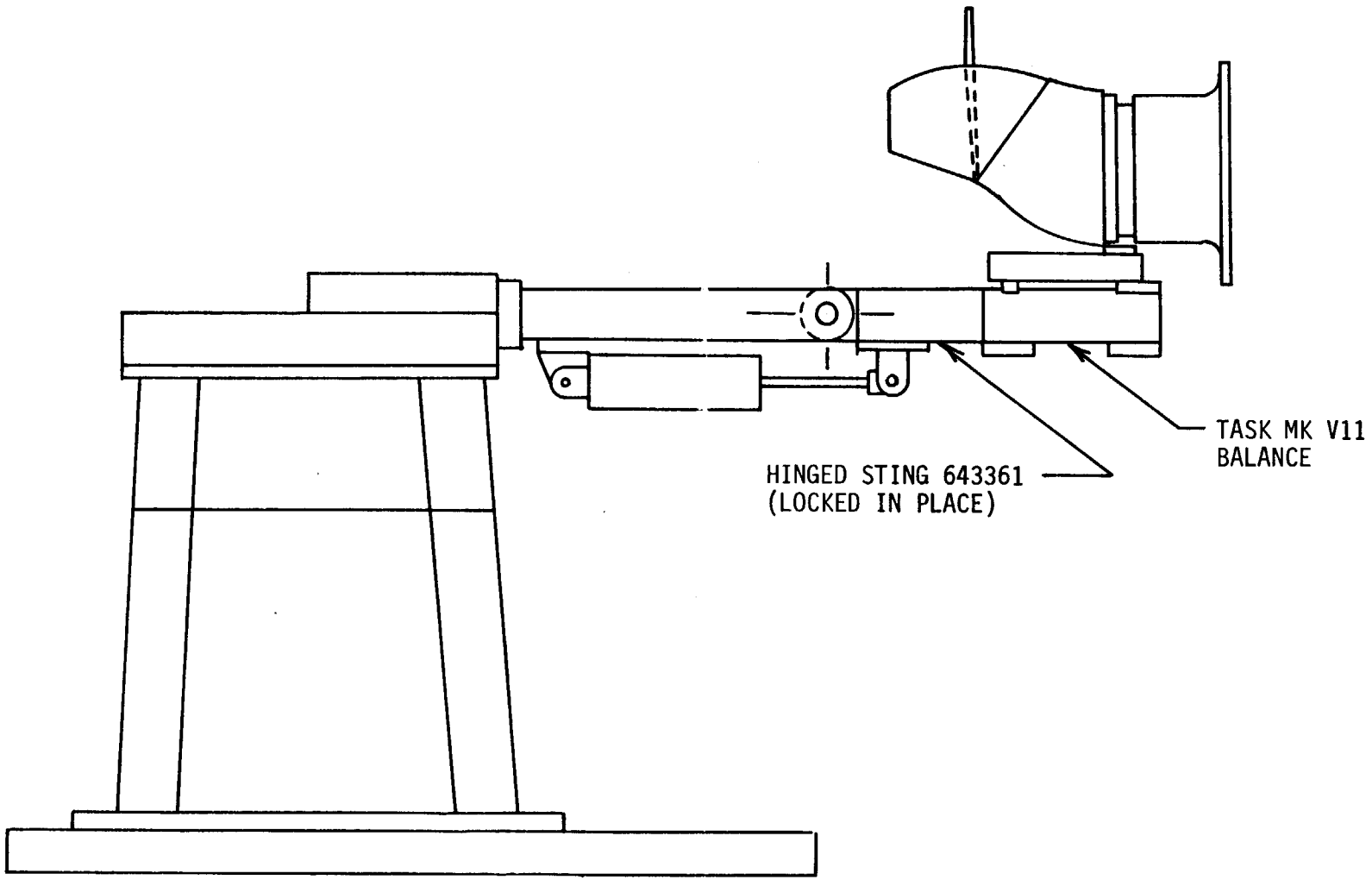

FIGURE 14 TANDEM FAN MODEL TEST FIXTURE INSTALLATION

5.4 Test Procedures

Each nozzle test run was preceded by a model configuration test setup. The test setup consisted of making the model changes as summarized in Table I and as follows:

(a) Select the fan-duct and Hub spacer which modifies the fan-nozzle coupling distance.
(b) Select the cruise or deflected nozzle position.
(c) Select the nozzle area by positioning the aft nozzle flap in the cruise mode or selecting the bottom duct lip configuration for the deflected mode.
(d) Select fan Hub 1 or 2
(e) Select shaft simulation configuration
(f) Add sidewall extensions or contour plate as required.

A specific model configuration test run was preceded by a warm-up period. The fan corrected speed was set in approximately five (5) unit increments from 50 to 100 percent and at least one data point taken at each condition for each of the configurations listed in Table I.

5.5 Data Reduction

Data were recorded by the Lewis Research Centers' automatic data systems and calculations made by a time-sharing digital computer system.

The data from the tests were recorded and/or reduced by the computer to include at least the following parameters:

Bellmouth

- Average bellmouth static pressure, PBAV
- Corrected bellmouth airflow, WBMC

Fan

- Fan corrected speed, PCDSPD
- Fan exit corrected airflow, WFANEC
- Fan exit Mach number, FANEMN
- Fan horsepower, FANHP
- Average fan exit total pressure ratio, FPRAV
- Average fan exit hub static pressure ratio, PRS2AV
- Average fan stator wall static pressure ratio, FSPAV
- Average fan exit total temperature ratio, FTRAV
- Fan exit rake total pressure ratios on each rake (I) and at each rake radius (J), FPR(I, J)
- Fan-exit ring total pressure ratio average, FPR(J)AV
- Fan stream ideal velocity, VIF
- Fan stream ideal airflow, WIF

Nozzle

- Thrust vector, T
- Flow deflection angle, PHID
- Pitching moment distance, D
- Thrust coefficient, CFN

- Thrust discharge coefficient, CD
- Nozzle pressure ratio, ENPR
- Specific corrected nozzle flow, WSN
- Surface static pressure ratio to freestream total, P/PTO
- Nozzle Mach number, MN

Duct and Hub

- Surface static pressure ratio to freestream total, P/PTO
- Mach number, M_0

Turbine

- Turbine flow ideal velocity, VIT
- Drive air parameters
- Turbine inlet total pressure, FDAP
- Turbine exit total pressure ratio, TTPR(I) and average, TTPRAV
- Turbine inlet total temperature, FDAT
- Turbine exit static pressure ratio, TSPRAV
- Turbine corrected airflow, WTC
- Turbine exit corrected airflow, WTEC
- Turbine temperature drop, TURBTD

- Turbine exit static/total pressure ratio, TEPSPT
- Turbine exit Mach number, TRBEMN
- Turbine output horsepower, TPH

79.45 cm Spacer

- Spacer wall static pressure, PSR
- Spacer exit static pressure, PS(I,J)
- Spacer exit total pressure ratios, PT16
- Spacer exit total temperature, TT16

6.0 Test Results

As shown in Table I, the test model was configured with fifteen (15) possible variables, but only six (6) occur in a given test. The model was configured with the nozzle in the cruise or deflected mode, and each nozzle operating mode could be adjusted for two (2) area positions as follows:

DEFLECTED	CRUISE
-	390.32 cm^2
-	465.80 cm^2
635.62 cm^2	-
772.98 cm^2	-

The close-coupled configuration had high fan exit pressure distortion. Therefore, a fan-duct spacer of 79.45 cm was added in order to move the nozzle farther aft of the fan exit and allow testing with reduced distortion. In addition, turbine air was dumped into the fan stream reducing the distortion in the total pressure profile at the nozzle entrance station.

It is desired in aircraft design to reduce the weight and drag penalty to a minimum. Therefore, a tandem fan-nozzle assembly with a short coupling distance and having a large value of nozzle exit venting would more nearly fulfill these requirements. Based on these facts a baseline design was selected, and all other deflected nozzle configurations are compared to this standard and are designated as modified baseline. The model design changes which result in the modification of the baseline is also included in the paragraph titles. The deflected nozzle-baseline design parameters utilized in the following data comparisons are as follows:

a) Nozzle in the full deflected mode.
b) Nozzle area equal to 772.98 cm^2
c) Turbine shaft simulator installed.
d) Fan exit Hub design 1.
e) No fan-duct spacer installed, $\Delta X = 0$.
f) No installed contour plate.
g) No installed sidewall plates.
h) No tape on nozzle flap hinge.

Comparable deflected configurations are those with fan-duct spacer distances of 3.81, 12.7 and 79.45 centimeters. The first two spacer configurations contained a turbine flow collector which dumped the turbine flow external of the model. The 79.45 cm spacer section had no collector, and the turbine air was dumped into the fan stream. These model configuration tests are identified as follows:

Nozzle Area, cm^2	Spacer Distance, cm	0	3.81	12.7	79.45
772.98	Computer Run	61	43	36	4

The cruise mode tests also had a configuration selected to be baseline design. The other cruise mode configurations are compared to the baseline design and are also designated as modified baseline. Similar to the deflected nozzle configuration, all of the modified cruise configurations are compared to the baseline cruise configuration. The cruise mode baseline consists of the following:

a) Nozzle in the full cruise mode
b) Nozzle area equal to 465.80 cm^2
c) Turbine shaft simulator installed
d) Fan exit Hub design 2
e) No Fan-duct spacer, $\Delta X = 0$

The baseline test run for the cruise nozzle is identified as Run Number 55. Comparable cruise configurations are those with fan-duct spacer distances of 3.81 and 12.7 centimeters. The long spacer, 79.45 cm - Computer Run Number 71, is also shown so that the effect of nozzle entrance distortion on the performance characteristics can be determined.

Nozzle Area, cm^2	Spacer Distance, cm	0	3.81	12.7	79.45
465.80	Computer Run	55	52	29	71

6.1 Baseline Comparison - Deflected Nozzle

The variation of nozzle thrust coefficient, thrust vector angle and normalized specific corrected nozzle flow as a function of nozzle pressure ratio and variation of fan-duct spacer, (0, 3.81, 12.7 and 79.45 cm) is shown in Table II.

TABLE II Thrust Vector Angle, Nozzle Thrust Coefficient and Normalized Specific Corrected Nozzle Flow Versus Nozzle Pressure Ratio - Baseline Deflected Nozzle - Nozzle Exit Area = 772.98 cm^2 - Hub 1 - No Contour Plate - Shaft In - ΔX = 0 cm, and Modified Baseline - ΔX = 3.81, 12.7 and 79.45 cm

ΔX ~ CM / ENPR OR PR16AD	0			3.81			12.7			79.45			79.45		
	PHID	CFN	WSN	PHID	CFN	WSN	PHID	CFN	WSN	PHID	CFNAD	W7SPCA	PHID	CFNAD	W7SPCA
1.10	93.2	.950	.141	92.7	.906	.146	91.8	.907	.146	-	-	-	-	-	-
1.15	93.3	.951	.164	92.7	.903	.171	92.2	.914	.168	90.5	.941	.173	90.4	.936	.173
1.20	93.7	.957	.182	92.7	.915	.188	92.5	.926	.189	90.5	.946	.194	90.2	.942	.194
1.25	94.0	.962	.195	92.8	.925	.201	92.4	.934	.201	90.5	.947	.212	90.5	.938	.211
1.30	95.1	.967	.206	94.0	.921	.212	93.0	.933	.211	90.5	.944	.225	90.6	.939	.225
1.35	96.0	.973	.209	95.7	.931	.219	94.6	.930	.217	90.6	.929	.237	90.5	.932	.236
% Δ	+3.0	+2.4	+48.2	+3.2	+2.8	+50	+3.1	+2.5	+48.6	+.11	-1.28	+37	+.11	-.42	+36.8
TEST RUN NO.	(3) 61			43			36			(2)(3) 74			(1)(2) 4		

(1) Run 4 had tape on the nozzle flap hinge to reduce leakage

(2) Turbine air dumped into duct with fan stream

(3) Highest Value of ENPR is 1.347

6.1.1 Thrust Vector Angle, PHID

These data show that as the coupling distance, (ΔX) is increased from 0 (baseline) to 79.45 cm the thrust vector of the nozzle (PHID) becomes more aligned with the vertical (90^0) centerline of the nozzle. The angle at a nozzle pressure ratio (ENPR) of 1.35 varies from 96^0 at $\Delta X = 0$ to 90.6^0 at $\Delta X = 79.45$ cm. The angle generally becomes increasingly larger as ENPR increases; for example, at $\Delta X = 0$ the angle changes from 93.2 to 96.0 degrees over the ENPR of 1.1 to 1.35 for an overall percent change of +3.0 percent. The percent change in thrust vector angle for the largest coupling, $\Delta X =$ 79.45 cm, configuration was +.11 percent with the angle being in the 90.2 to 90.6 degree range. A plot of PHID for the baseline configuration, $\Delta X = 0$, data is provided against ENPR in Figure 15 and against WSN in Figure 16.

6.1.2. Thrust Coefficient, CFN

The highest thrust coefficient (CFN) value, 0.973, was obtained with the baseline configuration, ($\Delta X = 0$) at a ENPR of 1.35. The general trend for $\Delta X = 0$, 3.81 and 12.7 cm is an increasing CFN, approximately +2.6 percent, for an increase in ENPR from 1.1 to 1.35. However, for a spacer $\Delta X = 79.45$ cm the CFN varied from 0.929 to 0.947 over the ENPR range of 1.1 to 1.35 which represents a 2.2 percent variation. A plot of the baseline configuration, ($\Delta X = 0$), data is provided in Figures 15 and 16.

6.1.3 Model Static Pressures

As shown in Figure 17 the static pressure ratio calculated from data measured at a given location increases with an increase in corrected fan speed. This trend is normal because the nozzle velocity is subsonic. Therefore, as the fan flow increases with fan speed and the nozzle area remains fixed, the flow channel static pressure will increase. It can be seen in Figure 17 that the general shape of each plotted static pressure path retains the pressure ratio trend from the lowest corrected fan speed to the highest. These data also show a number of additional trends.

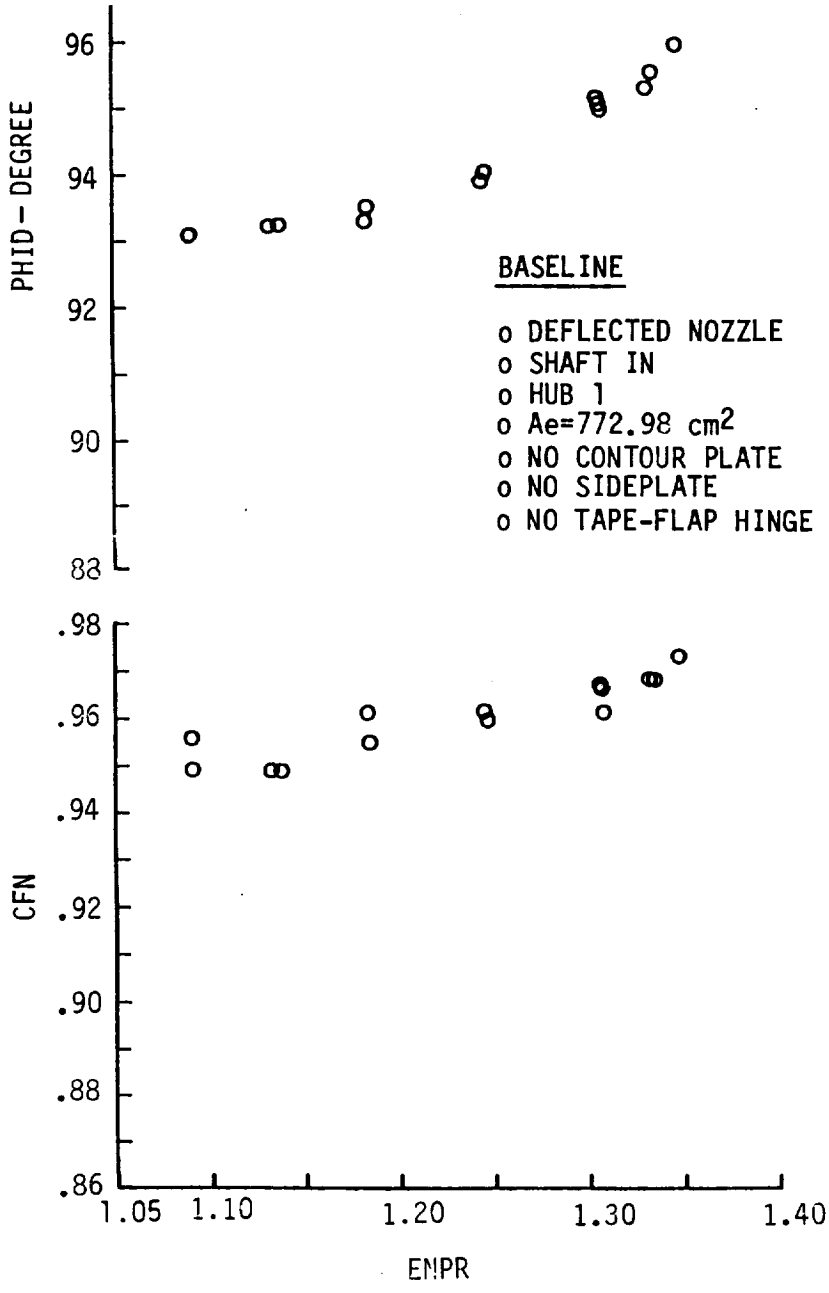

Figure 15 Thrust Coefficient and Thrust Vector Angle Versus Nozzle Pressure Ratio - Baseline Configuration - ΔX = 0 cm

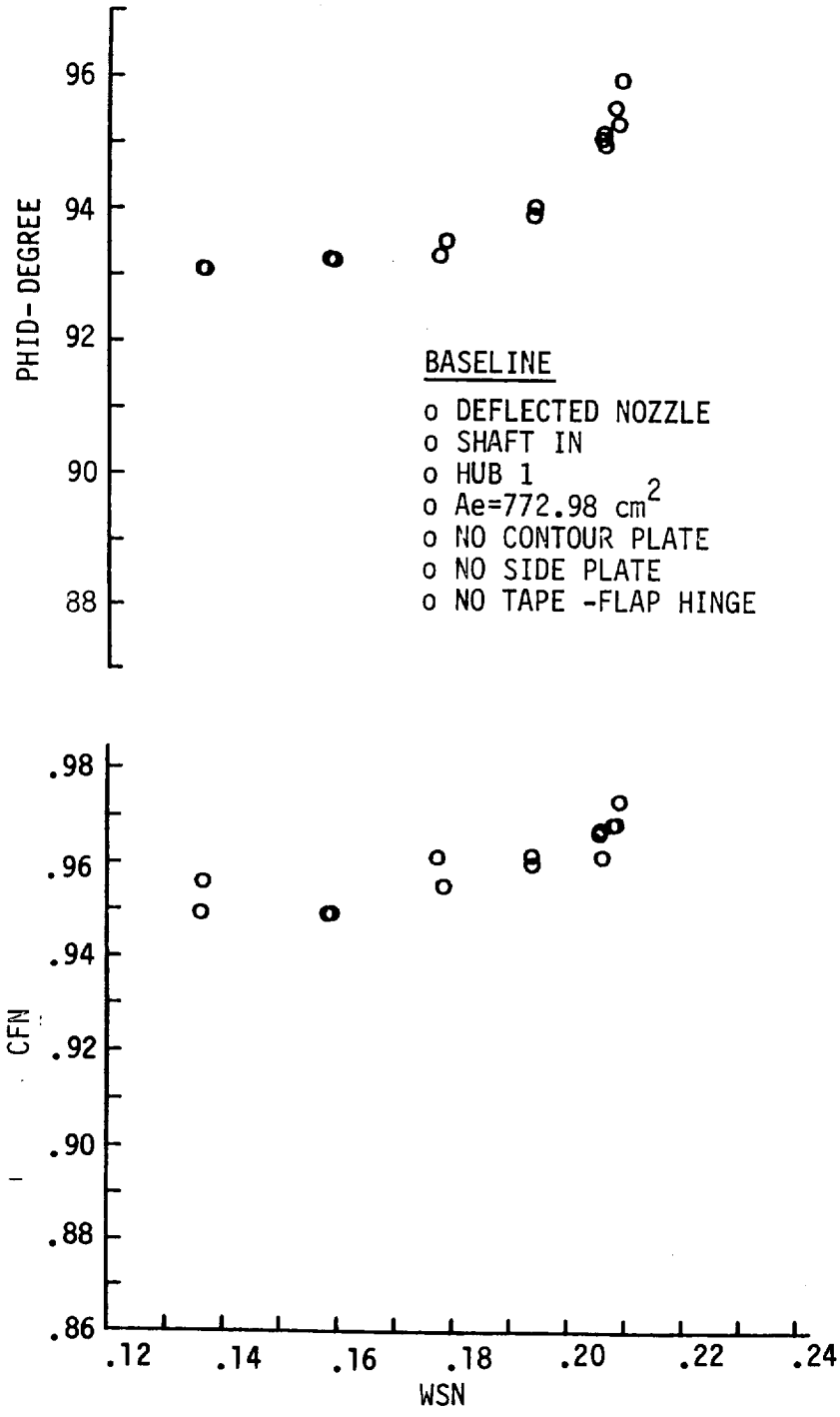

FIGURE 16 Thrust Coefficient and Thrust Vector Angle Versus Specific Corrected Nozzle Flow - Baseline Configuration - ΔX = 0 cm

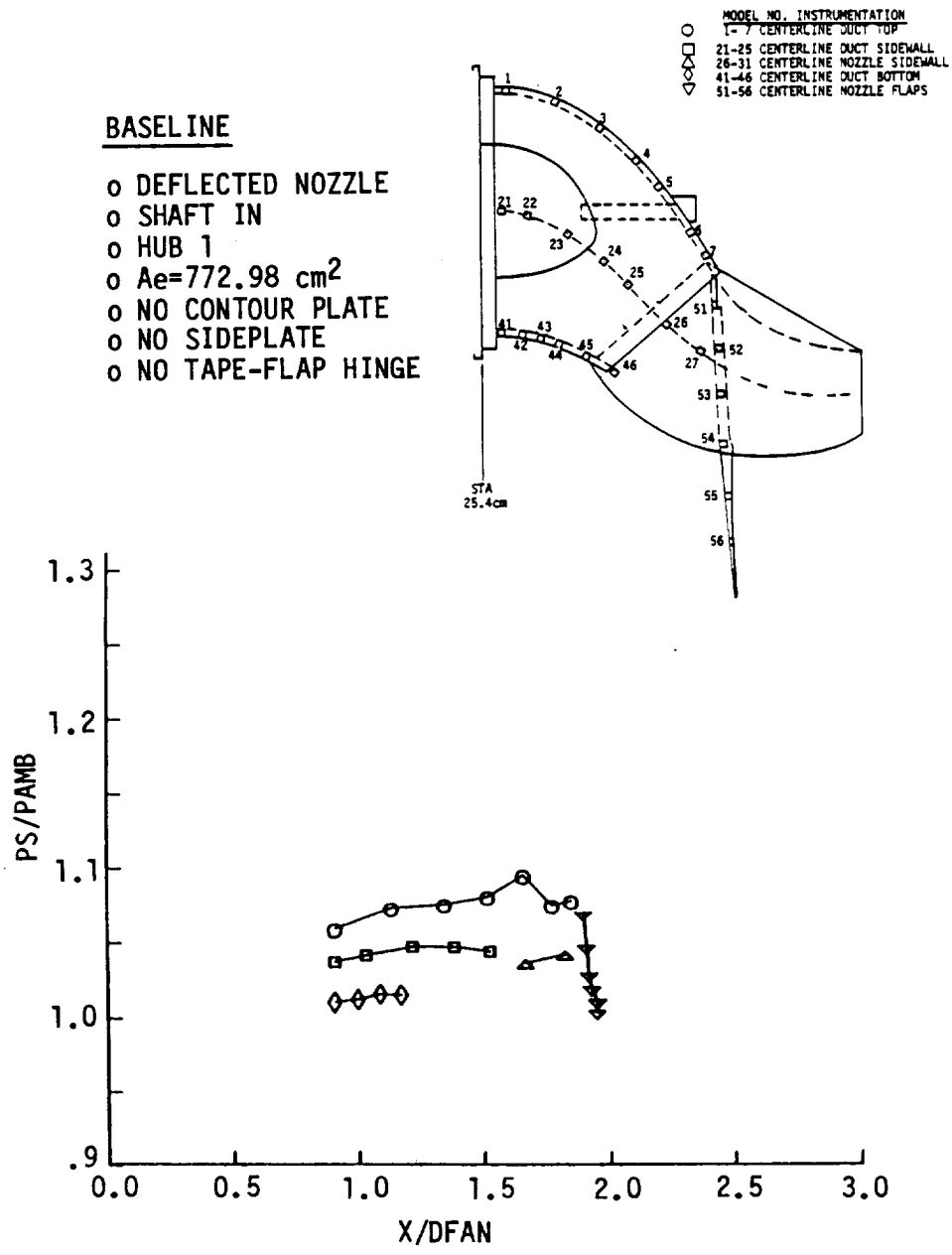

a) PCDSPD = 50%

Figure 17 Duct, Nozzle and Flap Static Pressure Ratio Versus Normalized Static Port Distance, Baseline Configuration, ΔX = 0 cm

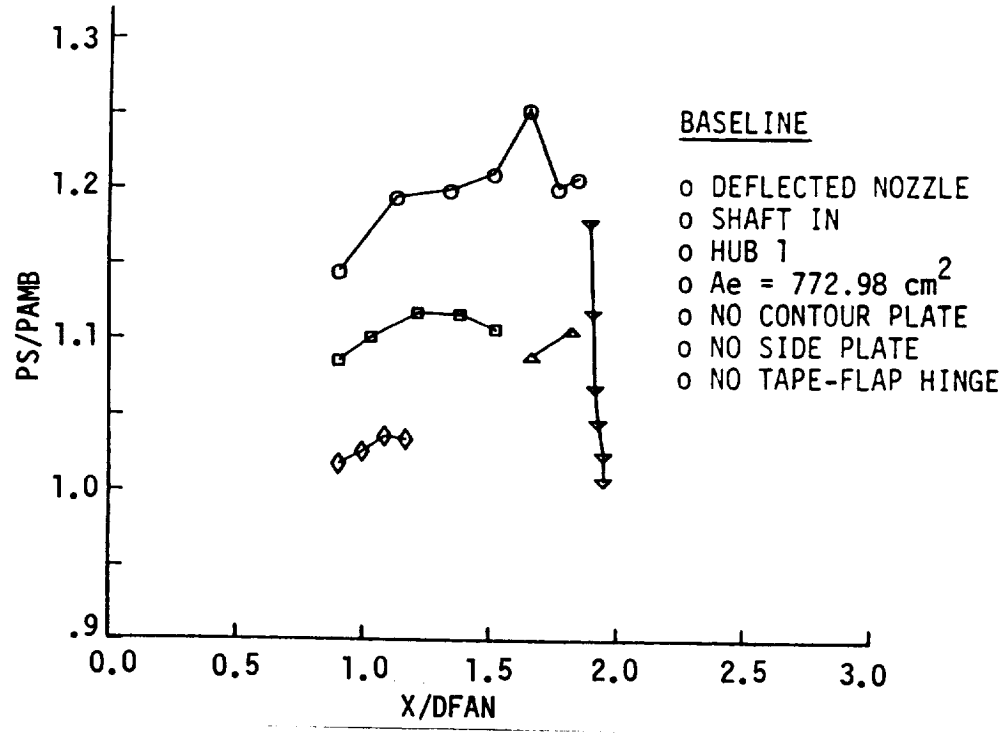

b) PCDSPD = 79.9%

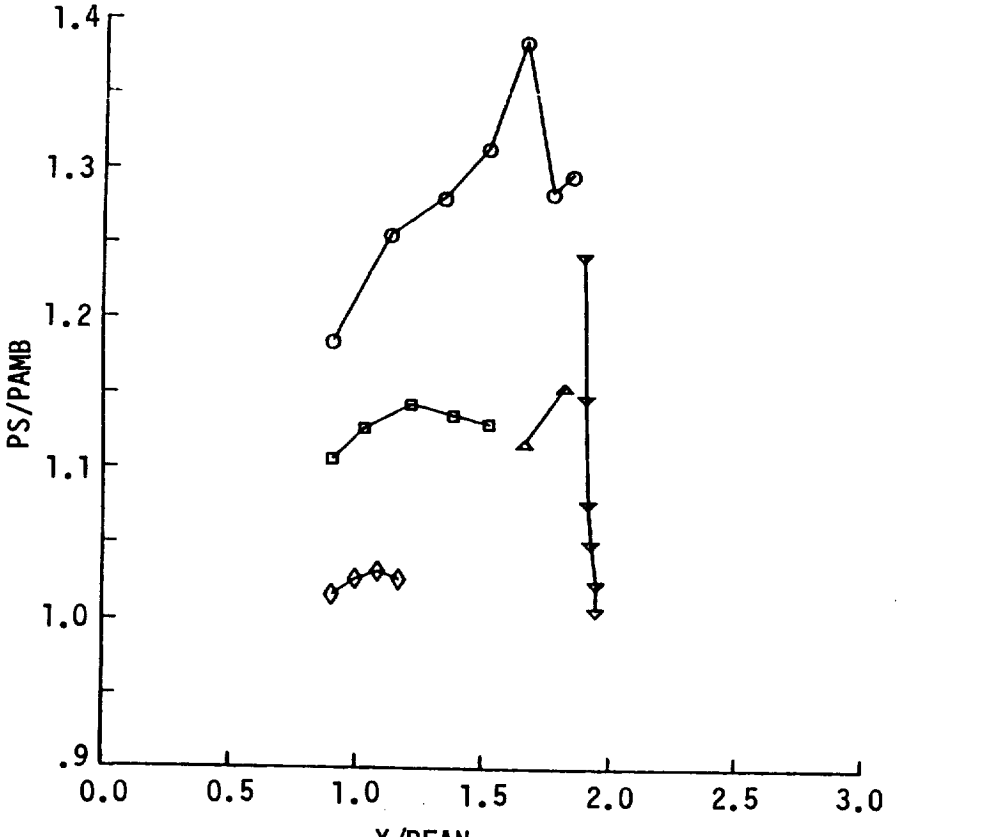

c) PCDSPD = 93%

FIGURE 17 (CONCLUDED)

The data for the duct sidewall and the duct bottom show an increase in static pressure for the first three data points and then decreases. The duct wall and fan Hub form a toroidal cylinder which has an increasing area from station 25.4 cm until the hub exit or the nozzle lip is reached. The velocity of the flow stream is decreasing with an increase in static pressure in this area of diffusion. The static pressure measurements on the top duct wall, show a considerable change in magnitude as the flow passes the first five (5) pressure taps (see Figure insert). The top duct wall and fan Hub form the same kind of cylindrical channel as discussed above. However, in this duct area there is also considerable duct turning which induces centrifugal effects to the flow stream. The centrifugal force is induced on the top duct wall and results in a larger static pressure increase than was seen on the side or bottom walls. Also the static pressure tap associated with the fifth data point of the duct top centerline data is located just above the simulated turbine shaft (see Figure insert). Most likely the exaggerated static pressure peak at this location is due to the flow disturbance induced by the flow stream discontinuity. The sixth and seventh data points are represented by pressure readings below the shaft. These pressure measuring locations result in a slightly decreased static pressure, but is more representative of the upstream flow characteristics at location four.

The nozzle flap static pressure taps lie almost on a vertical X/D fan line when the nozzle flap is in the deflected mode. The flow must make an abrupt change at the transition from the top duct wall to the vertical nozzle flap (See Figure insert). The flap static pressure decreased until ambient conditions are reached. The above conclusions are verified by the static pressure data of runs 33 (no contour plate), 50 (no contour plate) and 58 (with contour plate) which are based on a configuration with the simulated turbine shaft removed and the Hub design 2 installed. These static pressure ratios are plotted as a function of the X/D fan station and are shown in Figure 18. The data correspond to a corrected fan speed of approximately 90 percent and spacer distances of ΔX = 0, 3.81 and 12.7 cm. These data are typical of all deflected nozzle flow tests. Thus, no additional static pressure data are shown for the other deflected nozzle flow tests.

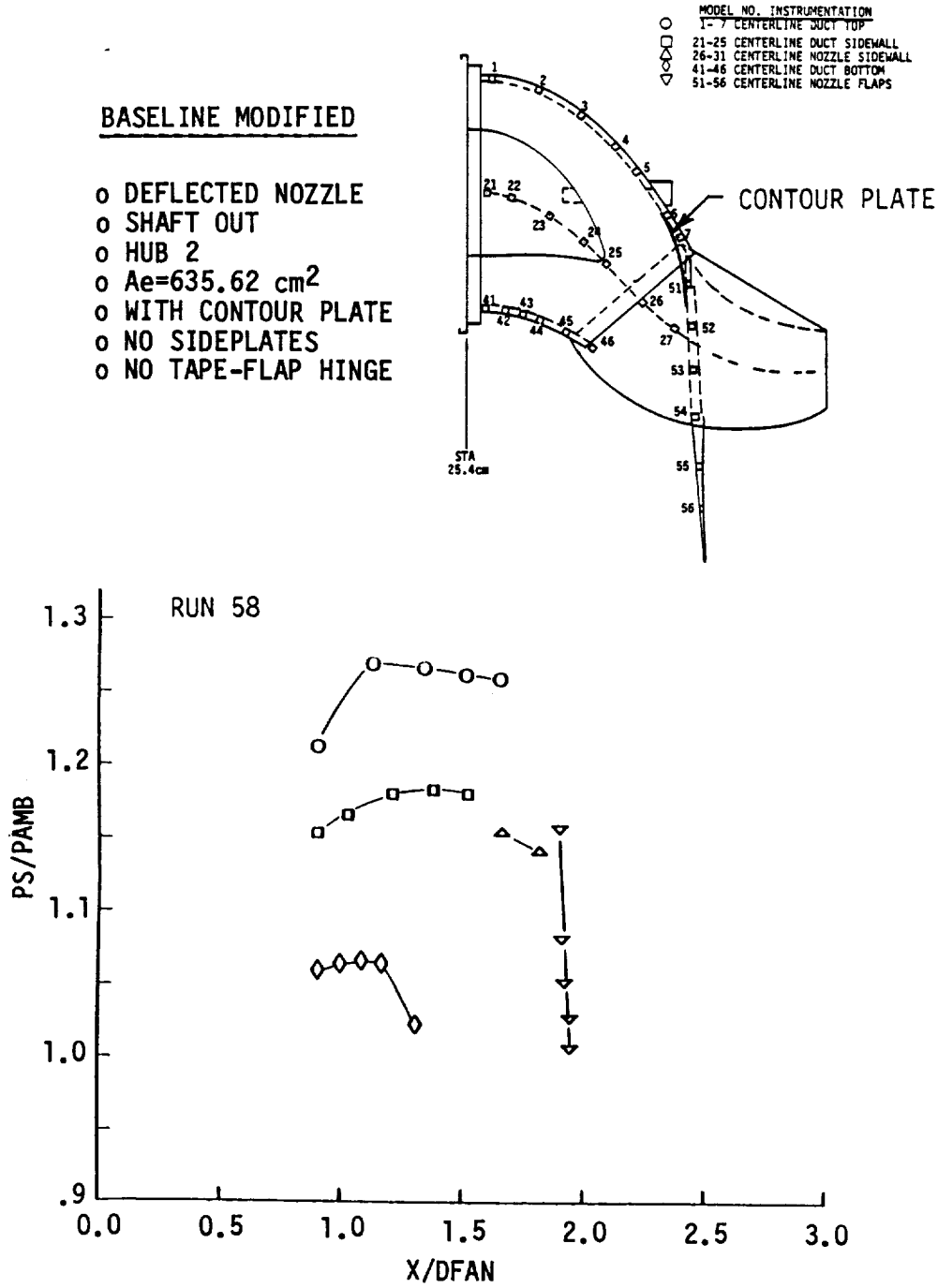

a) SPACER LENGTH = 0 cm

FIGURE 18 Duct, Nozzle and Flap Static Pressure Ratio Versus Normalized Static Port Distance, Modified Baseline - Shaft Out, Hub Design 2, PCDSPD = 90%

BASELINE MODIFIED

- o DEFLECTED NOZZLE
- o SHAFT OUT
- o HUB 2
- o Ae = 772.98 cm^2
- o NO CONTOUR PLATE
- o NO SIDEPLATES
- o NO TAPE-FLAP HINGE

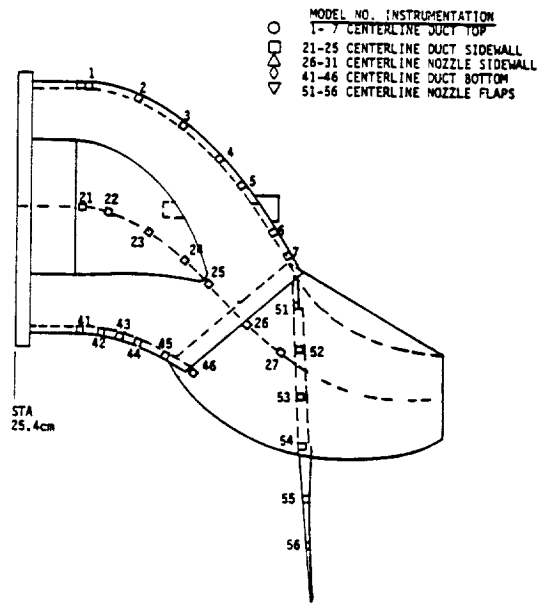

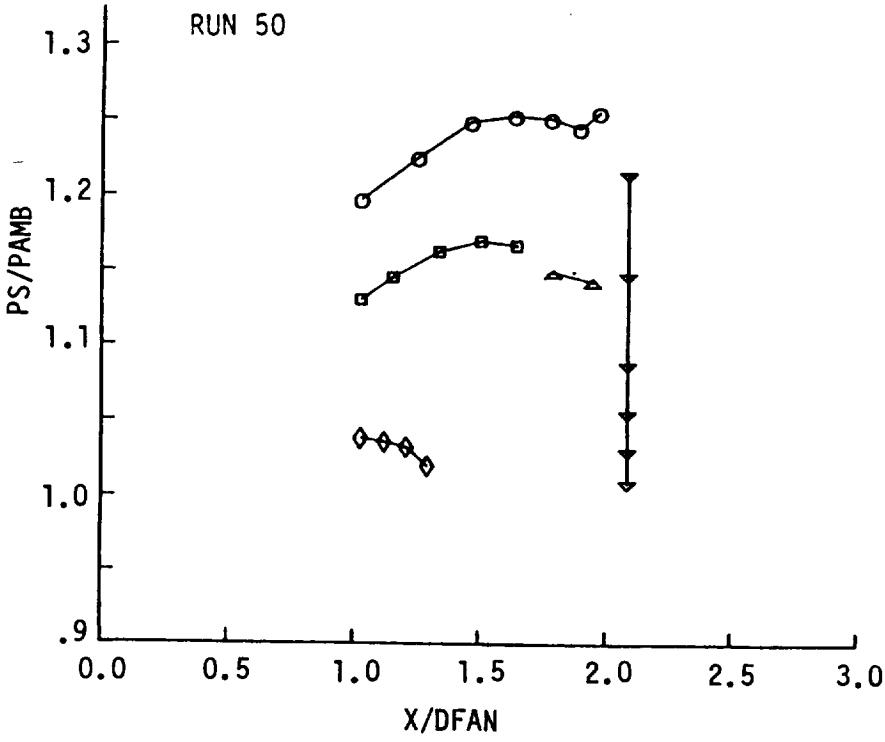

b) SPACER LENGTH = 3.81 cm

FIGURE 18 (CONTINUED)

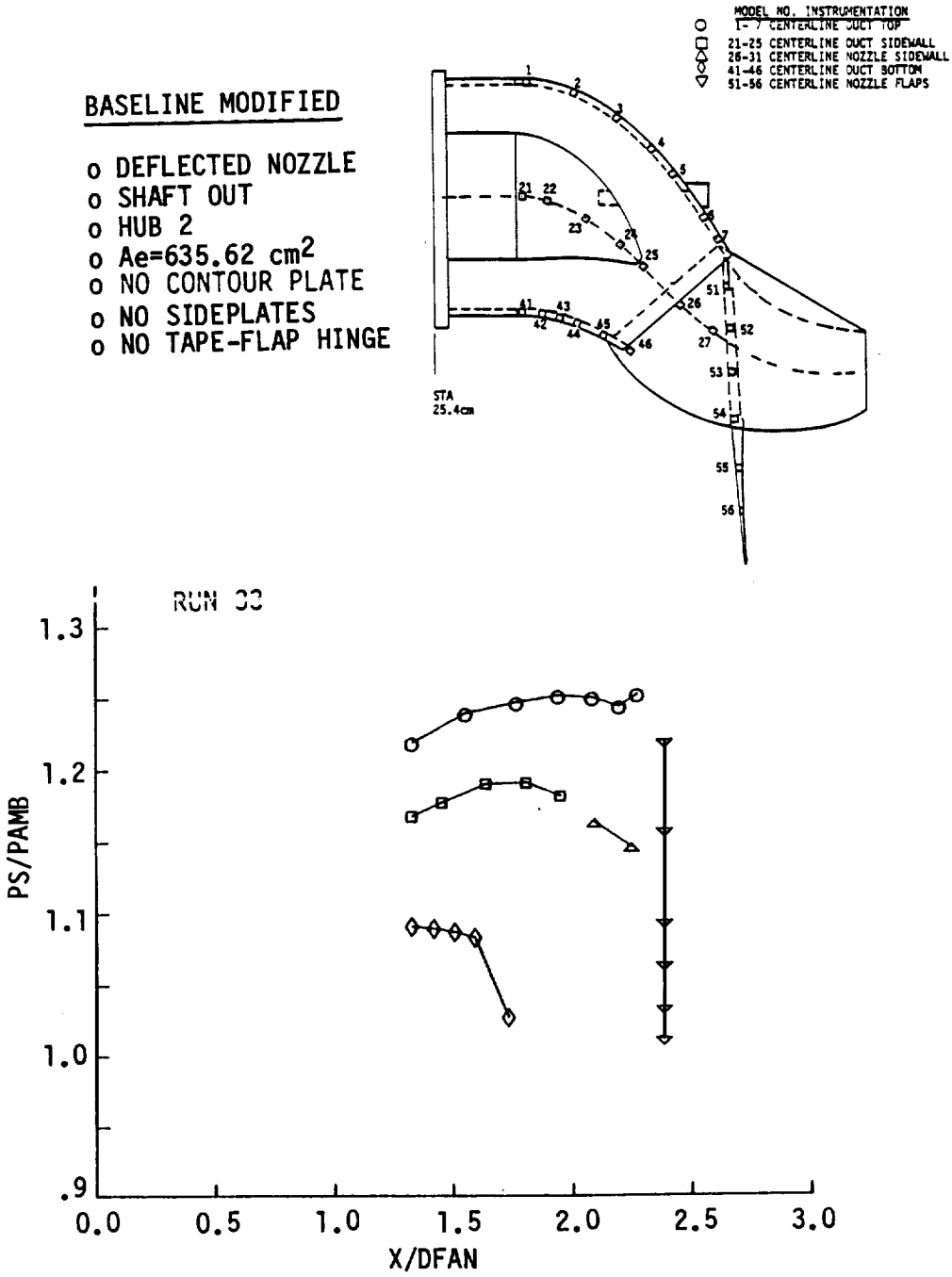

c) SPACER LENGTH = 12.7 cm

FIGURE 18 (CONCLUDED)

6.1.4 Fan Exit Total Pressure Distortion

The total pressure distortion at the fan exit is shown by plots of the rake radius station to flow channel height (R/H) as a function of the total pressure to free stream total pressure ratio (PT/PTO) on a given rake probe in Figure 19. The total pressure distortion can be compared for several circumferential stations from the center Hub to the outside wall and then for each radial station as a function of circumferential position at the fan exit. It was determined that the distortion is independent of the configuration and is basically only a function of the corrected fan speed. The total pressure ratio values tend to group together for all stations monitored except for ring 3, 4 and 5 on rake probe 5 and 6. The total pressure ratios at these latter stations become increasingly distorted as the corrected fan speed increases. The other remaining total pressure ratio monitoring stations remain grouped but as the corrected fan speed increases the grouping shifts to higher total pressure ratios and the distortion between the different probes increases. The total pressure ratio varies between 1.05 and 1.15 at the low corrected fan speed of about 50 percent to 1.05 and 1.56 at the corrected fan speed of about 98 percent. Therefore, the total pressure ratio variation at the low speed is approximately 19 percent and at the higher speeds it is near 36 percent.

There is also some radial total pressure distortion on each of the probes of the rake. The largest variation occurs on probe 5 which is located at approximatey the 350^{0} station which is almost the top centerline of the duct but as the model is mounted inverted in the test fixture, the probe would be on the bottom. The pressure distortion is caused by low loading on the fan blades tip and the turn the flow must make downstream of the fan exit. However, the above problem was resolved by adding the 79.45 cm spacer and dumping the tip turbine airflow into the fan stream. The results of the foregoing is shown in Figure 19(d).

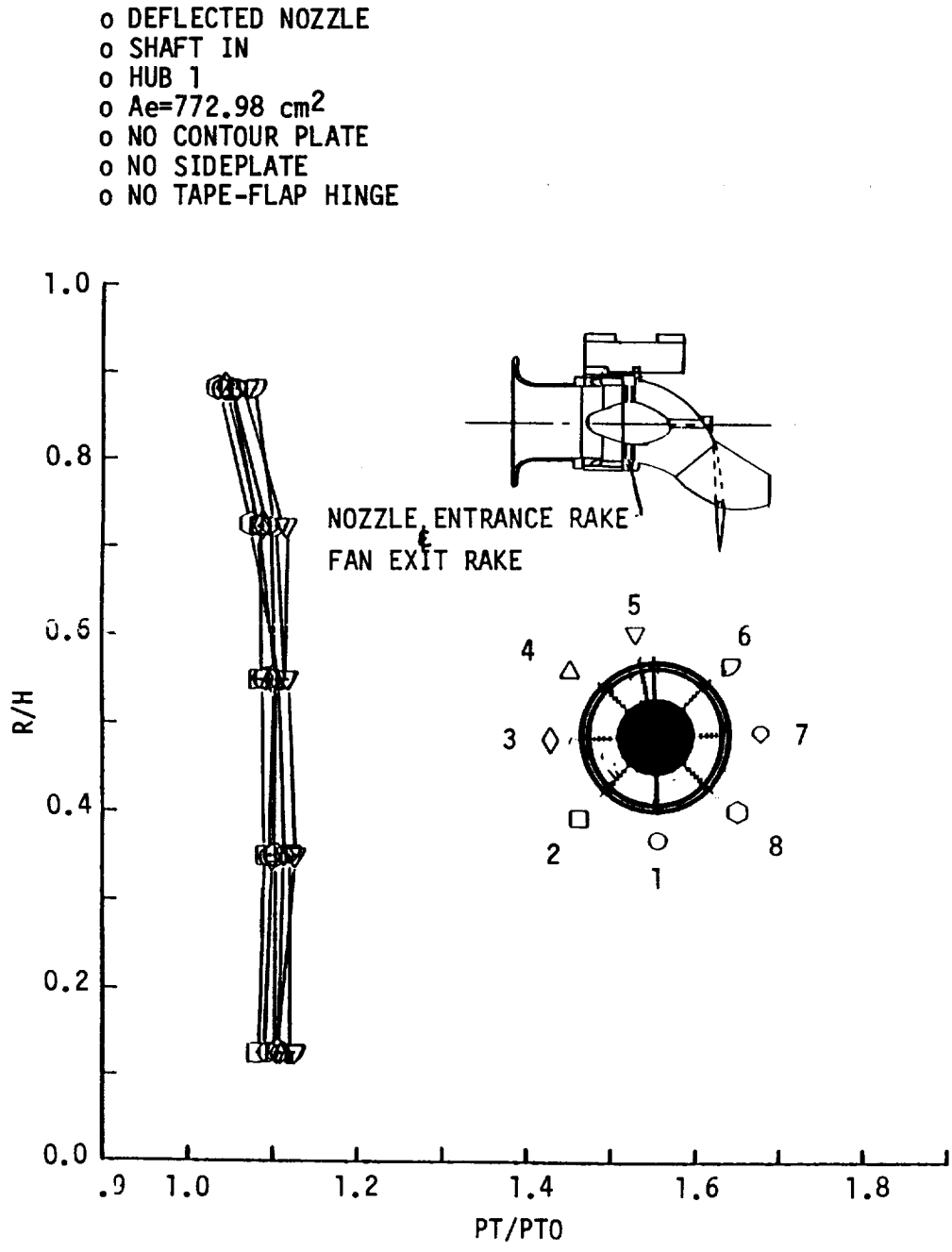

a) PCDSPD = 49.98%, ΔX = 0 cm

FIGURE 19 Rake Radius to Height Ratio Versus Total Pressure Ratio, Baseline Configuration - ΔX = 0 cm and Modified Baseline - ΔX = 79.45 cm

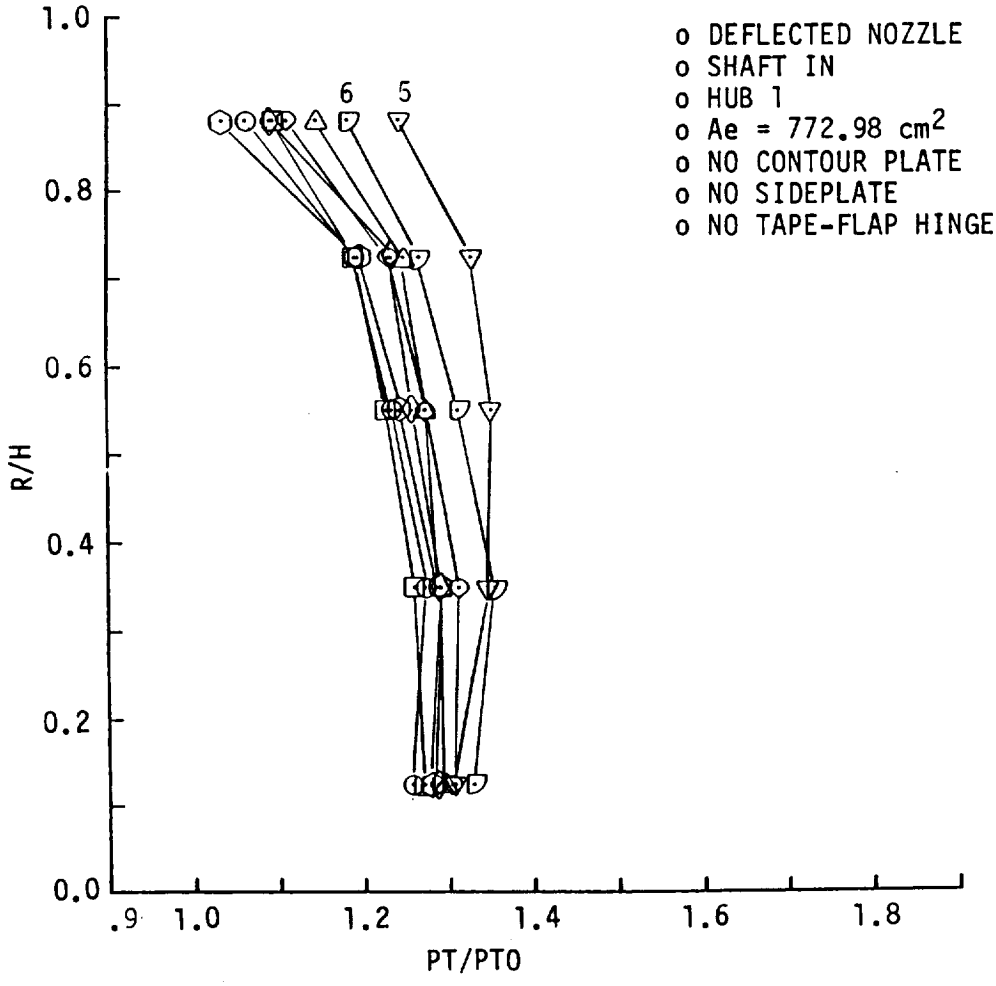

b) PCDSPD = 79.94%, $\triangle X$ = 0 cm

FIGURE 19 (CONTINUED)

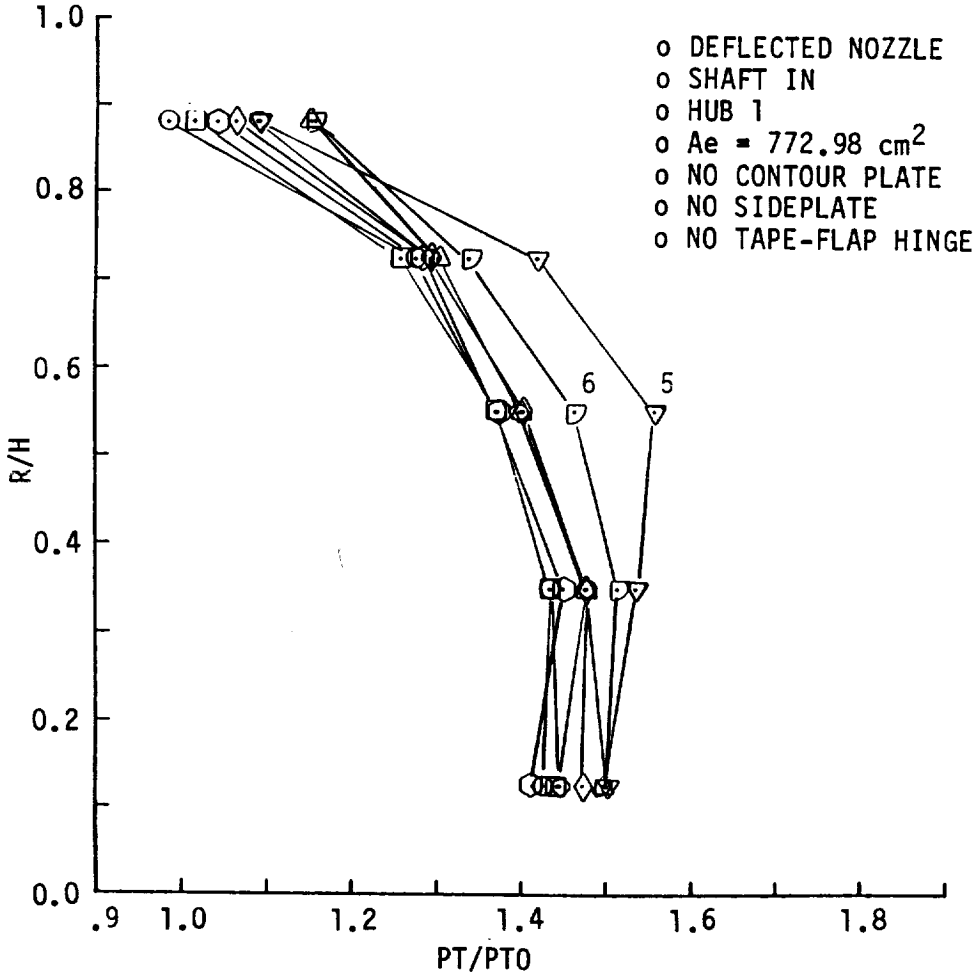

c) PCDSPD = 97.96%, $\triangle X$ = 0 cm

FIGURE 19 (CONTINUED)

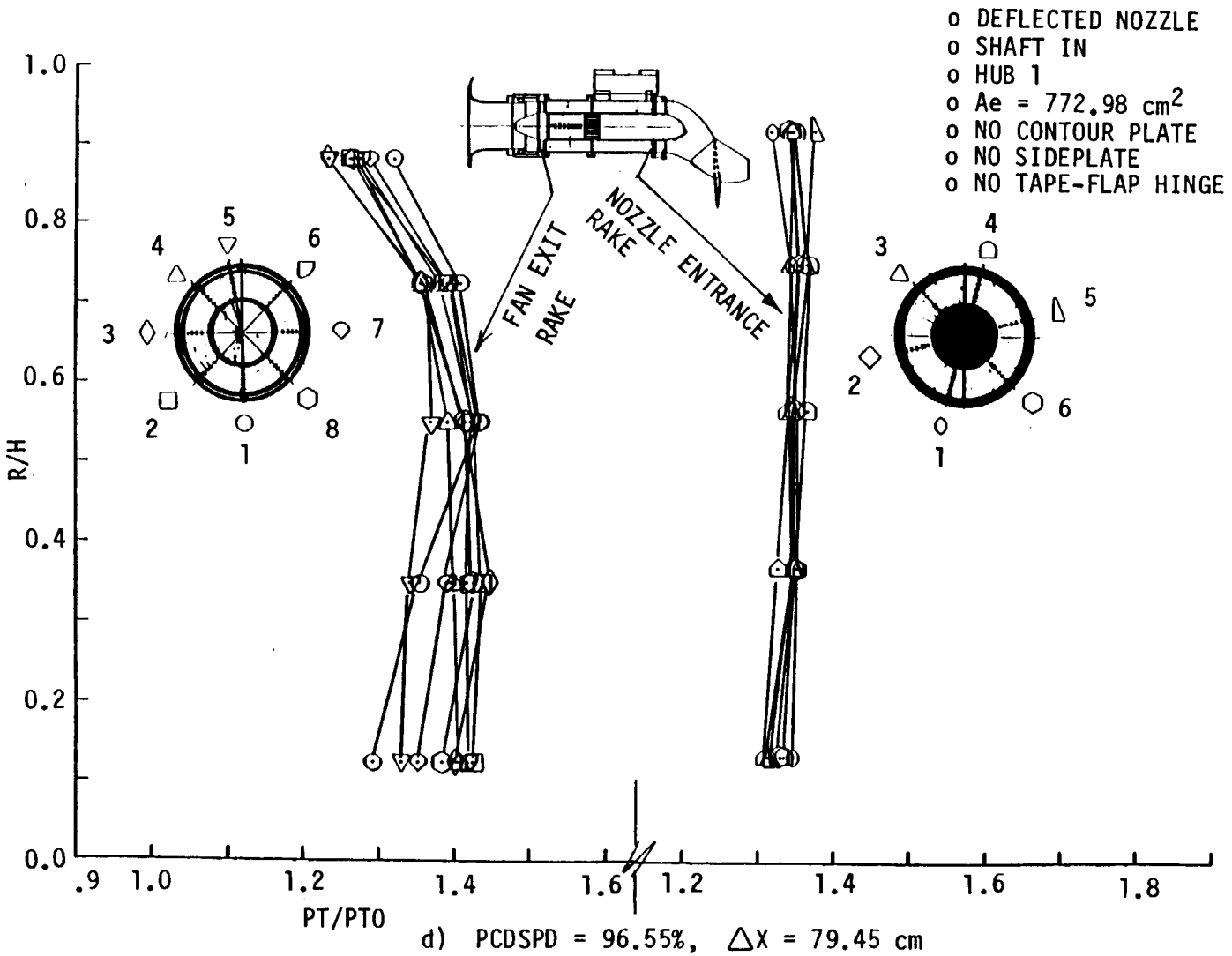

d) PCDSPD = 96.55%, ΔX = 79.45 cm

FIGURE 19 (CONCLUDED)

6.2 Modified Baseline - Deflected Nozzle - Ae = 635.62 cm^2 - Shaft In

This model configuration was tested in the following test runs.

Nozzle Area, cm^2	Spacer Distance, cm	0	3.81	12.7	79.45
635.67	Computer Runs	62	42	37	(1)(2)5, 73

NOTE: (1) Run 5 had tape on the nozzle flap hinge to reduce leakage.
(2) Runs 5 and 73 had turbine air dumped into the duct.

A comparison of the test data for this modified baseline configuration is presented in Table III. These data are directly comparable to the baseline data of Table II except that the nozzle area has been decreased from 772.98 cm^2 to 635.67 cm^2. This is accomplished by attaching a small panel on the bottom of the duct lip exit. This extension provides a slightly smoother exit contour and reduces nozzle venting.

As can be seen when comparing the data of Tables II (Ae = 772.98 cm^2) and III (Ae = 635.62 cm^2), the thrust vector alignment angle, PHID, changes toward the 90^0 vertical with the decrease in nozzle area. For example, at a nozzle pressure ratio of 1.35 for ΔX = 0, 3.81, and 12.7 cm; there occurred a decrease of 2, 2.8, and 3.6 percent, respectively, in the thrust vector alignment angle, PHID. PHID for the ΔX = 79.45 cm case has no appreciable change or improvement with the value being near 90.5^0. The data also shows that the CFN value for the ΔX = 0 cm configuration is decreased by approximately 0.6 percent with the decreased nozzle area. The CFN performance for ΔX = 3.81, 12.7 and 79.45 cm is improved by 3.4, 1.7 and 2.1 percent, respectively. These improvements occurred with the small nozzle exit area for constant nozzle pressure ratio but at a reduced WSN.

6.3 Modified Baseline - Deflected Nozzle - Shaft Removed

Tests were not performed for the modified baseline configuration (Ae = 635.67 cm^2) without a duct spacer (ΔX = 0), and shaft removed. However, the above configuration (Run 38) was tested with a duct spacer of ΔX = 12.7 cm. A comparison of this configuration (Run 38) with Run 37 (with shaft), indicated that the shaft simulation had no effect on PHID and CFN.

TABLE III Thrust Vector Angle, Nozzle Thrust Coefficient and Normalized Specific Corrected Nozzle Flow Versus Nozzle Pressure Ratio - Modified Baseline - Deflected Nozzle - Nozzle Exit Area = 635.62 cm^2 - Hub 1 - Shaft In - ΔX = 0, 3.81, 12.7, and 79.45 cm

ΔX ~ CM / ENPR OR PR16AD	0			3.81			12.7			79.45		
	PHID	CFN	WSN	PHID	CFN	WSN	PHID	CFN	WSN	PHID	CFNAP	W7SPCA
1.10	92.7	.945	.135	92.2	.922	.134	91.1	.926	.133	-	-	-
1.15	92.9	.945	.159	92.0	.927	.157	91.1	.942	.154	90.5	.936	.158
1.20	92.8	.947	.174	91.9	.934	.172	91.0	.942	.171	90.5	.952	.178
1.25	93.1	.964	.187	92.1	.954	.183	91.3	.936	.188	90.7	.948	.193
1.30	93.3	.961	.198	92.7	.957	.198	91.6	.955	.192	90.2	.963	.207
1.35	94.1	.967	.205	93.0	.963	.202	91.7	.950	.199	-	-	-
% Δ	+1.5	+2.32	+52.9	+.87	+4.4	+50.7	+.66	+2.6	+49.6	-.33	+2.7	+31.0
TEST RUN NO.	62			(1) 42			(2) 37			(3) 73		

(1) Highest ENPR is 1.3407

(2) Highest ENPR is 1.3249

(3) Turbine air dumped into the duct

6.4 Modified Baseline - Deflected Nozzle - Hub Design 2

This model configuration was tested in the following test runs.

Nozzle Area, cm^2	Spacer Distance, cm	0	3.81	12.7	79.45
772.98	Computer Runs	20	49	31	$(1)_2$, $(2)_{70}$
635.67	Computer Runs	19	48	32	1, 1b, 66, 69

NOTE: (1) Runs 1, 1b, 2 and 66 had tape on nozzle flap hinge to reduce leakage and turbine air dumped into duct

(2) Runs 1, 1b, 2, 66, 69 and 70 had turbine air dumped into duct

A comparison of the test data for this modified baseline configuration with each of the two deflected nozzle areas is presented in Table IV. In general when comparing these data with the baseline data in Table II it can be seen that by changing the fan Hub to design 2 and leaving the nozzle area at 772.98 cm^2 the thrust vector angle, PHID, more closely approaches the 90^o vertical and the thrust coefficient (CFN) increases for comparable specific corrected nozzle flow (WSN). The percent change of PHID over the ENPR is reduced while CFN is increased for the ΔX values of 0, 3.81 and 12.7 cm. As can be seen the data for ΔX = 79.45 cm shows a PHID decrease from 90.5^o (run 4 vs 74) to the range of 88.2^o to 88.9^o and slightly higher CFN values. The CFN deteriorates at the higher ENPR and especially those representing performance at near maximum corrected fan speeds, + 95%.

As also can be seen in Table IV, the PHID and CFN improve when the first lip spacer is installed and the nozzle exit area is decreased to 635.62 cm^2. These improvements also occur at smaller values of WSN.

In conclusion, the model modified to include the Hub design 2 with a nozzle area of 772.98 cm^2 is an improvement over the baseline standard. In addition, when the nozzle area is reduced to 635.62 cm^2 there are additional gains in performance. Figures 20 and 21 provide plotted data for test runs 49 and 48, respectively.

TABLE IV Thrust Vector Angle, Nozzle Thrust Coefficient and Normalized Specific Corrected Nozzle Flow Versus Nozzle Pressure Ratio - Modified Baseline - Hub Design 2 Shaft In

$A_e = 772.98\ cm^2$

ENPR OR PR16AD \ ΔX ~ CM	0			3.81			12.7			79.45			79.45		
	PHID	CFN	WSN	PHID	CFN	WSN	PHID	CFN	WSN	PHID	CFNAD	W7SPCA	PHID	CFNAD	W7SPCA
1.10	91.5	.936	.141	90.3	.933	.139	90.4	.925	.142	-	-	-	-	-	-
1.15	91.7	.944	.174	90.5	.936	.168	90.5	.936	.171	88.2	.950	.171	88.9	.961	.171
1.20	91.7	.942	.192	90.4	.939	.183	90.5	.942	.184	88.3	.966	.192	88.9	.957	.191
1.25	91.9	.949	.200	90.8	.947	.200	90.7	.948	.197	88.2	.957	.209	88.7	.960	.209
1.30	92.3	.957	.213	91.3	.956	.211	90.9	.950	.208	88.2	.952	.221	88.7	.960	.221
1.35	96.7	.961	.215	92.1	.965	.216	91.6	.966	.215	88.4	.940	.236	88.8	.961	.231
% Δ	+1.3	+2.7	+52.5	+2.0	+3.4	+55.4	+1.3	+4.4	+51.4	+.2	-1.0	+38.0	-.11	0	+35.1
TEST RUN NO.	20			49			31			(3) 70			(1) (2) 2		

$A_e = 635.62\ cm^2$

ENPR OR PR16AD \ ΔX ~ CM	0			3.81			12.7			79.45			79.45		
	PHID	CFN	WSN	PHID	CFN	WSN	PHID	CFN	WSN	PHID	CFNAD	W7SPCA	PHID	CFNAD	W7SPCA
1.10	91.5	.949	.131	91.0	.948	.132	90.6	.940	.134	-	-	-	-	-	-
1.15	91.6	.949	.165	91.1	.958	.157	90.6	.944	.156	88.7	.963	.158	88.6	.963	.158
1.20	91.6	.959	.173	90.9	.961	.172	90.6	.951	.172	88.8	.977	.178	88.6	.971	.176
1.25	91.5	.968	.190	91.0	.975	.189	90.6	.968	.185	88.9	.978	.192	88.7	.981	.191
1.30	91.7	.981	.195	91.1	.979	.198	90.6	.963	.195	88.9	.981	.206	88.9	.973	.205
1.35	92.2	.981	.606	91.7	.989	.204	90.7	.97	.199	-	-	-	-	-	-
% Δ	+.77	+3.4	+57.3	+.77	+4.3	+54.5	+.11	+3.2	+48.5	+.22	+1.8	+30.4	+.33	+1.0	+29.7
TEST RUN NO.	19			48			(1) 32			(2) 66			(3) 69		

(1) Highest value of ENPR is 1.33

(2) Tape on nozzle flap hinge to reduce leakage and turbine air dumped into duct

(3) Turbine air dumped into duct

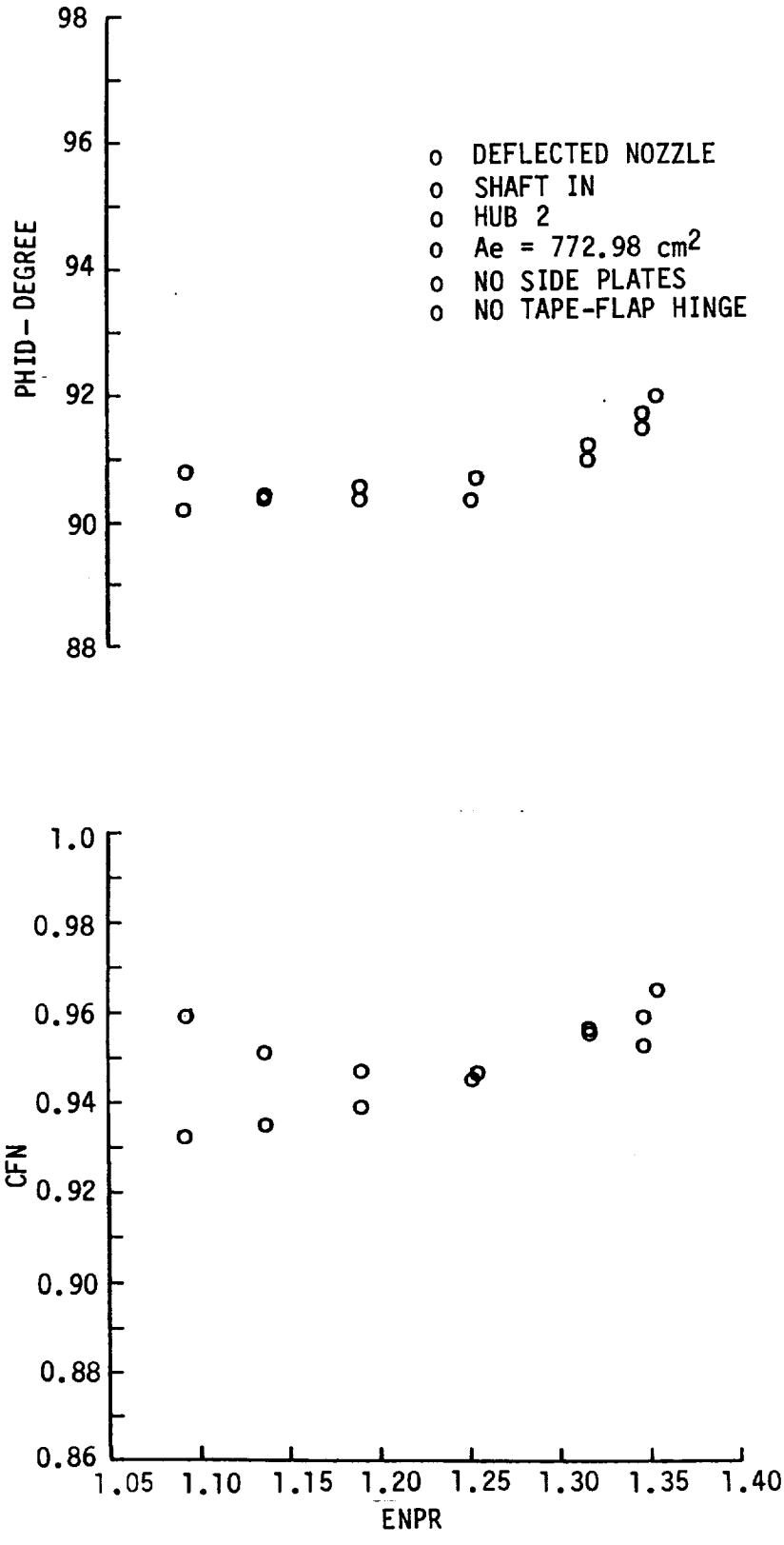

FIGURE 20A Thrust Coefficient and Thrust Vector Angle Versus Nozzle Pressure Ratio - Modified Baseline - Hub 2 - ΔX = 3.81 cm

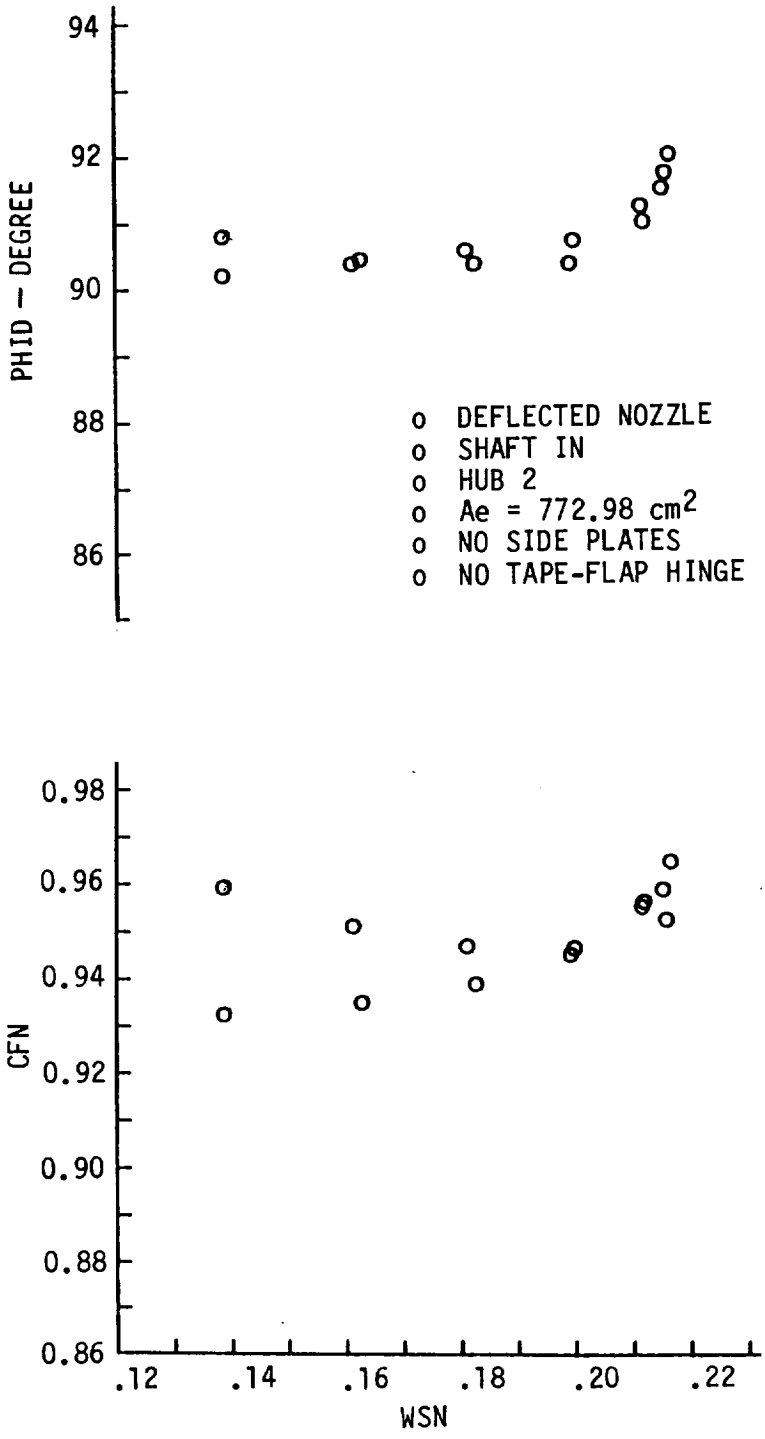

FIGURE 20B Thrust Coefficient and Thrust Vector Angle Versus Nozzle Flow - Modified Baseline - Hub 2 - ΔX = 3.81 cm

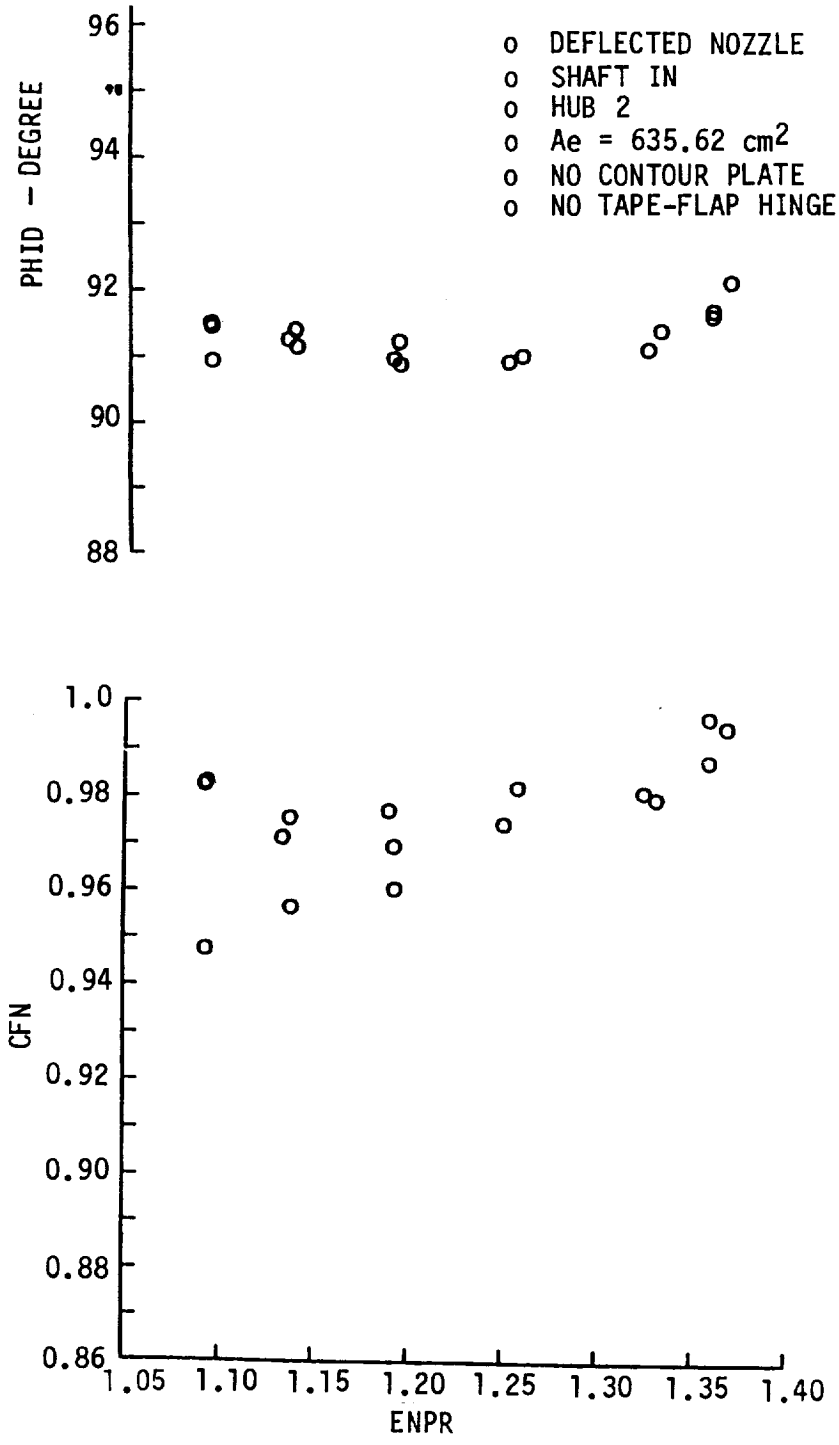

FIGURE 21A Thrust Coefficient and Thrust Vector Angle Versus Nozzle Pressure Ratio - Modified Baseline - Hub 2 - Ae = 635.62 cm^2 - ΔX = 3.81 cm

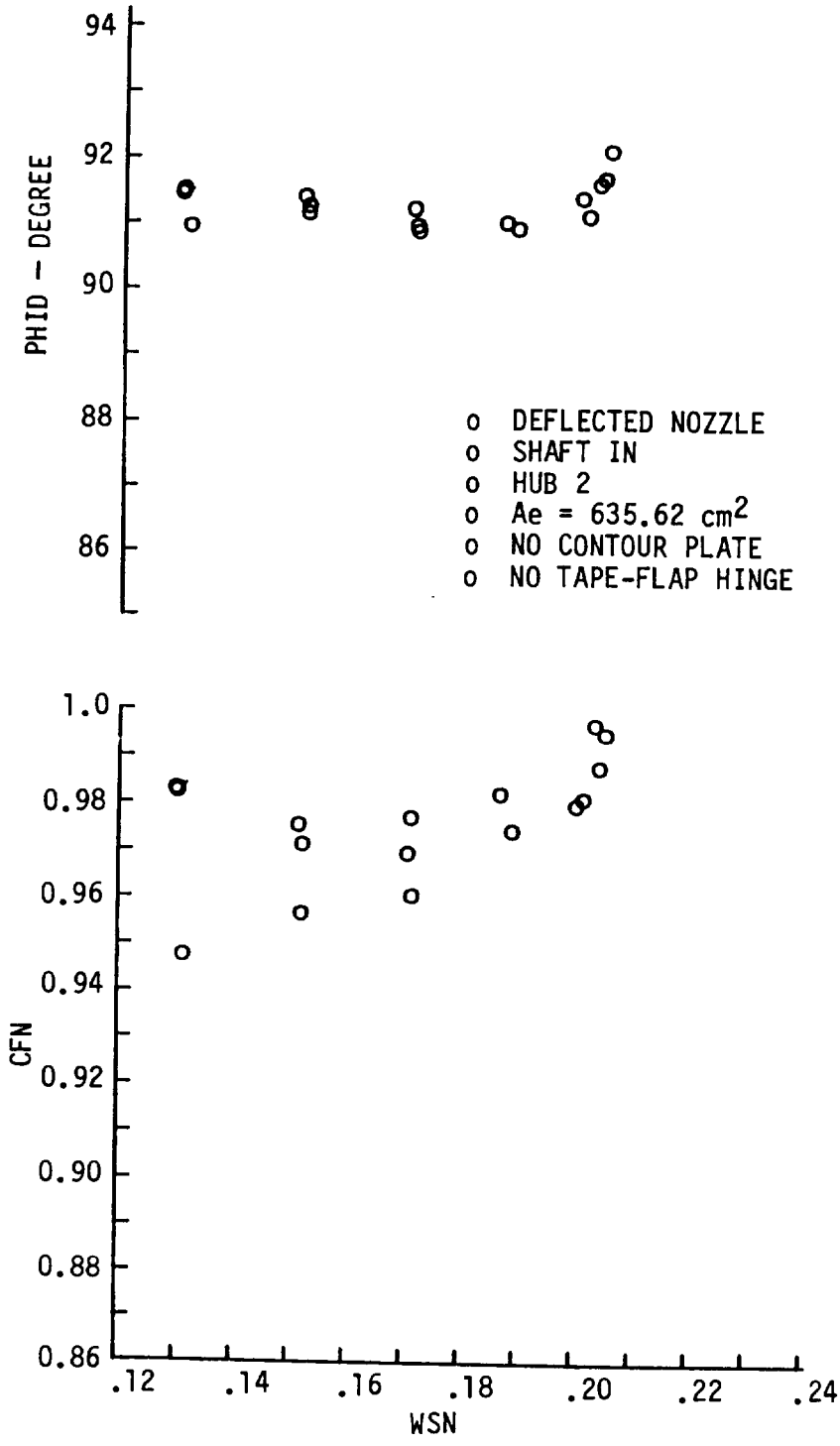

FIGURE 21B Thrust Coefficient and Thrust Vector Angle Versus Normalized Specific Corrected Nozzle Flow - Modified Baseline - Hub 2 - Ae = 635.62 cm^2 - ΔX = 3.81 cm

6.5 Modified Baseline - Deflected Nozzle - Hub Design 2 - Shaft Removed

This model configuration was tested in the following test runs.

Nozzle Area, cm^2	Spacer Distance, cm	0	3.81	12.7	79.45
772.98	Computer Runs	-	50	-	(1)3
635.67	Computer Runs	-	-	33	-

NOTE: (1) Run 3 had tape on the nozzle flap hinge to reduce leakage and turbine air dumped into duct.

A comparison of the test data for this modified baseline pertaining to each of the two deflected nozzle areas is presented in Table V. These data are also comparable to the data discussed in paragraph 6.4. The only difference in the test model was the removal of the simulated turbine shaft. If the data in Table V are compared to those of Table IV it can be seen that there are very small differences in the specific sets of data. The most noticeable difference occurs in the test data for a ΔX = 79.45 cm, run 3 versus run 70. The major additional model changes between these two test runs is the addition of tape on the nozzle flap hinge to reduce leakage for test run 3. As can be seen, the CFN is about 1 percent higher for comparable normalized specific corrected nozzle flow, WSN. This data lends some weight to the conclusion that leakage was occurring around the nozzle flap hinge.

6.6 Modified Baseline - Deflected Nozzle - Hub Design 1 - Contour Plate

The model configuration consisting of Hub design 1 and contour plate was tested in the test runs 8, 59 and 60. The only difference between test runs 59 and 60 is a nozzle area change. Run 60 is directly comparable to baseline test run 61 which had no contour plate.

Test run 8 is for a spacer distance of 79.45 cm and has the simulated turbine shaft removed from the model. The only other comparable test run is number 38 which was without a contour plate and had a spacer distance of 12.7 cm.

TABLE V Thrust Vector Angle, Nozzle Thrust Coefficient and Normalized Specific Corrected Nozzle Flow Versus Nozzle Pressure Ratio - Modified Baseline - Hub Design 2 - Shaft Removed

Ae = 772.98 cm^2

ΔX ~ CM / ENPR OR PR16AD	0			3.81			12.7			79.45		
	PHID	CFN	WSN	PHID	CFN	WSN	PHID	CFN	WSN	PHID	CFNAD	W7SPCA
1.10				90.2	.935	.144				-	-	-
1.15				90.5	.936	.170				88.7	.960	.171
1.20	NO TEST			90.6	.943	.187	NO TEST			88.6	.961	.192
1.25				90.7	.946	.201				88.8	.967	.210
1.30				91.1	.953	.213				88.9	.964	.221
1.35				91.7	.960	.216				89.0	.962	.232
% Δ				+1.7	+2.67	+50.				+.34	+.21	+35.7
TEST RUN NO.				50						(1)	3	

(1) Highest value of ENPR is 1.340

(2) Tape on nozzle flap hinge to reduce leakage and turbine air dumped into duct

Ae = 635.62 cm^2

ΔX ~ CM / ENPR OR PR16AD	0			3.81			12.7			79.45		
	PHID	CFN	WSN	PHID	CFN	WSN	PHID	CFN	WSN	PHID	CFNAD	W7SPCA
1.10							91.0	.935	.136			
1.15							90.8	.950	.156			
1.20	NO TEST			NO TEST			90.8	.954	.171	NO TEST		
1.25							90.7	.968	.186			
1.30							90.8	.979	.194			
1.35												
% Δ							-.2	+4.7	+42.6			
TEST RUN NO.							33					

A tabulated data comparison of the three test runs (8, 59 and 60) for this model configuration is presented in Table VI. As can be seen by the data of runs 60 and 59 the angle PHID and CFN improve for the decrease in nozzle area. This characteristic has been noted for other test run comparisons where the nozzle area was decreased from 772.98 cm^2 to 635.62 cm^2. However, when comparing the data of test run 60 with that of 61 in Table II it can be seen that the addition of the contour plate did not have any effect on the thrust vector angle. The CFN value decreased by 3 to 4 percent and the corrected nozzle flow at comparable nozzle pressure ratio has increased by 4-8 percent. The configurations with the longer spacer, and hence less total pressure distortion at the nozzle entrance, resulted in an improvement in the nozzle performance (Comparison Runs 8, 59).

6.7 Modified Baseline - Deflected Nozzle - Hub Design 2 - Contour Plate

This model configuration was tested in the following test runs.

Nozzle Area, cm^2	Spacer Distance, cm	0	3.81	12.7	79.45
772.98	Computer Runs	56	-	-	(1) 67
635.67	Computer Runs	57	-	-	-

NOTE: (1) Run 67 had tape on the nozzle flap hinge to reduce leakage and turbine air dumped into duct.

A comparison of the test data for the modified baseline is presented in Table VII. These data are also comparable to the data discussed in paragraph 6.4, Table IV. The only difference in the test model was the addition of a contour plate to smooth the interface between the top duct wall and the nozzle flap.

Study of the ΔX = 0 cm test data in Table VII and similar data in Table IV shows that the performance gains are very comparable. The data scans for run 56 showed a rather large shift in data values at the lower corrected fan speeds. When the normalized specific corrected nozzle flow (WSN) is approximately 0.14 the CFN varies from 0.92 to 0.936 for a nozzle pressure ratio of

TABLE VI Thrust Vector Angle, Nozzle Thrust Coefficient and Normalized Specific Corrected Nozzle Flow Versus Nozzle Pressure Ratio - Modified Baseline - With Contour Plate - Hub 1 - Shaft In

	Ae = 772.98 cm^2						635.67 cm^2		
ΔX ~ CM / ENPR OR PR16AD	0			79.45			0		
	PHID	CFN	WSN	PHID	CFNAD	W7SPCA	PHID	CFN	WSN
1.10	93.1	.920	.148	-	-	-	92.8	.927	.136
1.15	93.3	.921	.172	90.6	.937	.172	92.7	.931	.159
1.20	93.6	.920	.190	90.3	.940	.193	92.9	.938	.175
1.25	94.2	.915	.203	90.4	.939	.212	92.6	.944	.185
1.30	95.2	.929	.214	90.4	.939	.212	92.8	.959	.198
1.35	96.1	.933	.218	90.2	.933	.235	94.4	.968	.205
% Δ	+3.2	+1.4	+47.3	-.4	-.4	+36.6	+1.7	+4.4	+50.7
TEST RUN NO.	(2) 60			(1) (3) 8			59		

NOTE: (1) Run 8 is with shaft removed, tape on nozzle flap hinge to reduce leakage and turbine air dumped into duct.

(2) Highest value of ENPR is 1.3483.

(3) Highest value of ENPR is 1.3410.

TABLE VII Thrust Vector Angle, Nozzle Thrust Coefficient and Normalized Specific Corrected Nozzle Flow Versus Nozzle Pressure Ratio - Modified Baseline-Hub Design 2 - Contour Plate - Shaft In

	Ae = 772.98 cm^2						635.62 cm^2		
ΔX ~ CM / ENPR OR PR16AD	0			79.45			0		
	PHID	CFN	WSN	PHID	CFNAD	W7SPCA	PHID	CFN	WSN
1.10	91.8	.922	.145	-	-	-	91.3	.957	.137
1.15	91.8	.932	.171	88.3	.961	.171	91.5	.959	.160
1.20	92.0	.938	.188	88.4	.972	.190	91.5	.970	.176
1.25	92.1	.939	.200	88.5	.969	.208	91.5	.975	.188
1.30	92.4	.966	.211	88.5	.974	.220	91.7	.980	.198
1.35	92.4	.965	.214	88.5	.946	.234	92.1	.991	.206
% Δ	+.65	+4.7	+47.6	+.2	-1.6	+36.8	+.88	+3.4	+50.4
TEST RUN NO.	(1) 56			(3) 67			(2) 57		

(1) Highest value of ENPR is 1.333.

(2) Highest value of ENPR is 1.3434.

(3) Tape on the nozzle flap hinge to reduce leakage and turbine air dumped into duct.

1.09. The data are always clustered closely at the corrected fan speed of 95 percent. At the low nozzle pressure ratios (low specific air flow), there are two items working against the system. The balance is less accurate at these conditions. And a small error in weight flow results in a large error in CFN.

When test run 67, Table VII, data is compared to that of test run 70, Table IV, it can be seen that the thrust vector angle, PHID, is almost identical but the thrust coefficient, CFNAD, has improved by approximately +2.3 percent for comparable W7SPCA values. This improvement in CFNAD is believed to be the result of adding the contour plate. The contour plate most likely aligns and smooths the flow along the nozzle stream tube which results in a slight increase in the thrust vector. It appears that the contour plate can have some effects on performance when the nozzle entrance flow is less distorted, as the above example ($\triangle X$ = 79.45 cm).

6.8 Modified Baseline - Deflected Nozzle - Hub Design 2 - Contour Plate - Shaft Removed

This model configuration was tested in the following runs.

Nozzle Area, cm^2	Spacer Distance, cm	0	3.81	12.7	79.45
772.98	Computer Runs	-	-	-	-
635.67	Computer Runs	58	-	-	$^{(1)}6$

NOTE: (1) Run 6 had tape on the nozzle flap hinge to reduce leakage and turbine air dumped into duct.

This model configuration is the same as that of paragraph 6.5 except the simulated turbine shaft has been removed. Therefore, the data from runs 57 and 58, Ae = 635.67 cm^2, can be compared on a comparable basis. It was determined that the removal of the shaft had no effect on the performance values as were presented in paragraph 6.5.

When comparing the data between runs 58 and 6, which are comparable test points except for the spacer distance, it was determined that there were

noticeable differences. During data run 6 it was determined that PHID as a function of ENPR and WSN had a fairly constant trend at near 89^{o} while run 58 data showed about 91.5^{o} The data trends of CFN as a function of ENPR and WSN for the two test runs were very different. Test run 58 had increasing CFN values from around .96 to .99 while the test data of run 6 had a trend showing a fairly rapid increase initially as fan speed was increased but subsequently decreased. The CFN values were in the 0.96 to 0.975 range.

6.9 Modified Baseline - Deflected Nozzle - Hub Design 2 - Contour Plate - Shaft Removed - Sideplates

This model configuration was tested in test runs number 51 and 7. Test runs 7 and 51 were based on a spacer distance of 79.45 and 3.81 cm, respectively, and a nozzle exit area of 772.98 cm^2. These data are compared to the data of test run 6, paragraph 6.8, which is for an identical test model configuration except run 6 did not have extended sideplates on the nozzle exit wall and the nozzle exit area was set at 635.67 cm^2. Additionally, since it was previously concluded in paragraph 6.5 that shaft removal had very little effect on the perfomance parameters, data for run 67 (shaft in and no sideplates) is also presented. It can be seen in Figure 22 that the PHID has a constant shift as a function of PR16AD and W7SPCA and the data of test run 6 are more closely aligned to 90^{o}. The PHID of test runs 7 and 51 was near 91^{o} and for test run 67 it was near 88^{o}. However, the average data for the test scan of run 51 showed increasing values of CFN from around 0.95 to .98 but was shifted below the other three tests.

It can be seen in Figure 22 that the CFN data of run 67 has a sharp decrease at a PR16AD at approximately 1.362 and a W7SPCA of 0.227. This sharp decrease occurred at a corrected fan speed of 94.3 percent. The highest corrected fan speed tested during run 67 was 97.4 percent. This sharp decline in performance during test run 67 was noted during three separate test scans over the corrected fan speed range. A comparison of the data at maximum corrected fan speed is presented in the following table.

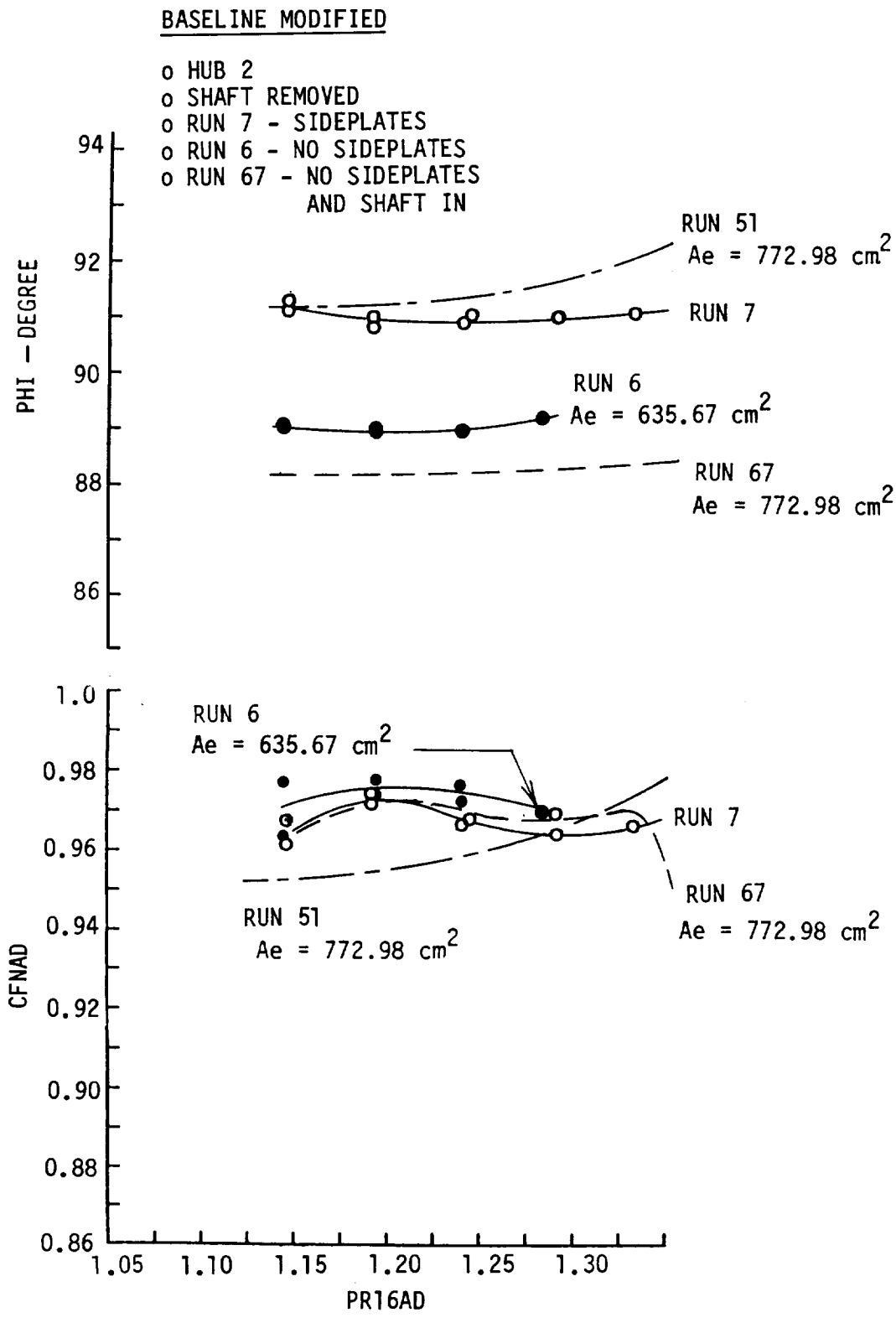

FIGURE 22A Thrust Coefficient and Thrust Vector Angle Versus Nozzle Pressure Ratio - Modified Baseline - Hub 2 - ΔX = 79.45 cm, Contour Plate, Tape on Nozzle Flap

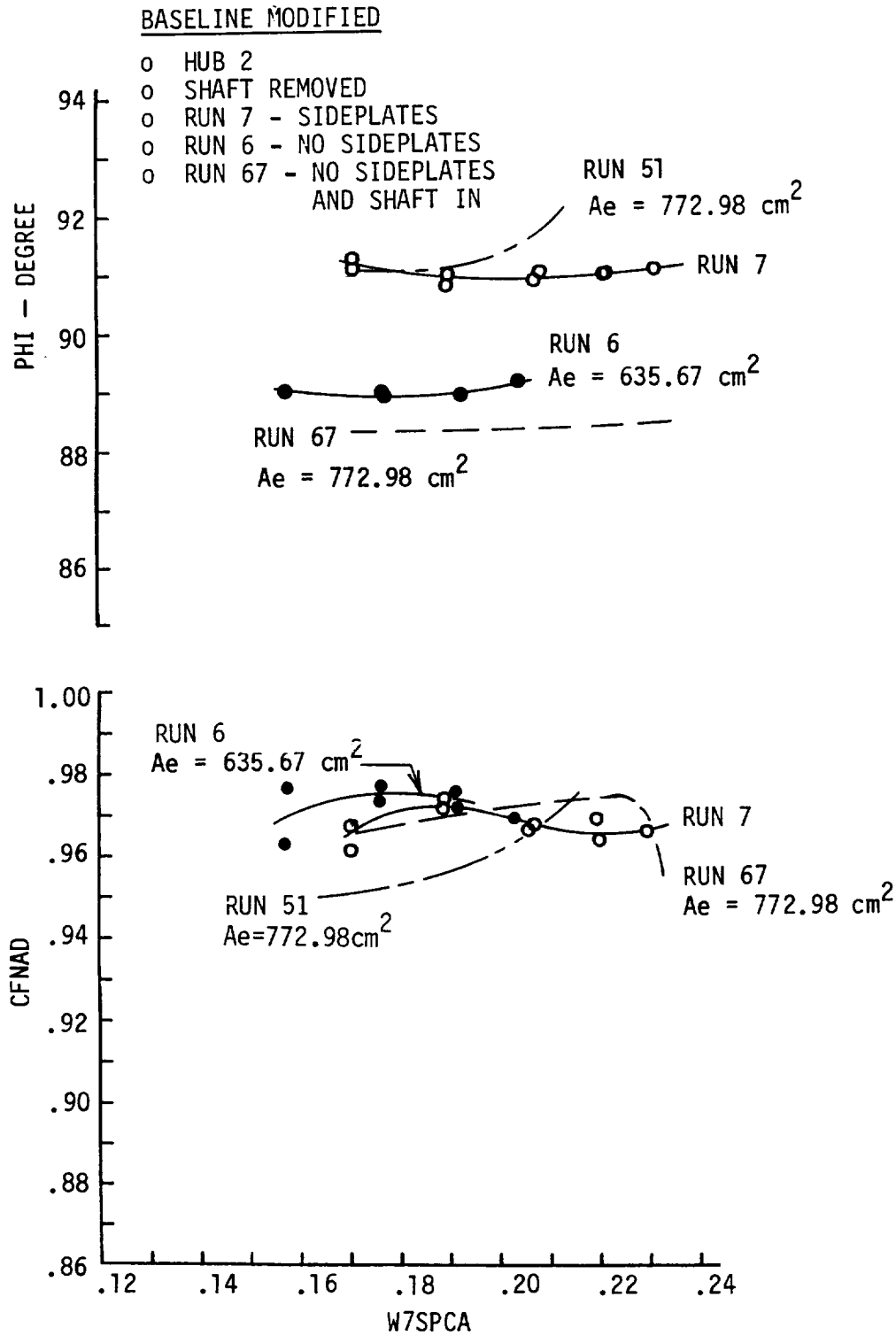

FIGURE 22B Thrust Coefficient and Thrust Vector Angle Versus Normalized Specific Corrected Nozzle Flow - Modified Baseline - Hub 2 - ΔX = 79.45 cm, Contour Plate, Tape on Nozzle Flap

NOZZLE AREA, cm^2	COMPUTER RUN	CORRECTED FAN SPEED PERCENT	PR16AD	W7SPCA	CFNAD	PHID
635.67	6	97.31	1.28	.202	.970	89.3
772.98	7	96.9	1.33	.229	.967	91.2
772.98	67	97.44	1.351	.234	.953	88.5

As can be seen, the nozzle area change effect appears in the W7SPCA values for run 6 versus 7 and 67. However, it would be difficult to see any appreciable improvements in performance by the addition of the sidewall nozzle extensions.

6.10 Cruise Nozzle

There were twelve (12) tests in the cruise mode that were based on the Hub 2 design. Ten (10) tests were for the simulated turbine shaft installed and two (2) with the shaft removed. Six (6) tests each were conducted at nozzle exit areas of 465.80 cm^2 and 390.32 cm^2.

There were ten (10) tests in the cruise mode that were based on the Hub 1 design. None (9) tests were for the simulated turbine shaft installed and one (1) with the shaft removed. Five (5) tests were conducted at a nozzle exit area of 465.80 cm^2 and 390.32 cm^2.

Since it was determined during the deflected nozzle data analysis that the Hub 2 design provided the most satisfactory performance, and the normal operating mode would be with the turbine shaft installed; these configurations were selected to be included in the cruise baseline model.

6.10.1 Baseline Comparison - Cruise Nozzle

The variation of nozzle thrust coefficient (CFN), thrust vector angle (PHID) and normalized specific corrected nozzle flow (WSN) as a function of nozzle pressure ratio (ENPR) and variation of fan-duct spacers, 0, 3.81, 12.7 and 79.45 cm, is shown in Table VIII.

TABLE VIII Thrust Vector Angle, Nozzle Thrust Coefficient and Normalized Specific Nozzle Flow Versus Nozzle Pressure Ratio - Baseline and Modified Baseline Cruise Mode - Hub Design 2 - Shaft In

Ae = 465.80 cm^2

ΔX ~ CM / ENPR OR PR16AD	0			3.81			12.7			79.45		
	PHID	CFN	WSN	PHID	CFN	WSN	PHID	CFN	WSN	PHID	CFNAD	W7SPCA
1.10	10.0	.885	.140	9.6	.892	.141	8.22	.903	.147	-	-	-
1.15	9.6	.899	.162	9.3	.898	.163	7.98	.905	.167	6.1	.965	.173
1.20	9.3	.905	.177	8.9	.900	.178	7.80	.911	.176	6.1	.972	.191
1.25	8.8	.910	.189	8.6	.911	.192	7.47	.932	.191	5.8	.966	.205
1.30	8.6	.919	.196	8.3	.921	.200	7.29	.933	.198	5.7	.974	.216
1.35	8.5	.929	.201	8.3	.929	.205	7.12	.948	.204	-	-	-
% Δ	-15.0	+4.97	+43.6	-13.5	+4.1	+45.4	-13.4	+5.0	+38.8	-6.6	+.9	+24.8
TEST RUN NO.	55			52			29			71		

Ae = 390.32 cm^2

ΔX ~ CM / ENPR OR PR16AD	0			3.81			12.7			79.45		
	PHID	CFN	WSN	PHID	CFN	WSN	PHID	CFN	WSN	PHID	CFNAD	W7SPCA
1.10	6.1	.933	.124	5.6	.929	.121	3.9	.949	.126	-	-	-
1.15	5.9	.944	.144	5.3	.943	.143	3.8	.948	.143	1.922	.974	.145
1.20	5.5	.970	.161	5.0	.966	.158	3.6	.976	.159	2.065	.972	.160
1.25	-	-	-	-	-	-	3.4	.994	.170	-	-	-
1.30	-	-	-	-	-	-	-	-	-	-	-	-
1.35	-	-	-	-	-	-	-	-	-	-	-	-
% Δ	-10.0	+4.0	+29.8	-10.7	+4.0	+30.6	-12.8	+4.7	+34.9	+7.4	-.20	+.10
TEST RUN NO.	54			53			30			72		

These data show that as the coupling distance, (ΔX) is increased from 0 to 79.45 cm the thrust vector angle (PHID) becomes more aligned with the horizontal (0^o) centerline of the cruise nozzle. The PHID at a ENPR of 1.30 varies from a low of 5.7^o to a high of 8.6^o when the nozzle area is set at 465.80 cm^2. These trends also occur for a decreasing spacer length (ΔX - 79.45, 12.7, 3.91 and 0 cm). However, when the nozzle area is reduced to 390.32 cm^2 the angle PHID increases from 2.06^o to 5.5^o for a ENPR of 1.20 and is also for a decreasing order of spacer length. The delta change in PHID between a spacer distance of 0 and 3.81 cm is small (0.5 degrees) but increases for ΔX = 12.7 and 79.45 cm.

The nozzle thrust coefficient (CFN) values for a nozzle exit area of 465.80 cm^2 are in general very different than the values at the smaller area of 390.32 cm^2. As can be seen from the data of Table VIII the CFN values for a spacer distance of 0 and 3.81 cm (Runs 55 and 52) are very similar with values near 0.898 at ENPR of 1.15 and 0.929 at ENPR of 1.35. The CFN values for the longer spacer distances are between 0.965 and 0.974 or an increase of about 6.5 percent. When the nozzle area is reduced to 390.32 cm^2 the CFN values are more closely grouped and are comparable to those for the longer spacers at the larger nozzle area. The CFN at ΔX = 0 cm and ENPR of 1.15 is 0.944 and increases to a maximum of 0.974 at the ΔX = 79.45 cm. This is a variation of about 3 percent. As the value of ENPR increases to around 1.20 the CFN value approaches a near constant value for all spacer lengths. The smaller nozzle area configurations were generally only tested to a maximum ENPR of around 1.22. The CFN values for the small nozzle configuration are larger for comparable WSN values. The nozzle pressure ratio is larger at a given WSN because of the smaller exit area of 390.32 cm^2.

A plot of the baseline cruise mode data is provided in Figure 23.

6.10.2 Modified Baseline - Cruise Nozzle - Shaft Out

This model configuration was tested in the following test runs.

Nozzle Area, cm^2	Spacer Distance, cm	0	3.81	12.7	70.45
475.80	Computer Runs	-	47	-	-
390.32	Computer Runs	-	46	-	-

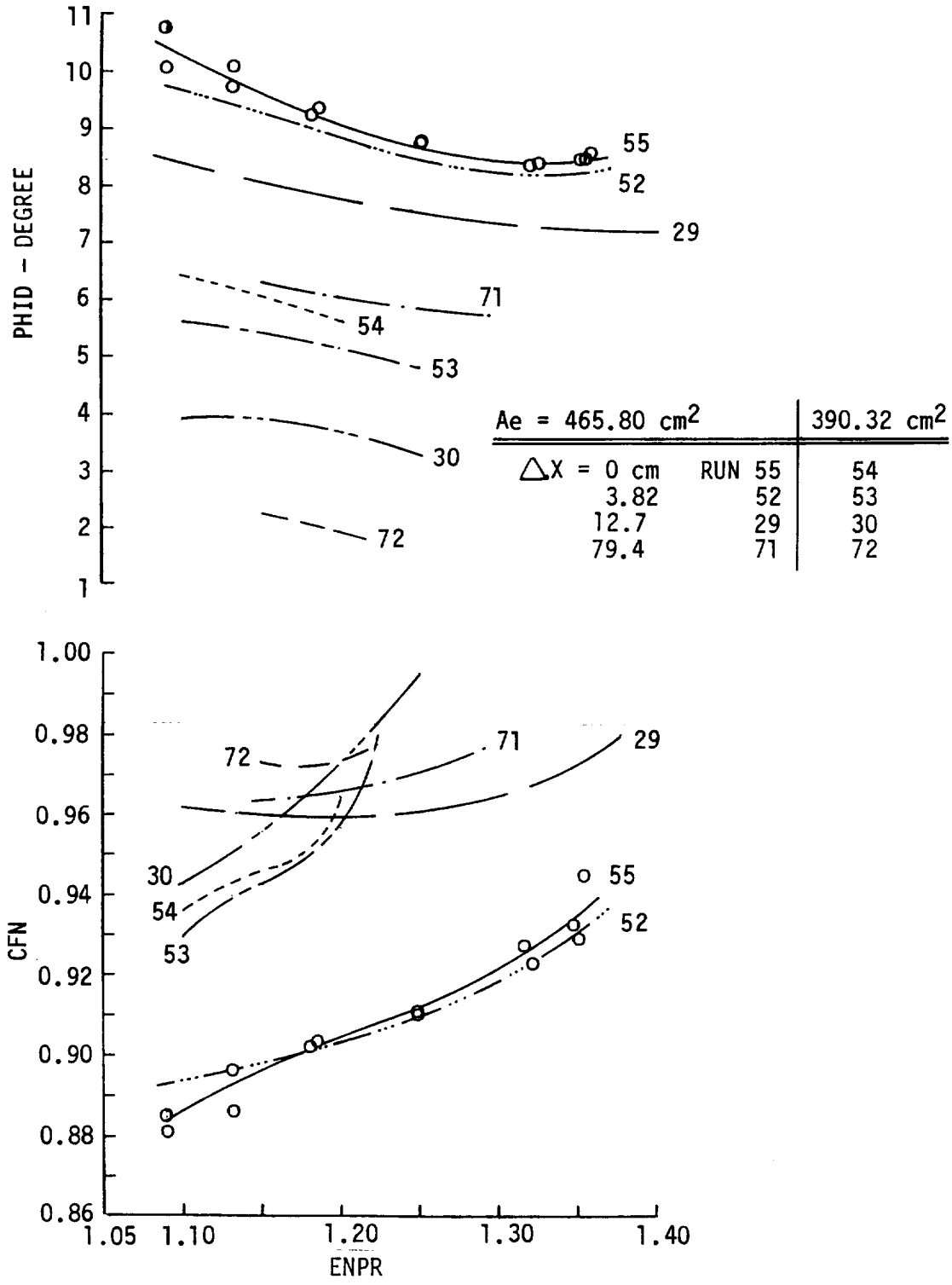

FIGURE 23A Thrust Coefficient and Thrust Vector Angle Versus Nozzle Pressure Ratio - Baseline Cruise Configuration - △X = 0 cm

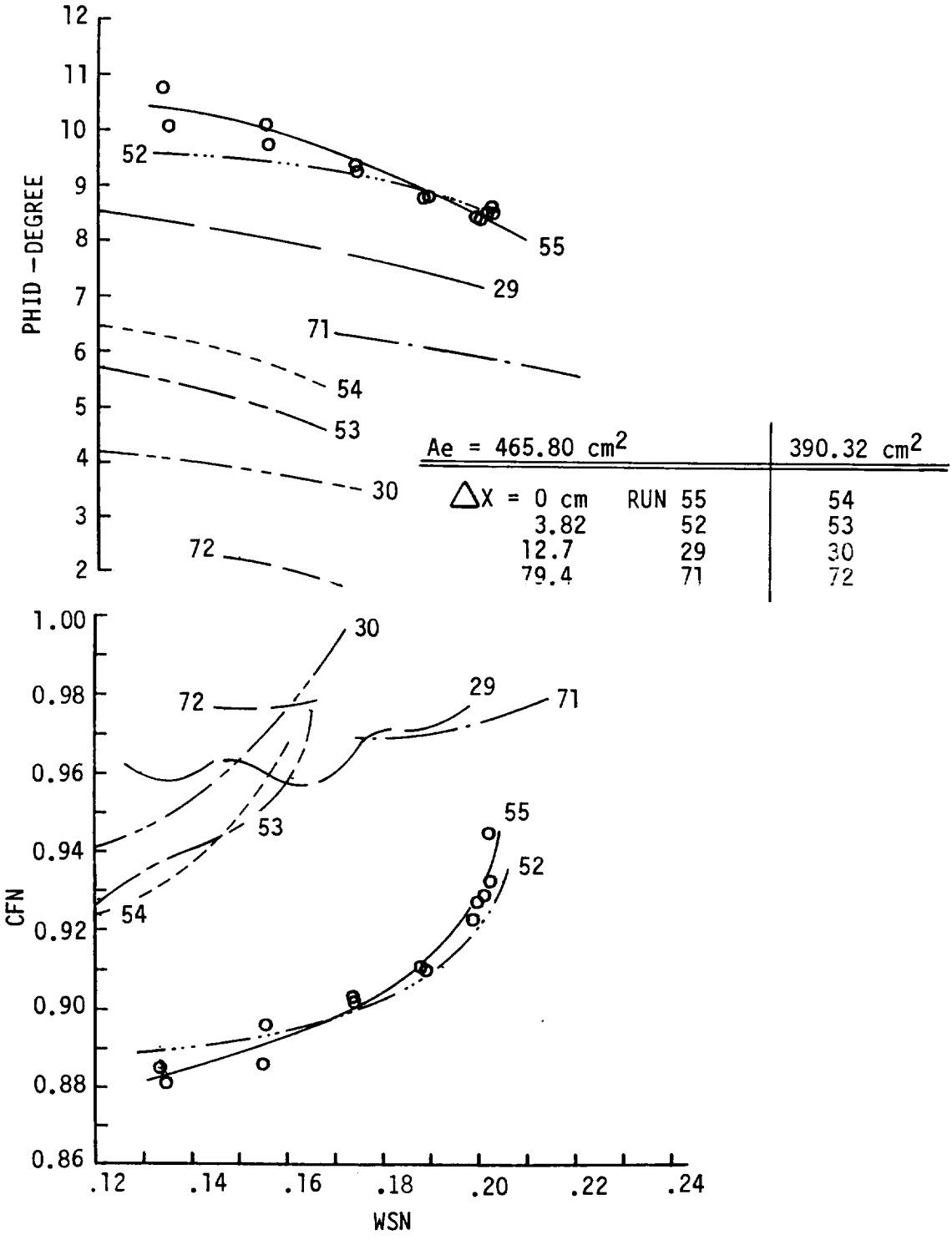

FIGURE 23B Thrust Coefficient and Thrust Vector Angle Versus Normalized Specific Corrected Nozzle Flow - Baseline Cruise Configuration - ΔX = 0 cm

A comparison of the test data for this modified configuration is presented in Table IX. When comparing these data with those of the cruise baseline, Table VIII, it can be seen that very small differences occur. Both nozzle areas show a decrease in the thrust vector angle of 12 to 22 percent. However the CFN values for the larger nozzle area increased by only 0.5 to 1.3 percent while the smaller nozzle area decreased by about 0.3 percent. The WSN values were also very comparable to the baseline.

6.10.3 Baseline - Cruise Nozzle - Model Static Pressures

If the static pressure ratios plotted in Figure 24 are compared to those in Figures 17 and 18, it can be seen that major changes occur in the regions of the bottom duct, nozzle side wall, nozzle flap and nozzle top wall. The changes are mainly due to the configuration change from the deflected nozzle mode to the cruise nozzle mode. It can be seen in Figure 24 that the PS/PAMB ratio is less than one for the last four (4) static locations on the nozzle top centerline. As previously discussed for the deflected nozzle static pressures, the flow along the top duct wall has centrifugal effect induced in the flow stream due to the rapid turn in the duct. These centrifugal effects result in increased static pressures relative to the centerline sidewall static pressures. The nozzle top wall which is downstream from the duct top wall has a reverse curved surface. These two wall surfaces form a lazy 'Z' which is skewed towards the duct (see figure insert). When the flow makes the turn from the duct section to the nozzle section, it separates from the wall resulting in a low pressure region. These static pressure characteristics can be seen in Figure 24 by referring to the data points corresponding to locations 1-11. It can be seen that the readings for the nozzle static pressure ratio are below 1.0 until the last data point which occurs at the nozzle exit. These readings are below those on the nozzle sidewall as indicated by the readings denoted as 26-31, Centerline Nozzle Sidewall. Also it can be seen that as the fan speed increases the static pressures in the duct increase and the static measurements for the top nozzle wall decrease to a low static pressure ratio of 0.89 at the last nozzle station before the exit plan is reached. The sidewall flow streams can be seen in the paint streak flow visualization pictures in Figure A-1. In the bottom picture it can be seen that the yellow

TABLE IX Thrust Vector Angle, Nozzle Thrust Coefficient and Normalized Specific Nozzle Flow Versus Nozzle Pressure Ratio - Modified Cruise Mode - Hub Design 2 - Shaft Out

	Ae = 465.80 cm^2			390.32 cm^2		
ΔX ~ CM / ENPR	3.81			3.81		
	PHID	CFN	WSN	PHID	CFN	WSN
1.10	8.2	.904	.145	4.0	.926	.127
1.15	8.0	.909	.163	4.0	.942	.143
1.20	7.8	.910	.179	3.9	.964	.159
1.25	7.8	.919	.189	-	-	-
1.30	7.6	.924	.197	-	-	-
1.35	7.3	.934	.203	-	-	-
% Δ	-11.0	+3.3	+40.0	-2.5	+4.1	+25.2
TEST RUN NO.	47			46		

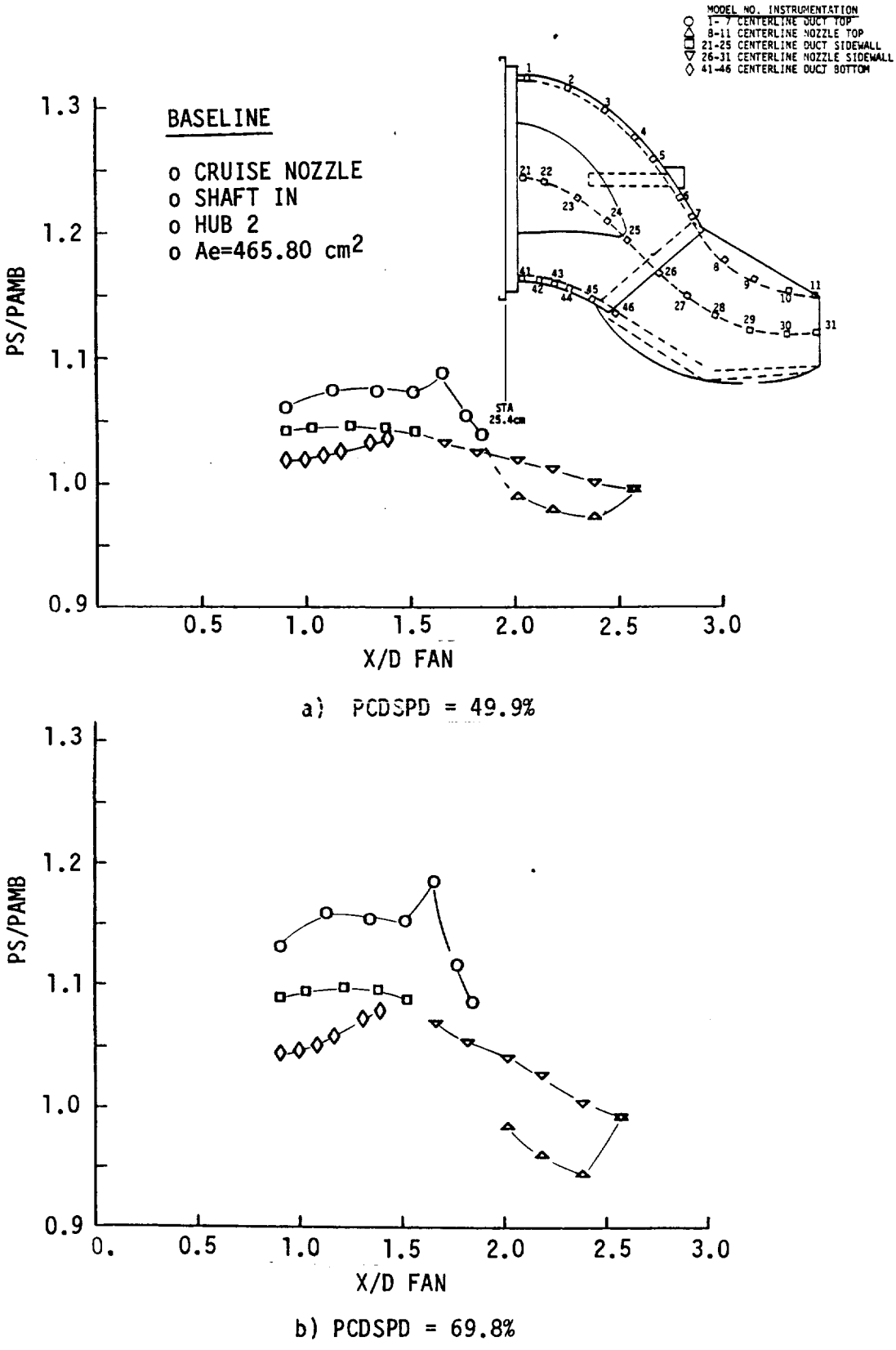

Figure 24 Duct, Nozzle, and Flap Static Pressure Ratio Versus Normalized Static Port Distance, Baseline Configuration, ΔX = 0 cm

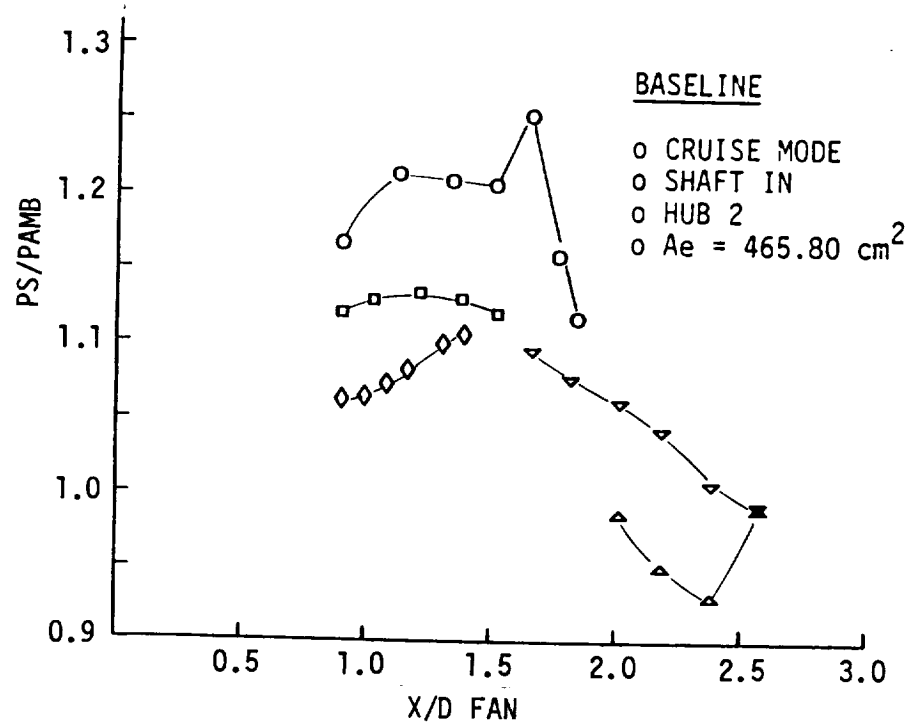

c) PCDSPD = 79.6%

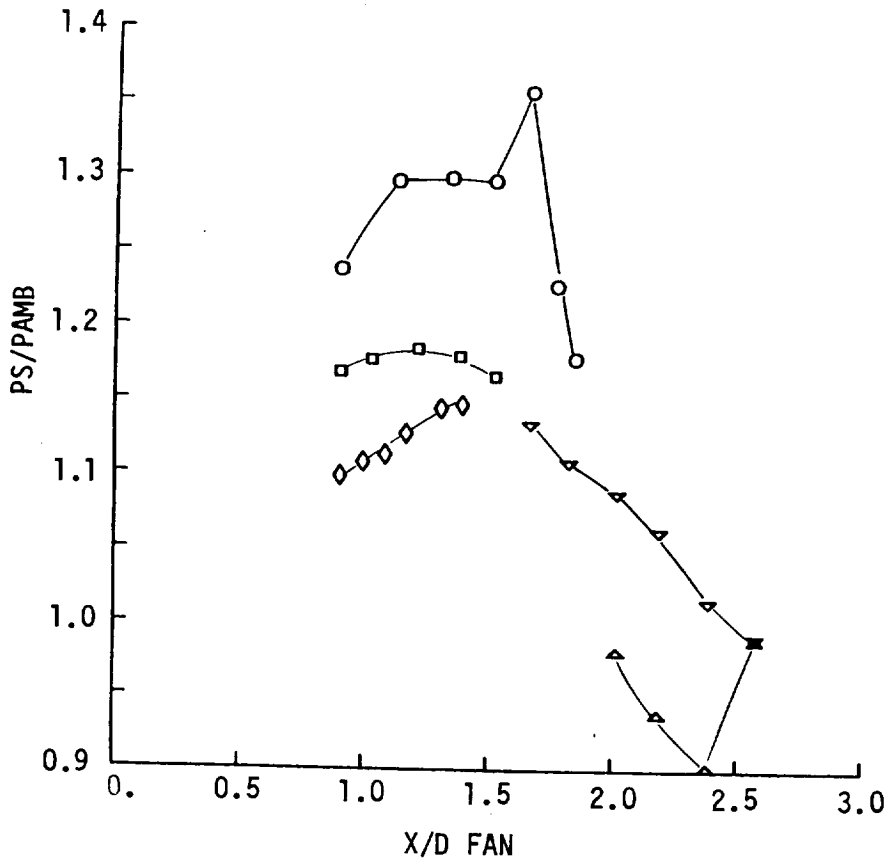

d) PCDSPD = 94.9%

FIGURE 24 (CONCLUDED)

and dark blue paints have covered the nozzle top surface very smoothly but the red and white paints that were dabbed as spots in the nozzle entrance did not follow the surface except near the wall and in line with the shaft.

6.10.4 Baseline - Cruise Nozzle - Fan Exit Total Pressure Distribution

The fan exit total pressure distortion for the cruise mode configuration is shown in Figure 25. Figure 25(d) shows the total pressure profiles at both the fan exit and nozzle entrance for the 79.45 cm spacer. If these plots are compared to those in Figure 19 it can be seen that the fan distortion is not effected by the model test configuration.

6.10.5 Modified Baseline - Cruise Mode - Hub 1 - Shaft In

This model configuration was tested in the following test runs.

Nozzle Area, cm^2	Spacer Distance, cm	0	3.81	12.7	79.45
465.83	Computer Runs	14	40	34	75
390.32	Computer Runs	15	41	35	76

The data for the nozzle area of 465.80 cm^2 shows that the best performance is obtained with the spacer distance of 79.45 cm followed in the decreasing order of 12.7 and 3.81 cm. However, when the nozzle area is reduced to 390.32 cm^2 the best performance is obtained with a spacer distance of 3.81 cm and then 12.7 cm (ENPR = 1.20).

When comparing the data of Table X to that of Table VIII it can be seen that the Hub 2 design generally provides the higher CFN values but has slightly higher thrust vector angles at comparable WSN and ENPR values.

6.10.6 Modified Baseline - Cruise Mode - Hub 1 - Shaft Out

This model configuration was tested only one time. The test was run 39 which was for a ΔX = 3.81 cm and a nozzle area of 465.80 cm^2. Comparing the data in Table XI with that of Table X it can be seen that the thrust vector angle increases by 1.5 to 7.8 percent and CFN increases about 0.7 percent at comparable WSN and ENPR values.

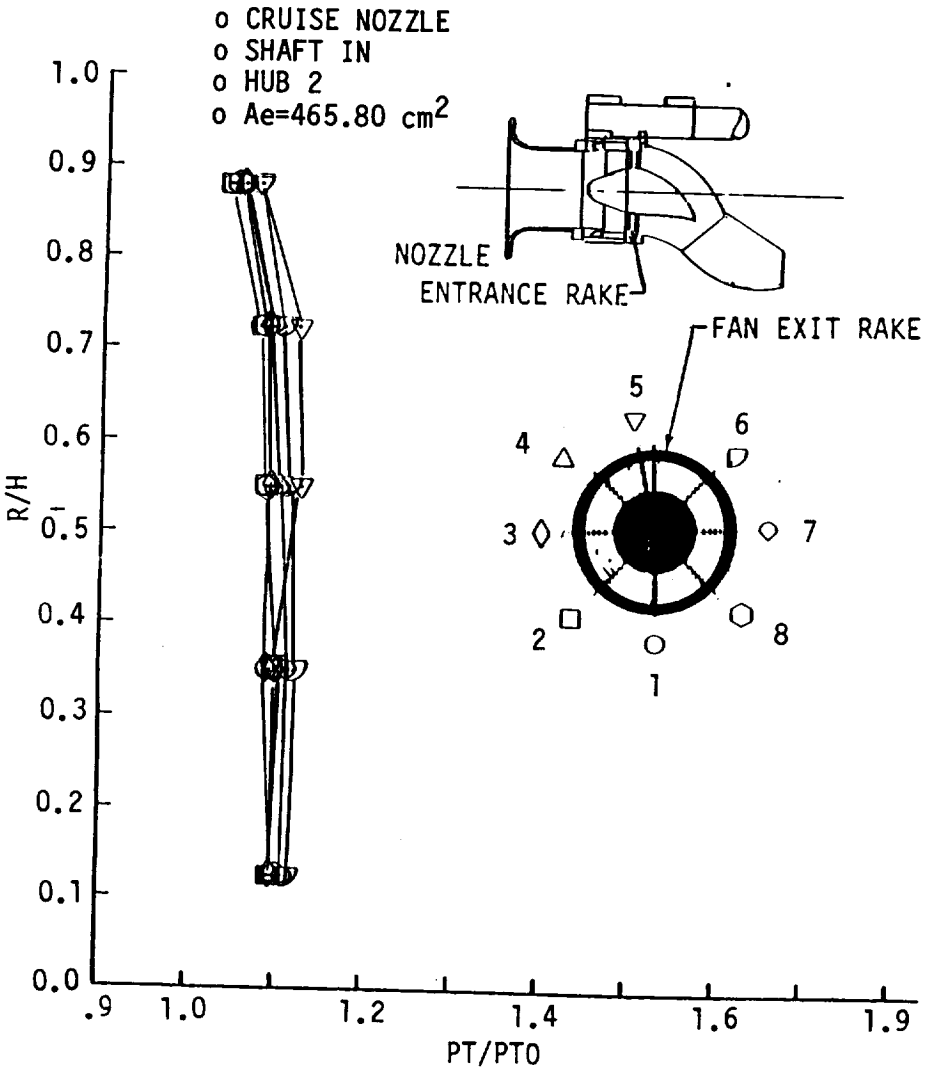

a) PCDSPD = 49.8%, ΔX = 0 cm

FIGURE 25 Rake Radius to Height Ratio Versus Total Pressure Ratio, Baseline Configuration, ΔX = 0 cm and Modified Baseline - ΔX = 79.45 cm

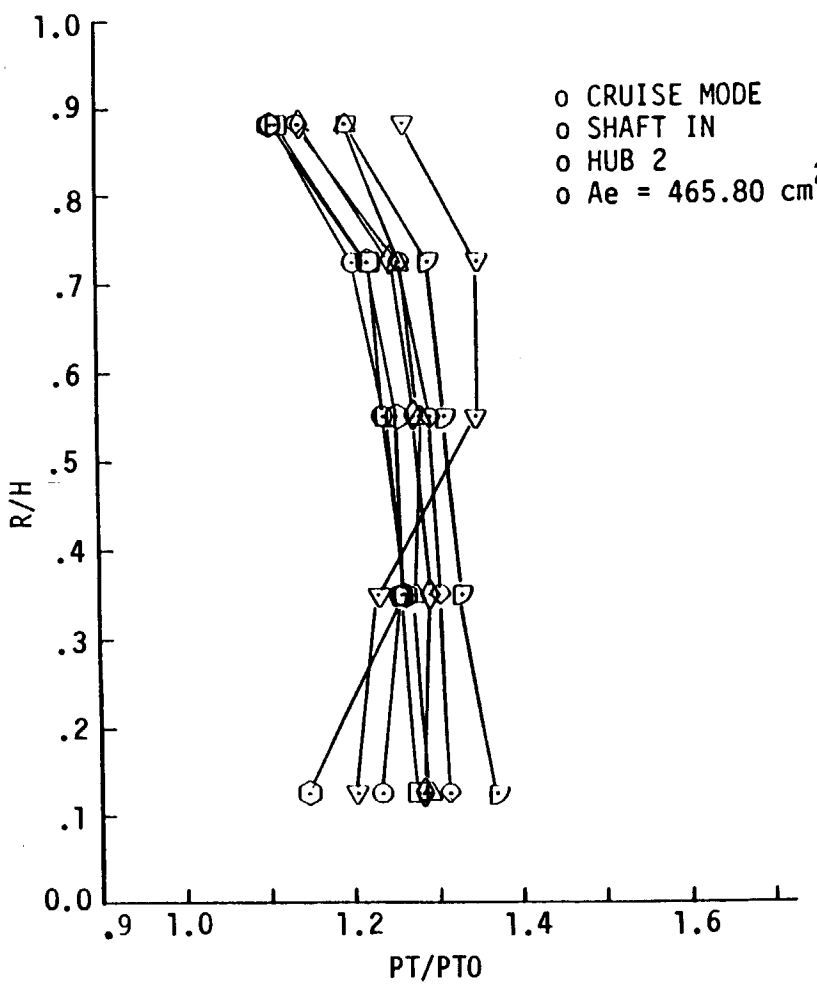

b) PCDSPD = 79.86%, ΔX = 0 cm

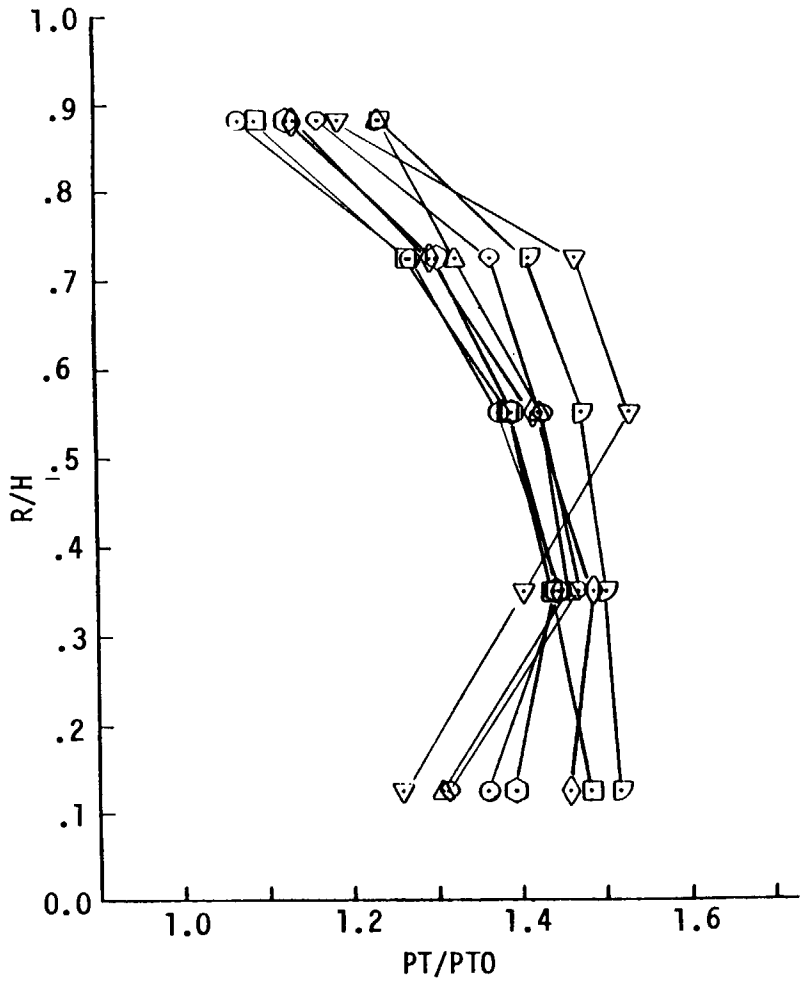

c) PCDSPD = 97.92%, ΔX = 0 cm

FIGURE 25 (CONTINUED)

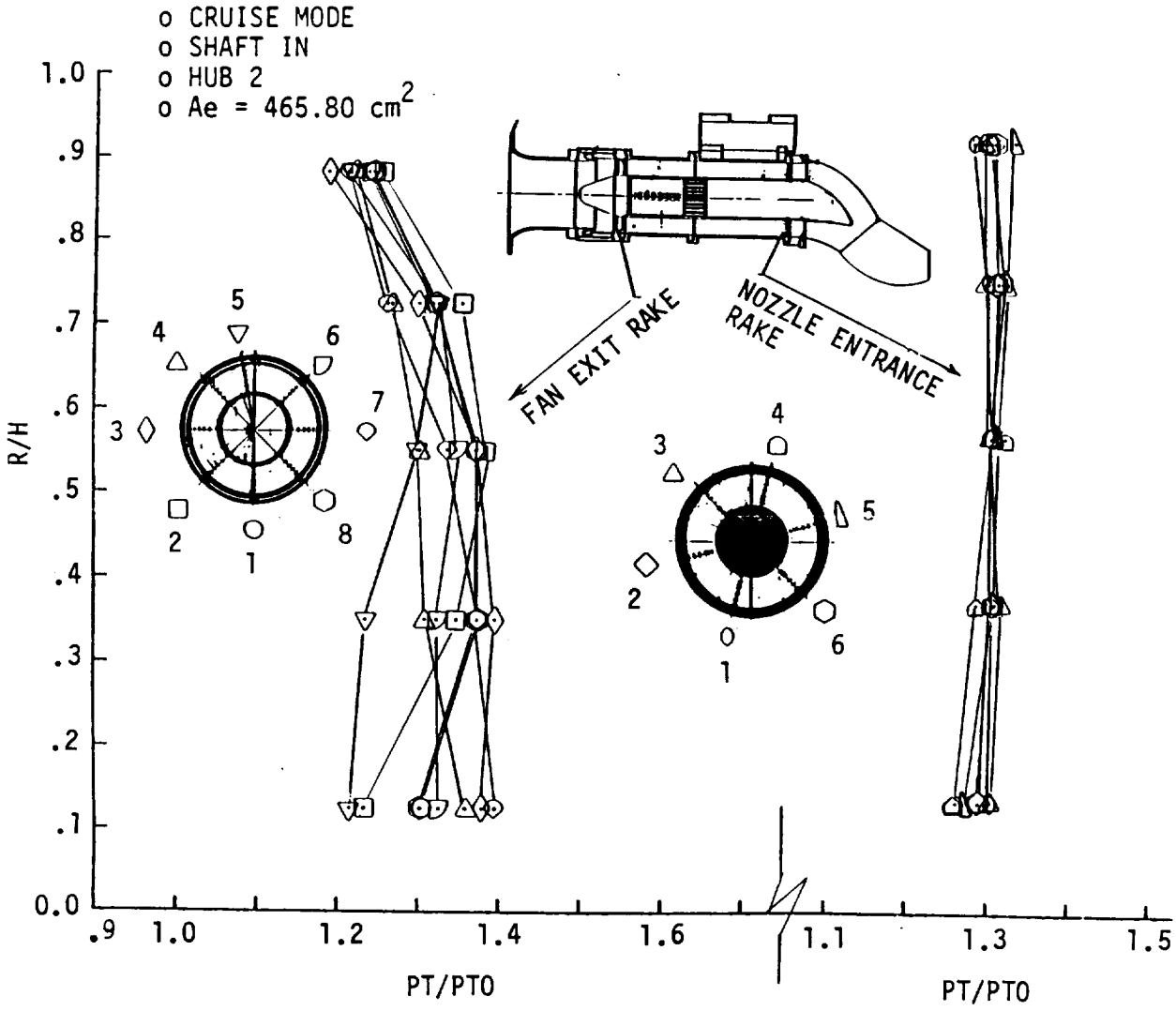

d) PCDSPD = 90.88%, ΔX = 79.45 cm

FIGURE 25 (CONCLUDED)

TABLE X Thrust Vector Angle, Nozzle Thrust Coefficient and Normalized Specific Nozzle Flow Versus Nozzle Pressure Ratio - Modified Baseline Cruise Mode - Hub Design 1 - Shaft In

$A_e = 465.80\ cm^2$

ENPR OR PR16AD \ ΔX ~ CM	0			3.81			12.7			79.45		
	PHID	CFN	WSN	PHID	CFN	WSN	PHID	CFN	WSN	PHID	CFNAD	W7SPCA
1.10	9.46	.886	.133	7.7	.889	.143	8.3	.903	.145	-	-	-
1.15	8.89	.894	.164	7.6	.894	.150	7.9	.899	.161	6.2	.958	.170
1.20	8.59	.904	.181	7.3	.911	.177	7.6	.904	.179	6.1	.936	.191
1.25	8.34	.911	.188	7.8	.914	.188	7.1	.819	.189	5.8	.956	.203
1.30	8.01	.922	.199	6.9	.923	.196	6.9	.932	.197	5.5	.954	.214
1.35	7.72	.931	.201	6.7	.928	.202	6.9	.936	.202	-	-	-
% Δ	-18.4	+5.1	+51.1	-14.1	+4.4	+41.3	-16.9	+3.7	+39.3	-11.3	-.4	+25.9
TEST RUN NO.	14			40			34			75		

$A_e = 390.32\ cm^2$

ENPR OR PR16AD \ ΔX ~ CM	0			3.81			12.7			79.45		
	PHID	CFN	WSN	PHID	CFN	WSN	PHID	CFN	WSN	PHID	CFNAD	W7SPCA
1.10	5.04	.949	.133	4.0	.937	.128	4.1	.928	.126	-	-	-
1.15	4.80	.945	.141	3.5	.955	.145	3.7	.942	.143	5.8	.959	.172
1.20	4.75	.961	.156	3.3	.971	.159	3.6	.967	.158	5.6	.961	.190
1.25	-	-	-	-	-	-	-	-	-	5.5	.962	.203
1.30	-	-	-	-	-	-	-	-	-	-	-	-
1.35	-	-	-	-	-	-	-	-	-	-	-	-
% Δ	-5.8	+1.3	+17.3	-17.5	+3.6	+24.2	-12.2	+4.2	+25.4	-5.2	+.3	+18.0
TEST RUN NO.	15			41			35			76		

TABLE XI Thrust Vector Angle, Nozzle Thrust Coefficient and Normalized Specific Nozzle Flow Versus Nozzle Pressure Ratio - Modified Baseline Cruise Mode - Hub Design 1 - Shaft Out

Ae = 465.8 cm^2 390.32 cm^2

ΔX ~ CM / ENPR	3.81			3.81		
	PHID	CFN	WSN	PHID	CFN	WSN
1.10	8.3	.894	.144			
1.15	8.0	.894	.158			
1.20	7.7	.897	.177	NO TEST		
1.25	7.4	.910	.189			
1.30	7.0	.921	.197			
1.35	6.8	.935	.204			
% Δ	-18.1	+4.6	+41.7			
TEST RUN NO.	39					

7.0 Summary of Results

7.1 Deflected Nozzle

A baseline configuration of the front tandem fan nozzle model was selected so that all other model configurations could be compared to the same standard. The baseline model constraints were as follows:

a) Nozzle in the full deflected mode.
b) Nozzle area equal to 772.98 cm.
c) Turbine shaft simulator installed.
d) Fan exit Hub design 1.
e) No fan-duct spacer installed, $\Delta X = 0$.
f) No installed contour plate.
g) No installed sideplates.
h) No tape on the nozzle flap hinge.

The front fan nozzle concept is a close-coupled configuration.

7.1.1 Hub Design 1

The following conclusions can be made for each of the model configurations containing Hub design 1.

<u>Baseline</u>

- The thrust vector angle, PHID, becomes more aligned with the vertical centerline of the nozzle as the fan-duct spacer distance is increased (Table II).

- The angle PHID is 96^{o} for a nozzle pressure ratio of 1.35, $\Delta X = 0$, and decreased to 90.5^{o} at $\Delta X = 79.45$ cm (Table II).

- The angle PHID increased as the nozzle pressure ratio increased from 1.1 to 1.35. The variation was 93.2^{o} to 96^{o} at ΔX = 0 cm and 90.2^{o} to 90.6^{o} at ΔX = 79.45 cm (Table II).

- CFN increased for spacer distances of 0, 3.81 and 12.7 cm as ENPR and WSN increased (Table II).

- CFN increased for a spacer distance of 79.45 cm as ENPR and WSN increased until the value of ENPR reached approximately 1.3 and then it decreased (Table II).

- CFN values were the largest for the spacer distance of 0 cm and ranged from 0.95 to 0.973 (Table II).

- The order of highest CFN values was ΔX = 0, 79.45, 12.7 and 3.81 (Table II).

- The lowest value of CFN occurred at a spacer distance of 3.81 cm with a range of values from 0.906 to 0.931 (Table II).

Baseline Modified

- A nozzle area decrease from 772.98 to 635.62 cm^2 resulted in improved performance parameters. PHID improved by 2 to 3 percent for spacer distances of 0, 3.81 and 12.7 cm. There were no appreciable changes to PHID values for a ΔX = 79.45 cm. The order of lowest PHID values occurred for spacer distances of 79.45, 12.7, 3.81 and 0 cm. The order of highest CFN values occur at spacer distances of ΔX = 0, 79.45, 3.81 and 12.7 cm. In addition lower values of WSN occur for comparable baseline ENPR values (Table III).

- No performance effect was noticed when the simulated turbine shaft was removed. Static pressures measured on the duct wall above and below the shaft did show noticeable differences.

- When the model has a contour plate installed along the duct-nozzle interface, no improvements were obtained for the angle PHID. However, CFN values decreased by 3 to 4 percent and the WSN values increased by 4 to 8 percent for comparable values of ENPR. These conclusions were based on test runs 61 versus 60 and 62 versus 59 (Table II, III and IV).

- When a contour plate is added and the nozzle area is decreased to 635.62 cm^2 the same trend as above was noted, test runs 59 versus 60. It was also concluded based on data of test run 59 versus 62 that no appreciable performance or static pressure effects occurs because the contour plate was installed (Table II and III).

7.1.2. Hub Design 2

The following conclusions can be made for the Hub 2 design in comparison to the Hub 1 design.

- It was determined that considerable changes in performance parameters occurred when Hub 1 was replaced by Hub 2. The highest PHID and CFN values occurred in the order of ΔX = 79.45, 12.7, 3.81 and 0 cm. The values of PHID, CFN and WSN in the order of the ΔX spacer distance above and at an ENPR of 1.3 are (1) 88.2^{o}/.952/.221, (2) 90.9^{o}/.950/.208, (3) 91.3^{o}/.956/.211, (4) 92.3^{o}/.957/.213, and for a ENPR of 1.15 they are (1) 88.2^{o}/.950/.171, (2) 90.5^{o}/.936/.171, (3) 90.5^{o}/.936/.168, (4) 91.7^{o}/.944/.174. Thus, it was concluded that Hub 2 resulted in a 1.8 to 3.3 percent improvement in PHID, 1.0 to 3.6 percent improvement in CFN and 0.6 to 4.2 percent decrease in WSN at comparable nozzle pressure ratios (Table II and IV).

- The changes in static pressures due to the Hub 2 installation occurred in the duct sidewall and bottom. The sidewall static ports remain in a high static pressure region because of the hub shape. The bottom duct and Hub 2 form a relatively flat constant flow channel which results in slightly higher static pressures along the bottom duct to the nozzle exit lip.

- When the Hub 2 design was modified by decreasing the nozzle area to 635.62 cm^2 the CFN values increase as was noted for the Hub 1 design. However, the angle PHID did not show any significant changes. Most changes of PHID were within $\pm$0.5 percent of those for a nozzle area of 772.98 cm^2. In comparison to the Hub 1 design and a nozzle area of 635.62 cm^2 the Hub 2 design had PHID improvements in the range of 1.4 to 2.6 percent Table II and IV).

- The Hub 2 tests with the shaft removed, showed no noticeable effects on performance (Table IV and V).

- When the contour plate is installed (close-couple configuration) there were in general no effects on performance. However, some improvements were noted for the spacer distance of 79.45 cm (non close-couple configuration) (Table IV and VII).

- Side plates had no effect on the performance.

7.2 Cruise Nozzle

A baseline configuration of the front tandem fan nozzle model was selected so that all cruise model configurations could be compared to the same standard. The baseline model was based on the results of the data analysis of the deflected mode nozzle configuration. The cruise nozzle baseline model constraints were as follows:

a) Nozzle in the full cruise mode
b) Nozzle area equal to 465.80 cm^2
c) Turbine shaft simulator installed
d) Fan exit Hub design 2
e) No fan-duct spacer $\triangle X$ = 0 cm

7.2.1 Hub Design 2

The following conclusions can be made for each of the model configurations containing Hub design 2.

Baseline

- The thrust vector angle, PHID, becomes more aligned with the horizontal centerline of the nozzle as the fan-duct spacer distance is increased (Table VIII).

- The angle PHID is 8.5^o at a nozzle pressure ratio (ENPR) of 1.35 and increases to 10.0^o at a ENPR of 1.10 (Table VIII).

- The angle PHID decreases as the nozzle pressure ratio increases from 1.1 to 1.35. The variation was 10^o to 8.5^o at $\triangle X$ = 0 cm (baseline) and 6.1^o to 5.7^o at $\triangle X$ = 79.45 cm (modified baseline), (Table VIII)..

- CFN values were the smallest for the spacer distance of $\triangle X$ = 0 cm (baseline) and ranged from 0.885 to 0.929 (Table VIII).

- The order of highest CFN values was $\triangle X$ = 79.45, 12.7, 3.81 and 0 cm (baseline), (Table VIII).

Baseline Modified

- A nozzle area decrease from 465.80 cm^2 to 390.32 cm^2 resulted in improved performance values. PHID improved by approximately 40 percent at the spacer distance of 0 cm and 43 percent at the spacer distance of 3.81 cm. The order of lowest PHID values

is ΔX = 79.45, 12.7, 3.81 and 0 cm. CFN improved by approximately 7.2 and 7.3 percent at spacer distances of 0 and 3.81 cm, respectively. The order of highest CFN values occur at spacer distances of ΔX = 79.45, 12.7, 0 and 3.81 cm. Lower values of WSN occur for comparable baseline ENPR values (Table VIII).

- The largest value for CFN occurred at a spacer distance of 79.45 cm (modified baseline) with a range of 0.965 to 0.974 (Table VIII).

- When the simulated turbine shaft was removed at the Ae = 465.80 cm^2 and ΔX = 3.81 cm the angle PHID and CFN improved by about 14.0 and 0.92 percent, respectively (Tables VIII and IX). When the nozzle area is decreased to 390.32 cm^2 the performance parameters have an additional improvement. The value of PHID is 3.9^o and CFN is 0.964 at a nozzle pressure ratio of 1.2 (Table IX).

7.2.2 Hub Design 1

The following conclusions can be made for the Modified Baseline - Hub 1 design in comparison to the Baseline-Hub 2 design.

- The angle PHID had slight improvements with the larger change occurring at a ΔX = 3.81 cm. PHID decreased from 9.6^o to 7.7^o at ENPR of 1.1 and decreased from 8.3^o to 6.7^o at ENPR of 1.35. The PHID at ΔX = 79.45 cm had very small changes. CFN had a significant decrease at the ΔX = 79.45 cm. CFN changed from 0.965 to 0.958 at ENPR of 1.15 and from 0.974 to 0.954 at ENPR of 1.30 (Table VIII, X).

- When the Hub 1 design has the nozzle area reduced to 390.32 cm^2 the values of PHID and CFN once again have significant improvements (Table X).

- When changes are noted for the Hub 1 (Modified Baseline) in comparison to Hub 2 (Baseline) with a nozzle exit area of 390.32 cm^2 and ΔX = 0 cm, it can be seen that the angle PHID changes are in the range of 6.1^o - 5.5^o (Table VIII) to 5.04^o - 4.75^o (Table X) at ENPR values of 1.10 - 1.20, approximately a 16 percent improvement. The CFN decreased from the range of 0.933 - 0.970 (Table VIII) to 0.949 to 0.961 (Table X) over the ENPR range of 1.1 to 1.2, approximately 0.4 percent. There are significant angle PHID differences with a spacer distance of 79.45 cm.

- When the shaft is removed from the model for the Hub 1 design, Ae = 465.80 cm^2, ΔX = 3.81 cm, there are slight increases in angle PHID. However, the CFN values are lower for a given WSN and ENPR (Tables X and XI).

8.0 Conclusions and Recommendations

High nozzle performance in the deflected mode was verified for all of the spacer distances and corrected fan speeds. The thrust vector angle, PHID, is usually between 88^o and 92^o, the thrust coefficient, CFN, in the range of 0.90 to 0.98 and the normalized specific corrected flow in the range of 0.136 and 0.234; depending on corrected fan speed and model configuration. The three major contributors to performance improvement were determined to be Hub design, nozzle exit area and fan-duct spacer distance. Shaft removal, the addition of a contour plate and sideplates had very little or no effect on performance parameters. Hub 2 design results in 1.8 to 3.3 percent improvement in the thrust vector angle, 1.0 to 3.6 percent improvement in thrust coefficient at comparable nozzle pressure ratios. Additional improvements occur when the nozzle area is reduced to 635.62 cm^2. The highest CFN in the vertical mode occurs with no fan-duct spacer (ΔX = 0 cm) while the best CFN for the cruise mode occurs with the largest fan-duct spacer installed (ΔX = 79.45 cm).

Based on the performance data analysis presented in this report and the preceeding conclusions, the following configuration is recommended:

- The Hub 2 design should be used in front tandem fan nozzle designs.

- Good nozzle thrust coefficient (CFN = 0.94) can be obtained with no fan duct spacer.

- The smaller nozzle area of 635.62 cm^2 should be used because it provides less nozzle venting and has a slightly smoother nozzle exit lip.

- Further design and testing should be conducted in the area of fan hub shape and lower nozzle lip shape.

Based on the results of this test and those of References 1 and 2, it is further recommended that the total Tandem Fan nacelle be tested statically, at transition speeds, and at cruise velocities.

- Further design and testing should be conducted in the area of cross flow reduction.

REFERENCES

1. "Additional Testing of the Inlets Designed for a Tandem Fan V/STOL Nacelle", A. H. Ybarra, NASA CR-165310 (Vought Technical Report 2-53020/1R-52726), June 1981.

2. "Low Speed Test of the Aft Inlet Designed for a Tandem Fan V/STOL Nacelle", W. W. Rhoades and A. H. Ybarra, NASA CR-159752 (Vought Technical Report 2-30320/0R-52360), February 1980.

3. NASA Contract NAS3-21467, "Design and Fabrication of Front Nozzle Model", 27 June 1978.

4. "Design Report Model 1109-A 12-inch Tip-Turbine Fan TR77-101, Revision A", G. Linsker, Tech Development Incorporated TD-1109M, 4 February 1977.

APPENDIX A
Flow Visualization Studies

To improve the understanding of the local flow patterns that occur at the duct exit and in the nozzle passage, flow visualization tests were performed.

Artist oil pigments were mixed with penetrating oil to obtain a viscosity just high enough to ensure no flow under gravity forces. A number of different colored paint spots were dabbed on the model. The fan was brought up to a specified corrected fan speed and held at that speed for a sufficient span of time so that paint flow would have fully outlined the flow patterns.

Five tests were performed with the nozzle in the cruise mode and twenty-seven in the deflected mode. Approximately half of the tests were performed with Hub design 1 and 2, respectively. Nine tests had the contour plate installed.

Four typical paint streak photographs are shown in Figures A-1, A-2, A-3 and A-4.

Figure A-1 shows the flow visualization for the cruise mode model containing Hub 2 and the shaft installed. Smooth streamlines are indicated along the top nozzle wall (model inverted) and sidewalls. The nozzle flap has non-uniform flow in line with the fan Hub as shown by the discontinuity in the yellow paint. The red and white paint on the bottom of the Hub fairing indicate flow swirl from left to right (looking forward).

Figure A-2 shows the flow test for the deflected mode, Ae = 772.96 cm^2, Hub 2, with shaft and sideplates. This test shows flow swirl from left to right on the top duct wall at the duct-nozzle flap interface, and the streamlines are generally sloped from left to right on the nozzle flap. The flow on the nozzle flap and sidewalls indicates fairly uniform flow. The sharp turning radius of the flow can be seen by the dark blue, red and yellow paint on the duct right sidewall. Flow interference by the shaft is clearly seen by the white paint flow around and downstream of the shaft.

THIS PAGE BLANK

Figure A-1 Flow Visualization Test - Cruise Mode - Ac = 465.3 cm^2 - Hub 2 - With Shaft - 80% Corrected Fan Speed

THIS PAGE BLANK

Figure A-2 Flow Visualization Test - Deflected Mode - Ae = 772.96 cm^2 - Hub 2 - With Shaft - With Sideplates - 80% Corrected Fan Speed

THIS PAGE BLANK

Figure A-3 Flow Visualization Test - Deflected Mode - Ae = 488.77 cm^2 - Hub 2 - With Shaft - No Sideplates - With Contour Plate - 90% Corrected Fan Speed

THIS PAGE BLANK

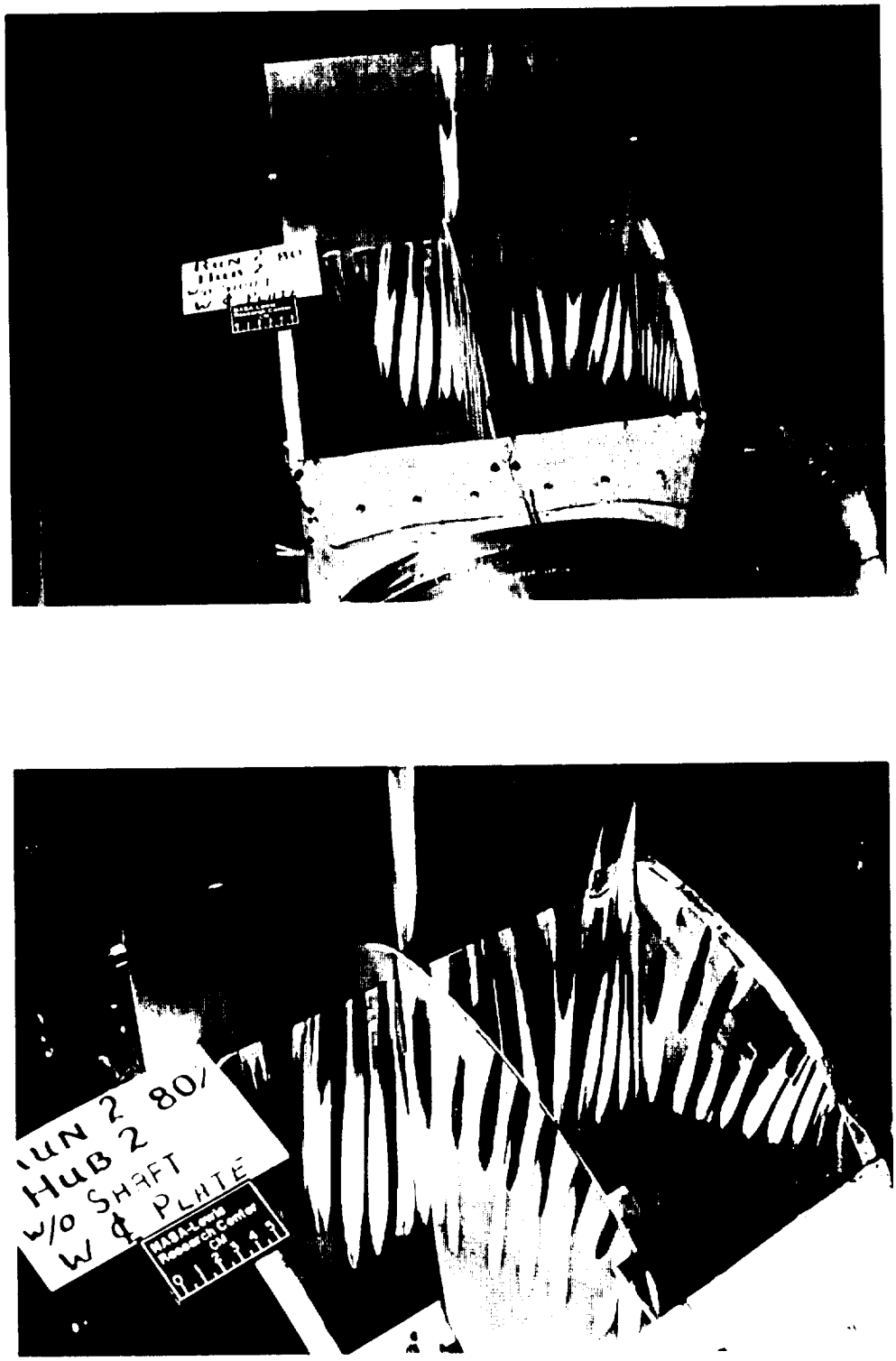

Figure A-4 Flow Visualization Test - Deflected Mode - Ae = 488.77 cm^2 - Hub 2 - Without Shaft - No Sideplates - No Contour Plate - With Center Plate - 80% Corrected Fan Speed

THIS PAGE BLANK

Figure A-3 shows the flow effect related to the addition of the contour plate to smooth the duct top wall and nozzle flap interface. As can be seen when comparing Figures A-2 and A-3, the flow distortion at the nozzle flap and duct wall was eliminated, but the remaining flow streams appear to be very comparable. Also, the sidewall lip spillover is reduced by the sidewall extension plates.

Figure A-4 shows that the addition of a center plate in the nozzle exit eliminates the cross flow on the nozzle flap as was noted in Figures A-2 and A-3.

THIS PAGE BLANK

APPENDIX B
DATA REDUCTION EQUATIONS

The Tandem Fan front nozzle tests were performed with two different instrumentation systems in the static test facility at the NASA Lewis Research Center. The instrumentation of the various components is provided in Section 5.0.

This appendix provides the data reduction equations used to calculate the various parameters based on the measured test data. All data were measured, recorded and calculated in standard English units, therefore, the calculations presented in this appendix are presented in that nomenclature with comparable metric units provided in parenthesis, for example lbm/ft^3 (kg/m^3).

I. TURBINE DRIVE AIR

a) Air Density, FDEN, LBm/FT^3 (kg/m^3)

$$FDEN = 2.69966 \left(\frac{VDAP}{VDAT}\right)$$

VDAP = Venturi Inlet Pressure, Psia (kPa)

VDAT = Inlet Temperature, ^oR (^oK)

b) Venturi Pressure Ratio, R

$$R = \frac{VDAP - VDELP}{VDAP}$$

VDELP = Venturi delta pressure, Psid (kPa)

c) Expansion Factor, VENEF

$$VENEF = \left\{ \frac{1}{FGAM} R^{\frac{2}{GAM}} \left(\frac{1-R^{FGAM}}{1-R}\right) \left(\frac{1-VBETA^4}{1-VBETA^4 R^{\frac{2}{GAM}}}\right) \right\}^{\frac{1}{2}}$$

VBETA = Throat to inlet diameter ratio

GAM = Ratio of specific heats

FGAM = (GAM - 1.0)/GAM

d) Thermal Expansion Factor, VENFA

$$VENFA = 1.0 + [13.1 \times 10^{-6}(VDAT-535.0)]$$

e) Venturi Weight Flow, WVEN, LBm/sec (kg/sec)

$$WVEN = 0.52502 \sqrt{(FDEN)(VDELP)} \left[\frac{(VENFC)(VENEF)(VENTD)^2(VENFA)}{\sqrt{1.0-VBETA^4}} \right]$$

VENFC = Flow Coefficient, 0.995

II. TURBINE CONDITIONS

a) Turbine Exit Total Pressure Ratios, TTPR

$$TTPR\ (I=1 \rightarrow 8) = \frac{FDAP}{TETP(J)}$$

FDAP = Inlet Total Pressure, Psia (kPa)

J = 6 different measuring locations

b) Average Turbine Exit Total Pressure Ratio, TTPRAV

$$TTPRAV = \frac{\Sigma TTPR(I=1 \rightarrow 8)}{8}$$

c) Turbine Exit Static Pressure Ratio, TSPR

$$TSPR\ (I) = \frac{FDAP}{AVD.WD}$$

AVD.WD = 61, 65, 69, 73
62, 66, 70, 74

d) Average Turbine Exit Static Pressure Ratio, TSPRAV

$$TSPRAV = \frac{\sum_{I} TSPR\ (I)}{I}$$

e) Turbine Corrected Airflow, WTC, LBm/sec (kg/sec)

$$WTC = WVEN \left(\frac{14.696}{FDAP}\right) \sqrt{\frac{FDAT}{518.7}}$$

FDAT = Inlet Total Temperature, $^{O}R(^{O}K)$

f) Turbine Temperature Drop, TURBTD, $^{O}R(^{O}K)$

TURBTD = FDAT - TETTAV

TETTAV = Average Turbine Exit Total Temperature, $^{O}R(^{O}K)$

g) Turbine Exit Static-to-Total Pressure Ratio, TEPSPT

$$TEPSPT = \frac{TTPRAV}{TSPRAV}$$

h) Turbine Exit Mach Number, TRBEMN

$$TRBEMN = \sqrt{5.0\ [(TEPSPT)^{\frac{-2}{7}} - 1.0]}$$

i) Turbine Exit Corrected Airflow, WTEC, LBm/sec (kg/sec)

$$WTEC = \frac{(ATUBE)(49.432)(1.728)(TRBEMN)}{(1.0+.2\ TRBEMN^2)^3}$$

ATUBE = 0.1067 FT^2 (m^2)

j) Turbine Exit Airflow, WTE, LBm/sec (kg/sec)

$$WTE = WTEC \left[\frac{FDAP}{(14.696)(TTPRAV)}\right] \sqrt{\frac{518.7}{TETTAV}}$$

k) Turbine Leakage Ratio, TELR

$$TELR = \frac{WVEN - WTE}{WVEN}$$

1) Turbine Output Horsepower, TOHP, HP (Watts)

$$TOHP = 0.25\ (TURBTD)(WVEN)\left(\frac{778}{550}\right)$$

III. FAN CONDITIONS

a) Corrected Fan Speed, RPM2C, RPM

$$RPM2C = \frac{RPM2}{\sqrt{\frac{TTO}{518.7}}}$$

RPM2 = measured fan speed

TTO = freestream total temperature, $^{o}R(^{o}K)$

b) Percent Fan Speed, PMDSPD

$$PMDSPD = \frac{(RPM2)(100)}{18144}$$

c) Percent Corrected Fan Speed, PCDSPD

$$PCDSPD = \frac{(RPM2C)(100)}{18144}$$

d) Fan Exit Total Pressure Ratio, FPR (I,J)

$$FPR\ (I,J) = \frac{PT}{PTO}$$

PT = total pressure at rake location (I,J) where I = 1⟶8 (rake), J=1-5 (Ring), Psia (kPa)

PTO = freestream total pressure, Psia (kPa)

e) Average Total Pressure - Complete Rake, FPRAV

$$FPRAV = \frac{\sum FPR\ (I,\ J)}{40}$$

f) Average Total Pressure Ratio - each Ring, PRNGAV (J)

$$PRNGAV\ (J) = \frac{FPR\ (I=1,8,J)}{8}$$

J = RING 1 → 5, constant for each calculation series

g) Average Total Pressure - Each Rake Probe, PRKAV

PRKAV(I) = FPR (I, J = 1-5)

I = Rake Probe number

h) Average Fan Hub Exit Static Pressure, PRS2AV

$$PRS2AV = \frac{PRS2\ (I=1-8)}{8}$$

PRS2(I) = static pressure ratio on fan hub

i) Average Fan Exit Total Temperature Ratio, FTRAV

$$FTRAV = \frac{\sum FTR\ (I=1 \rightarrow 16)}{16}$$

FTR (I) = total temperature ratio on each rake

j) Bellmouth Corrected Airflow, WBMC, LBm/sec (kg/sec)

$$WBMC = \frac{A_{fan}\ XK \sqrt{\left(\frac{PTO}{PBAV}\right)^{\frac{2}{7}} - 1}}{\left(\frac{PTO}{PBAV}\right)^{\frac{6}{7}}}$$

A_{fan} = 12 inch diameter fan area, FT^2 (m^2)

XK = 190.331; Inlet = 1

PBAV = Average of Bellmouth Static Pressures, Psia (kPa)

k) Bellmouth Airflow, WMB, Lbm/sec (kg/sec)

$$WBM = WBMC \left(\frac{PTO}{14.696}\right) \sqrt{\frac{51.87}{TTO}}$$

l) Fan Temperature Rise, FANDT, $^{o}R(^{o}K)$

FANDT = (FTRAV - 1.0) TTO

m) Fan Horsepower, FANHP, HP (Watts)

$$FANHP = 0.25\ (FANDT)(WBM)\quad \left(\frac{778}{550}\right)$$

n) Fan Exit Corrected Airflow, WFANEC, LBm/sec (kg/sec)

$$WFANEC = WBM \sqrt{\frac{(FTRAV)(TTO)}{518.7}} \quad \left(\frac{14.696}{(FPRAV)(PTO)}\right)$$

o) Fan Exit Mach No., FANEMN

$$\frac{WFANEC}{0.6} = \frac{(49.432)(1.728)\ FANEMN}{(1. + 0.2\ FANEM^2)^{3}}$$

IV. LOADS

a) Thrust Vector, T, LBf (kN)

$$T = \sqrt{FN^2 + A^2}$$

b) Flow Angle, PHI, degree

$$PHI' = \left[\text{ARCTAN}\ \left(\frac{FN}{A}\right)\right]\quad \frac{180}{\pi}$$

$$PHI = 180 - PHI'$$

c) Moment Arm, FT (m)

$$D = \frac{MPITCH}{T}$$

d) Fan Stream Ideal Velocity, VIF, FT/sec (m/sec)

$$VIF = 109.563\quad \frac{(FTRAV)(TTO)}{(1. - FPRAV)^{\frac{.4}{1.4}}}$$

e) Fan Stream Ideal Airflow, WIF, LBm/sec (kg/sec)

$$WIF = (AEXIT)(2.0556)\left[\frac{(FPRAV)(PTO)}{\sqrt{(FTRAV)(TTO)}}\right]\sqrt{\frac{1}{(FPRAV)^{\frac{2}{1.4}} - (FPRAV)^{\frac{2.4}{1.4}}}}$$

f) Turbine Flow Ideal Velocity

$$VIT = (109.563)\sqrt{TETTAV\left\{1. - \left[\frac{(PTO)(TTPRAV)}{FDAP}\right]^{\frac{.4}{1.4}}\right\}}$$

g) Mass Weighted Total Pressure, PTMW, Psia (kPa)

$$PTMW = \frac{\left[\frac{(FDAP)(WVEN)}{TTPRAV}\right] + [(FPRAV)(PTO)(WBM)]}{(WVEN + WBM)}$$

h) Mass Weighted Total Temperature, TTMW, $^{o}R(^{o}K)$

$$TTMW = \frac{(TETTAV)(WVEN) + (FTRAV)(TTO)(WBM)}{(WVEN + WBM)}$$

i) Mass Weighted Ideal Airflow, WIMW, LBm/sec (kg/sec)

$$WIMW = (AEXIT)(2.0556)\sqrt{\frac{PTMW}{TTMW}\left[\frac{PTMW}{\sqrt{TTMW}} - \frac{PTO}{PTMW}\right]^{\frac{2.4}{1.4}}}$$

V. NOZZLE

a) Thrust Coefficient, CFN

$$CFN = \frac{32.174\ T}{(WBM)(VIF)}$$

b) Discharge Coefficient, CD

$$CD = \frac{WBM}{WIF}$$

c) Specific Corrected Nozzle Flow, WSN, LBm/sec IN^2 (kg/sec m^2)

$$WSN = \frac{WBM\sqrt{\frac{(FTRAV)(TTO)}{518.7}}}{\frac{(FPRAV)(PTO)\ Ao}{14.696}}$$

$Ao = 95.00\ IN^2$

d) Nozzle Pressure Ratio, ENPR

$$ENPR = \frac{PTMW}{PTO}\ ;\ PTO = PAMB \text{ in static case}$$

THIS PAGE BLANK